Experimental investigation of myocardial hypertrophy in health and disease

PhD dissertation

Balázs Tamás Németh, MD

Semmelweis University
Doctoral School of Basic Medicine

Tutor: Tamás Radovits, M.D., Ph.D.

Opponents: Attila Borbély, M.D., Ph.D.
Levente Kiss, M.D., Ph.D.

Head of the Final Examination Committee:
Emil Monos, M.D., D.Sc.

Members of the Final Examination Committee:
Anikó Görbe, M.D., Ph.D.
Csaba Csonka, M.D., Ph.D.

Budapest
2019

Contents

1. List of Abbreviations

AAB – abdominal aortic banding

ACEi – angiotensin converting enzyme inhibitor

Akt – protein kinase B

ANOVA – analysis of variance

ANP – atrial natriuretic peptide

AWT – anterior wall thickness

Bcl-2 – B-cell lymphoma 2

BNP – B-type natriuretic peptide

BW – body weight

CaMKII – Ca^{2+}/calmodulin dependent kinase II

Cat – catalase

cDNA – complementary DNA

cGMP – cyclic guanosine monophosphate

CI – cardiac index

cMRI – cardiac magnetic resonance imaging

CNP – C-type natriuretic peptide

CO – cardiac output

CytC – cytochrome C

DAB – diaminobenzidine

DNA – deoxyribonucleic acid

dP/dt_{max} – maximal increment of LV pressure

dP/dt_{max}-EDV – dP/dt_{max} – end-diastolic volume relationship

dP/dt_{min} – maximal decrement of LV pressure

E_a – arterial elastance

ECM – extracellular matrix

EDRF – endothelium-derived relaxing factor

EDTA – ethylenediamine-tetraacetic acid

E_{es} – end-systolic elastance

EF – ejection fraction

Eff – efficiency

EIA – enzyme immunoassay

ERK – extracellular signal-regulated kinase

Errα – estrogen-related receptor α

ESPVR – end-systolic pressure-volume relationship

Ex – exercised animal

FS – fractional shortening

GAPDH – glyceraldehyde-3-phosphate dehydrogenase

GPCR – G-protein coupled receptor

H&E – hematoxylin and eosin staining

H_2O_2 – hydrogen peroxide

HDAC – histone deacetylase

HF – heart failure

HFpEF – heart failure with preserved ejection fraction

HFrEF – heart failure with reduced ejection fraction

HHD – hypertensive heart disease

HR – heart rate

HRP – horse radish peroxidase

HSP70 – heat shock protein 70 kDa

HW – heart weight

IGF-1 – insulin-like growth factor-1

IGF-1R – IGF-1 receptor

IgG – immunoglobulin G

IL-1β – interleukin-1β

IP_3 – inositol-1,4,5-triphosphate

IR – insulin receptor

JNK – c-Jun N-terminal kinase

LiW – liver weight

LuW – lung weight

LV – left ventricle, left ventricular

LVEDD – LV end-diastolic diameter

LVEDP – LV end-diastolic pressure

LVEDV – LV end-diastolic volume

LVESD – LV end-systolic diameter

LVESP – LV end-systolic pressure

LVESV – LV end-systolic volume

LVH – LV hypertrophy

LVM – LV mass

LVMi – LV mass index

MAP – mean arterial pressure

MAPK – mitogen activated protein kinase

MEF-2 – myocyte enhancer factor 2

MHC – myosin heavy chain

MHCα/β – myosin heavy chain α/β

MKP-1, -4 – MAPK phosphatase 1 and 4

MLP – muscle LIM protein

mTOR – mammalian target of rapamycin

NADPH – nicotinamide adenine dinucleotide phosphate

NFAT – nuclear factor of activated T cells

NIH – National Institutes of Health

NO – nitric oxide

NOS1 – neuronal NO synthase

NOS3 – endothelial NO synthase

NOX – NADPH oxidase

Nrf1 – nuclear respiratory factor 1

NT-proBNP – N-terminal pro-B-type natriuretic peptide

O_2^- – superoxide anion

PCR – polymerase chain reaction

PDE – phosphodiesterase

pGC – particulate guanylate cyclase

PGC1α – peroxisome proliferator activated receptor γ coactivator 1α

PI3K – phosphoinositide 3-kinase

PKA – cAMP dependent kinase

PKG – cGMP dependent kinase

PLC – phospholipase C

Pln – phospholamban

PPARα – peroxisome proliferator activated receptor α

p-Pln – phospho-Pln

PRSW – preload recruitable stroke work

P-V – pressure-volume

p-VASP – phospho-vasodilator-stimulated phosphoprotein

PWT – posterior wall thickness

RIPA – radio-immunoprecipitation assay lysis buffer

RNA – ribonucleic acid

RNS – reactive nitrogen species

ROS – reactive oxygen species

rTDT – recombinant terminal deoxynucleotidyl transferase

RV – right ventricle, right ventricular

RWT – relative wall thickness

RyR2 – ryanodine receptor 2

SDS – sodium dodecyl sulphate

Sed – sedentary animal

SERCA2a – sarcoplasmic and endoplasmic reticulum Ca^{2+}-ATPase isoform 2a

sGC – soluble guanylate cyclase

SOD-2 – superoxide dismutase 2

SV – stroke volume

SW – stroke work

TCAP – titin CAP protein

TGFβ – tissue growth factor β

TL – tibia length

TNFα – tumor necrosis factor α

Tris – 2-amino-2-(hydroxymethyl)propane-1,3-diol

TRPC – transient receptor potential cation channel

Trx1 – thioredoxin 1

TTBS – tris-buffered saline with Tween-20

TUNEL – terminal deoxyuridine triphosphate nick-end labeling

VAC – ventriculo-arterial coupling

VASP – vasodilator-stimulated phosphoprotein

τ – time constant of active LV relaxation

2. Introduction

The vast majority of adult mammalian cardiomyocytes are terminally differentiated and therefore do not proliferate under physiological conditions. The heart still retains its capability to respond to environmental demands, and cardiomyocytes can grow in reaction to various physiological or pathological stimuli. Primary triggering events for cardiac hypertrophy are mechanical stress and neurohumoral stimulation, which induce various cellular responses including changes in gene expression, protein synthesis and cell metabolism, leading to the development and progression of cardiac hypertrophy (Francis *et al.*, 1993; Lyon *et al.*, 2015; Maillet *et al.*, 2013). Growth of the body, pregnancy or physical exercise induces physiological enlargement of the heart, which occurs through hypertrophy of the individual cardiomyocytes, and is characterized by normal or enhanced contractility coupled with normal architecture and organization of cardiac structure (Weeks & McMullen, 2011). Therefore, physiological myocardial hypertrophy is generally not considered to be a risk factor for heart failure. In contrast, pathological cardiac hypertrophy is associated with hemodynamic overload, injury and loss of cardiomyocytes resulting in cardiac remodeling (Sano *et al.*, 2007; Shimizu *et al.*, 2010). The occurring pathophysiological changes include, but are not limited to metabolic derangement, altered calcium handling, inflammation, cell death and fibrosis. Although pathological and physiological myocardial hypertrophy might appear to be similar phenotypically, it has long been known that they differ fundamentally in the signaling pathways that drive their development (Shimizu & Minamino, 2016).

Mortality share of cardiovascular diseases has continuously been increasing for decades, now accounting for approximately 40% of deaths caused by non-communicable diseases (Figure 1.). Long standing pathological hypertrophy is a major underlying cause of heart failure (HF). Pressure overload, a highly prevalent cause of pathological myocardial hypertrophy induces adverse remodeling of the left ventricle (LV) that can result in HF with preserved ejection fraction (HFpEF). HFpEF is increasingly investigated, as its burden is similar to HF with reduced ejection fraction [HFrEF, (Kelly *et al.*, 2015)]. Although effective pharmacological and device therapies have been developed to decrease the burden of HFrEF (Emdin *et al.*, 2015), clinical trials targeting patients with HFpEF have had neutral results to this date (Emdin *et al.*, 2015;

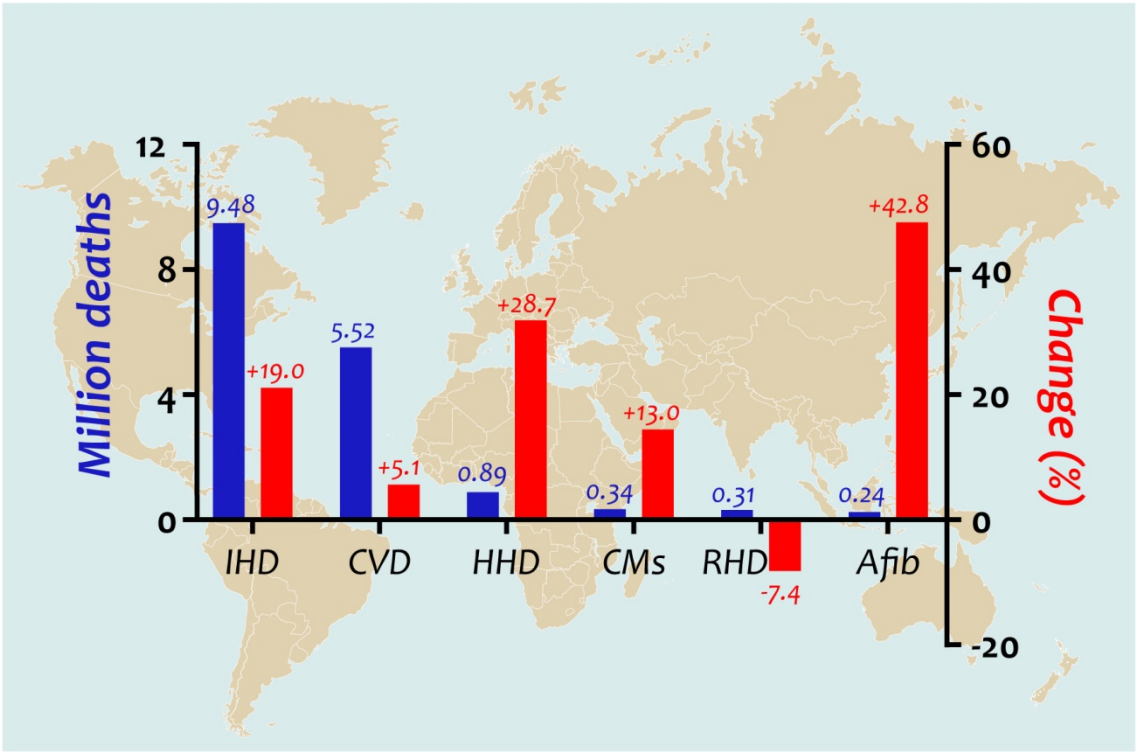

Figure 1. Leading causes of cardiovascular mortality worldwide and their change between 2006 and 2016

For the first time in human history, non-communicable diseases cause more deaths every year than epidemics worldwide, approximately 40% of which deaths are of cardiovascular origin. As such, cardiovascular conditions are the leading causes of mortality on our globe. This figure details the most frequent cardiovascular diseases resulting in death, showing the annual number of deaths and the percent change of death rate in 2016 compared with 2006 (GBD 2016 Mortality Collaborators, 2017).

Afib – atrial fibrillation; CMs – cardiomyopathies; CVD – cerebrovascular disease; HHD – hypertensive heart disease; IHD – ischemic heart disease; RHD – rheumatic heart disease

Kelly *et al.*, 2015). Therefore, new therapeutic approaches might be feasible in addressing the growing public health burden of HFpEF.

A feasible option to improve outcomes of HFpEF patients might be to target and alter molecular pathways currently not involved in pharmacological therapies. Such an interesting target is the second messenger cyclic GMP (cGMP) and its downstream signaling in cardiomyocytes. cGMP generated in response to nitric oxide (NO) production is an important intracellular regulator of many physiological and pathophysiological processes in the cardiovascular system, including cardiac remodeling (Tsai & Kass, 2009). It has previously been shown that elevated cytosolic

levels of cGMP originated either from blockade of its degrading enzyme, phosphodiesterase type 5 (PDE-5) (Takimoto *et al.*, 2005a) or from increasing its production by stimulating or activating its producing enzyme, soluble guanylate cyclase (sGC) (Fraccarollo *et al.*, 2014; Frankenreiter et al., 2018; Korkmaz *et al.*, 2009) preserved myocardial structure and function in experimental ischemia-reperfusion models. Therefore, elevating myocardial cGMP levels might prove to be an effective new method of preventing the development of pathological myocardial hypertrophy. A new group of drugs named sGC activators has been developed in order to counteract the impairment of the NO-cGMP pathway (Evgenov *et al.*, 2006). Cinaciguat (BAY 58-2667) is the most potent member of the sGC activators developed to this date (Stasch *et al.*, 2002), which is capable of activating even inactive forms of sGC (Schmidt *et al.*, 2009).

In the following brief review of the literature, I will summarize our knowledge of physiological and pathological myocardial hypertrophy, redox and NO/cGMP signaling in health and disease, as well as the concept of sGC activation, a novel therapeutic option as a preamble of my work.

2.1. Physiological myocardial hypertrophy

2.1.1. Cardiac structural changes in physiological myocardial hypertrophy

Physiological myocardial hypertrophy occurs naturally during growth or pregnancy, and is also the response of the heart to regular exercise. The diameter of human cardiomyocytes increase approximately 3-fold during growth from infancy to adulthood, and there is a linear relationship between body weight and cardiac weight. Cardiomyocytes in an adult heart retain their ability to increase the amount of contractile proteins within them in response to moderate mechanical stress, and the mode of sarcomere addition, discussed below in more detail, will define the final hypertrophic phenotype. Importantly, adverse events characteristic to remodeling such as fibrosis do not develop during this type of growth, resulting in maintained cardiac structure, function, and metabolism (Gibb & Hill, 2018).

Exercise is associated with a similar enlargement of the heart that is generally thought to be harmless and even beneficial in healthy people. Different types of exercise, however, affect cardiac enlargement differently, as the heart conforms the type of hemodynamic load imposed on the cardiovascular system (Maillet *et al.*, 2013). Dynamic sports, such as running or swimming, induce volume overload of the heart since there is an intensive dilatation of the skeletal muscle vasculature, leading to increased venous return to the heart (Pluim *et al.*, 2000). Thus, athletes trained in sports requiring sustained isotonic movement develop eccentric cardiac hypertrophy that is characterized by chamber enlargement and proportionate thickening of the ventricular walls (Figure 2.). In this setting, cardiomyocytes grow both in length and width. In contrast, sports involving development of muscular tension against increased resistance, such as weightlifting or wrestling, induce pressure overload of the heart. As such, static exercise leads to concentric LV hypertrophy (LVH), where wall thickness increases without proportionate dilation of the LV, leading to decreased LV cavity dimensions [Figure 2.; (Bernardo *et al.*, 2010)]. Cardiomyocytes usually increase in thickness more than in length during concentric hypertrophy (Heineke & Molkentin, 2006; Selby *et al.*, 2011). There are also sports that combine dynamic and static components, such as cycling or rowing, where endurance training is completed against elevated resistance. This combined type of exercise results in the greatest degree of LV chamber dilatation and

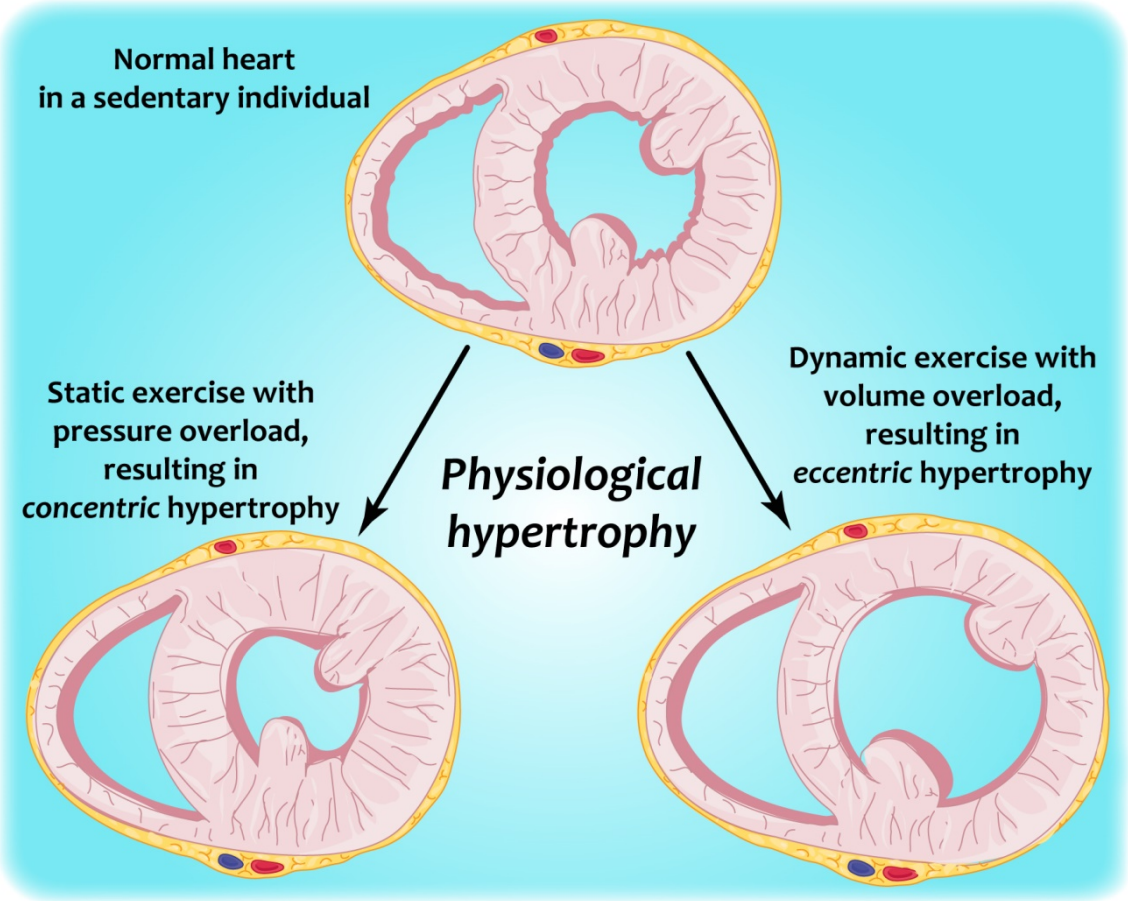

Figure 2. The proposed two extremes of cardiac wall and chamber alterations in physiological myocardial hypertrophy

Classical view of cardiac hypertrophy in response to exercise was dichotomous: dynamic types of exercise were thought to induce eccentric hypertrophy due to the volume overloading of the heart, while static sports would induce pressure overload of the left ventricle, therefore causing concentric hypertrophy. More recent investigations highlighted that the final phenotype of hypertrophy is dependent upon the ratio of dynamic and static components of the exercise, and that it is more of a continuum than two easily separable extremes (Mitchell et al., 2005).

increase in wall thickness (Barbier *et al.*, 2006; Pelliccia *et al.*, 1991; Pluim *et al.*, 2000). Therefore, it is now widely accepted that the phenotype of hypertrophy resulting from any type of exercise is dependent upon the ratio of the static and dynamic components of that particular exercise (Mitchell *et al.*, 2005). Furthermore, factors such as gender, ethnicity or age also influence the final observable phenotype (Colombo & Finocchiaro, 2018; Pavlik *et al.*, 2013). It must also be noted here, however, that

extreme exercise associated with competitive sport might result in a maladaptive hypertrophic response, which is still a diagnostic challenge for clinicians to differentiate from innocuous changes based on observation of phenotypic deteriorations alone (De Innocentiis *et al.*, 2018; Gabrielli *et al.*, 2018).

In contrast to the LV, response of the right ventricle (RV) to exercise training was not investigated in detail until relatively recently, mostly because of its more complex geometry and location inside the chest. Echocardiographic investigation of the RV is difficult at best, and many times accurate measurements are not possible due to anatomical reasons. The development of cardiac magnetic resonance imaging (cMRI) allowed for a more complex and accurate characterization of RV structural and functional changes following exercise. Similarly to LV alterations, RV volume, mass and stroke volume have all been observed to increase in athletes (Scharhag *et al.*, 2002). Contrary to the LV, however, RV hypertrophy and dilatation seem to occur only following dynamic training, while static exercise does not influence RV dimensions (Eijsvogels *et al.*, 2016; Weiner & Baggish, 2012). A possible downside of endurance training might be that atrial enlargement in athletes predisposes them to an increased risk of atrial fibrillation (D'Ascenzi *et al.*, 2015; Wilhelm *et al.*, 2012).

2.1.2. Functional changes associated with exercise training

While structural changes of the LV have been described somewhat consistently, functional alterations are not so well characterized. This discrepancy stems from the fact that the overwhelming majority of studies investigating the athlete's heart phenomenon have utilized conventional echocardiography to describe cardiac function (Utomi *et al.*, 2013), and while this modality is optimal for the investigation of structural alterations, it is not as reliable when it comes to functional parameters. The value of both fractional shortening (FS) and ejection fraction (EF), which are the most common systolic indices that have been used to evaluate cardiac function in athletes, is dependent upon multiple factors including loading conditions and heart rate. cMRI, although less influenced by anatomical variations and thus capable of providing better spatial resolution, can only measure these parameters as well. Meta-analyses based on studies utilizing these non-invasive modalities concluded that systolic function is preserved or somewhat enhanced in athletes compared with sedentary controls during resting conditions (Fagard, 2003; Fagard, 1996; Pluim *et al.*, 2000; Scharf *et al.*, 2010a; Scharf *et al.*, 2010b), but a

significant effect of study-to-study heterogeneity was noted (Utomi *et al.*, 2013). EF and FS investigated in these studies reflect chamber mechanics, which, especially in rest, might leave subtle, but important differences unnoticed. Investigation of intrinsic myocardial mechanics therefore might provide a better insight into the real functional alterations characterizing exercise-induced hypertrophy (Simsek *et al.*, 2013). Our research group has published a more detailed characterization of athlete's heart in a rat model (Radovits *et al.*, 2013), utilizing the invasive pressure-volume (P-V) analysis that is capable of providing load independent indices of both systolic and diastolic function. Athlete's heart in humans, however, cannot ethically be investigated with an invasive method, given its generally harmless nature. Development of the novel echocardiographic imaging modes tissue Doppler and speckle-tracking imaging allows for a more detailed and more accurate assessment of LV systolic function that correlates well with invasive measurements (Kovacs *et al.*, 2015). The results of studies implementing these modalities provided similar data, i.e. normal or supernormal cardiac systolic and diastolic function was found in athletes (Beaumont *et al.*, 2017; D'Andrea *et al.*, 2006; Kovacs *et al.*, 2014; Richand *et al.*, 2007).

Despite its clinical importance, LV diastolic function is an entity that has been difficult to assess (George *et al.*, 2010). The gold standard measure of LV active relaxation, τ, is the time constant of isovolumic pressure decline in the LV from LV pressure at maximum decrement of LV pressure (dP/dt_{min}) to the level of LV end-diastolic pressure (LVEDP), and was first described by Weiss et al. in 1976 (Weiss *et al.*, 1976), and later modified by Raff & Glantz (Raff & Glantz, 1981). Similarly to systolic LV parameters, however, routinely implementing invasive measurements to evaluate τ is not justifiable in healthy people. Therefore, alternative methods such as estimation of blood flow velocity through the mitral valve utilizing pulsed Doppler echocardiography are widely used to assess LV diastolic function (Nagueh *et al.*, 2009; Rakowski *et al.*, 1996), with the limitation that this method measures both active relaxation and myocardial stiffness, therefore incorporating passive components of diastolic function. Trans-mitral flow velocity comprises two components; peak early (E) and peak atrial (A) filling velocities. In the normal heart, most diastolic filling occurs during the early filling phase, so that E is characteristically greater than A, and the ratio E/A is usually >1.0 (Rakowski *et al.*, 1996). E/A was found to be normal or slightly enhanced in athletes as well (Fagard,

2003; Schmidt-Trucksass *et al.*, 2001; Sharma *et al.*, 2002). In some studies, however, the A wave was unusually lower than the E wave that can probably be ascribed to the lower heart rate, which prolongs the diastolic filling period and reduces the atrial component (Fagard *et al.*, 1987). To conclude, studies estimating LV diastolic function are consistent that diastolic function is not compromised in athletes despite the presence of cardiac hypertrophy.

2.1.3. Molecular pathways underlying physiological myocardial hypertrophy

Several pathways have been implicated in the background of physiological myocardial hypertrophy, the most important of which being hormones such as insulin, insulin-like growth factor-1 or thyroid hormone, and also signal transduction activated by mechanical forces. These factors induce physiological myocardial hypertrophy via the activation of several signaling pathways converging on phosphoinositide 3-kinase (PI3K), Akt, AMP-activated protein kinase or mammalian target of rapamycin (mTOR). In the following, I will briefly review the literature on these pathways.

2.1.3.1. Mechanical forces and signal transduction

Mechanotransduction enables cardiomyocytes to convert mechanical stimuli into biochemical events through the modulation of specific signaling molecules, giving them the ability to regulate hypertrophic or atrophic response depending on the extent and duration of mechanical stress imposed on them. Molecular pathways implicated in mechanotransduction and their significance in cardiac hypertrophy and failure has been extensively reviewed recently by Lyon and colleagues (Lyon *et al.*, 2015). Key loci within cardiomyocytes in this regard are the sarcomere, the intercalated discs and the sarcolemma, which, through a plethora of proteins, are all interconnected, functioning as a complex sensor of mechanical stimuli. At the sarcomere, titin and attached proteins (such as muscle LIM protein [MLP], titin-Cap [TCAP] or calsarcin-1) serve mainly as a stretch sensor and stress response signalosome (Frey *et al.*, 2004a; Gautel, 2011; Knoll *et al.*, 2002; Miller *et al.*, 2003). In the intercalated discs, N-cadherin was shown to mediate an adaptive response of the cardiomyocyte cytoskeleton to changes in mechanical stimuli (Chopra *et al.*, 2011; Kostetskii *et al.*, 2005). Besides the intercalated discs at the ends of cardiac myocytes, sarcolemma-associated proteins and complexes along the lateral surfaces of elongated myocytes (such as integrins) have been described as foci of force transmission. By forming a connection between the

extracellular matrix (ECM) and the contractile apparatus, costameric structures also facilitate the maintenance of mechanical integrity of the sarcolemma (Manso *et al.*, 2013; Sharp *et al.*, 1997). Furthermore, there is evidence that cardiomyocyte stress sensing might be dependent on the direction of the mechanical stimulus (Gopalan *et al.*, 2003; Simpson *et al.*, 1999), which may be related to different modes of hypertrophic growth (Kerckhoffs *et al.*, 2012).

2.1.3.2. Thyroid hormone-related signaling

Thyroid hormones have significant biological effect mainly during postnatal growth (Stubbe *et al.*, 1978), which effect is partially mediated by the activation of PI3K/Akt/mTOR signaling (Kinugawa *et al.*, 2005) (Figure 3.). Whether this hormone promotes physiological cardiac hypertrophy in adults, however, is still controversial, but studies indicate that thyroid hormone effect convert pathological to physiological cardiac hypertrophy (Pantos *et al.*, 2011; Pantos *et al.*, 2007; van Rooij *et al.*, 2007).

2.1.3.3. Insulin and insulin-like growth factor-1 signaling

Insulin and insulin-like growth factor-1 (IGF-1) signaling are the most well-known pathways in the development of physiological hypertrophy (Figure 3.). Their pathways converge on Akt (also known as protein kinase B), which is the main mediator of their downstream effects in cardiac myocytes (Catalucci *et al.*, 2009a; Catalucci *et al.*, 2009b; Kemi *et al.*, 2008; Kim *et al.*, 2003), although IGF-1 has another canonical pathway through extracellular-signal-regulated kinase (ERK), and a non-canonical pathway through G_i/phospholipase C (PLC)/inositol-1,4,5-triphosphate (IP_3)/Ca^{2+} signaling (Troncoso *et al.*, 2014). Both insulin and IGF-1 are critically important in the pre- and postnatal growth of the heart, and both are involved in regulating cell proliferation, growth, differentiation, metabolism, and survival (Saltiel & Kahn, 2001; Takeda *et al.*, 2010; Tatar *et al.*, 2003; Ungvari & Csiszar, 2012; Vinciguerra *et al.*, 2009; Vinciguerra *et al.*, 2012). Genetic deletion of IGF-1 leads to a significant decrease in body weight during development and usually results in embryonic lethality or death from respiratory failure shortly after birth (Liu *et al.*, 1993; Powell-Braxton *et al.*, 1993; Shimizu & Minamino, 2016). Similarly, cardio-specific deletion of insulin receptor (IR) results in a significant reduction of cardiomyocyte size and heart weight, with persisting fetal gene expression profile, mitochondrial dysfunction and reduced cardiac function (Belke *et al.*, 2002; Boudina *et al.*, 2009; Sena *et al.*, 2009). Ikeda and colleagues demonstrated

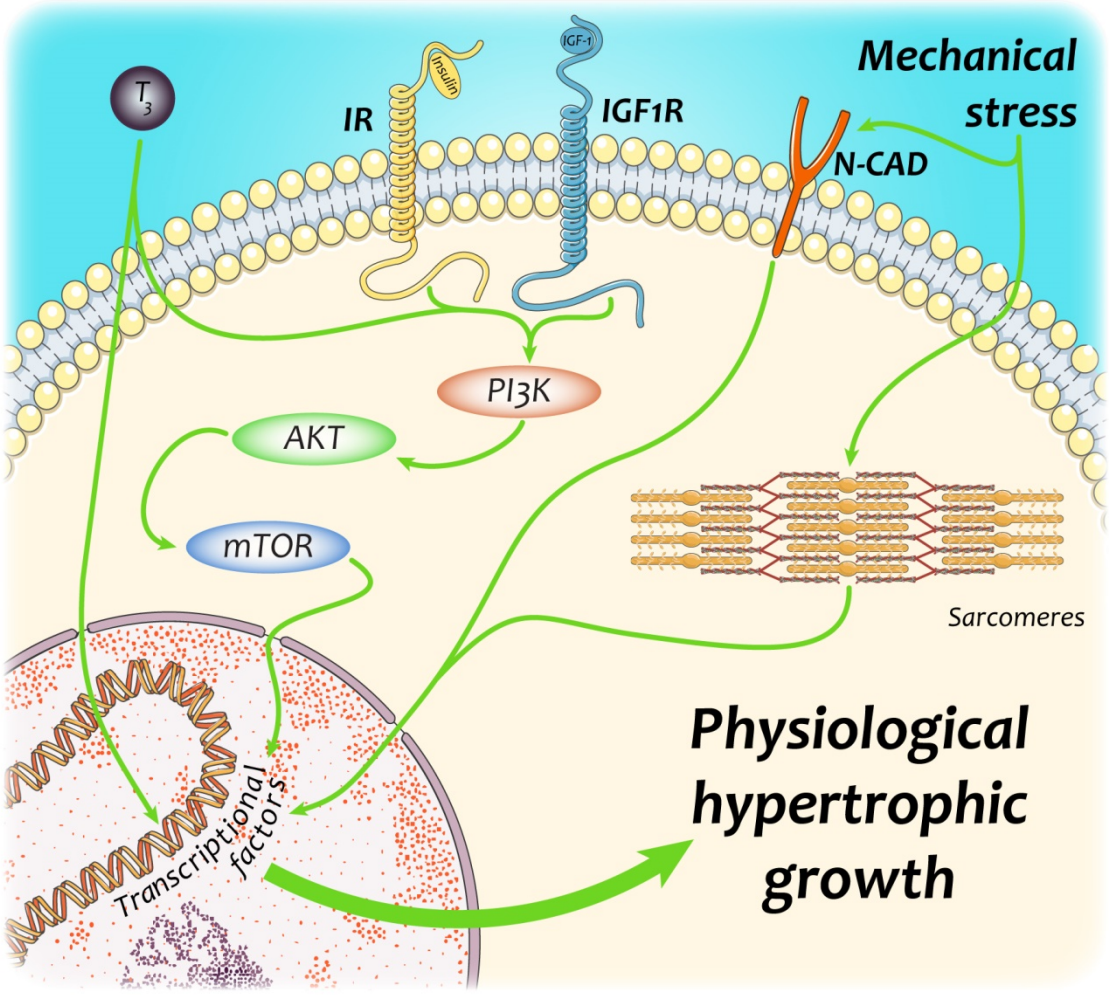

Figure 3. Major molecular factors governing the development of physiological hypertrophy

Physiological hypertrophic growth is induced mainly by growth factors such as insulin, IGF-1, or thyroid hormone, and also by periodical mechanical stress occurring during strenuous exercise either through pressure- or volume overload. The effects of hormonal factors are mediated mostly via the PI3K/Akt/mTOR signaling pathway, while mechanical stress exerts its effects through the sarcolemma, intercalated discs and sarcomeres (Lyon et al., 2015).

Akt – protein kinase B; IGF-1 – insulin-like growth factor-1; IGF1-R – IGF-1-receptor; mTOR – mammalian target of rapamycin, N-CAD – N-cadherin; PI3K – phosphoinositide-3-kinase; T_3 – triiodothyronine

the role of IGF-1 and IR mediated signaling in regulating the hypertrophic response induced by exercise in an elegant series of experiments. Deletion of the receptors of

insulin or IGF-1 in cardiomyocytes is associated with reduced or normal baseline cardiac growth, respectively, while the hypertrophic response to exercise is normal in both cases. When homozygous deletion of either IR or IGF-1 receptor (IGF-1R) is aggravated with the deletion of one of the alleles of the other receptor, exercise-induced cardiac hypertrophy becomes attenuated as well. The phenotypic changes in exercise-induced hypertrophy in *Igf1r*$^{+/-}$*-Ir*$^{-/-}$ mice were found to be more severe, which suggests that insulin is more closely involved in physiological hypertrophy related to exercise than IGF-1 (Ikeda *et al.*, 2009). Nevertheless, cardiac level of IGF-1 was shown to be higher in athletes than in sedentary controls, and exercise increased the serum level of IGF-1 (Neri Serneri *et al.*, 2001; Poehlman *et al.*, 1994), suggesting a significant role of IGF-1 in the development of physiological hypertrophy in humans.

Akt is the best characterized downstream effector of both insulin and IGF-1 mediated signaling, and was shown to promote cardiac hypertrophy via modulation of a variety of signaling pathways. Akt was shown to improve Ca^{2+}-handling, enhance cardiac contractility and promote physiological cardiac hypertrophy by activating or suppressing numerous transcription factors (Figure 3.) (Catalucci *et al.*, 2009a; Catalucci *et al.*, 2009b; Condorelli *et al.*, 2002; Matsui *et al.*, 2002; McMullen *et al.*, 2003; Pallafacchina *et al.*, 2002; Shioi *et al.*, 2000; Shioi *et al.*, 2002; Yamashita *et al.*, 2001). Taken together, interrelated pathways of insulin and IGF-1 signaling in physiological hypertrophy, although both are known to contribute to the phenotypic changes associated with it, need to be further elucidated.

2.2. Pathological myocardial hypertrophy

2.2.1. Main structural changes in pathological compared with physiological myocardial hypertrophy

While physiological stimuli, such as growth, pregnancy or exercise induce cardiac hypertrophy that is associated with maintained structure and function, various pathological conditions such as hypertension, myocardial infarction, diabetes mellitus, valvular heart disease or cardiomyopathies evoke hypertrophic growth that significantly alters the composition of the myocardium. This hypertrophic response of the heart to different stressors has been believed to be, at least initially, adaptive and to have a compensatory function by diminishing wall stress and thus decreasing myocardial oxygen consumption according to the law of Laplace (Grossman *et al.*, 1975; Hood *et al.*, 1968; Sandler & Dodge, 1963). It was shown later, however, that the presence of LVH developed in response to pathological stimuli, is associated with a significant increase in the risk of heart failure and malignant ventricular arrhythmias (Koren *et al.*, 1991; Levy *et al.*, 1990).

Similarly to physiological myocardial hypertrophy, two main phenotypes of pathological myocardial hypertrophy can be distinguished: (1) concentric hypertrophy due to pressure overload originating most commonly from hypertension or stenotic valvular disease, which is characterized by parallel addition of sarcomeres and lateral growth of individual cardiomyocytes; and (2) eccentric hypertrophy due to volume overload (valvular regurgitation or arteriovenous fistulas) or prior infarction, characterized by addition of sarcomeres in series and longitudinal cell growth (Dorn *et al.*, 2003; Frey *et al.*, 2004b). Furthermore, pathological LVH is usually associated with an increased rate of cardiomyocyte death and fibrotic remodeling that promote systolic and diastolic dysfunction, rendering it maladaptive in the long term (Berk *et al.*, 2007; Spinale, 2007). The combination of LVH with increased levels of biomarkers of subclinical myocardial injury (high-sensitivity cardiac troponin T, N-terminal pro–B-type natriuretic peptide [NT-proBNP]) identifies patients at highest risk for developing symptomatic HF, especially HFrEF (Heinzel *et al.*, 2015; Messerli *et al.*, 2017; Seliger *et al.*, 2015). In the following, I will summarize the consequences of longstanding hypertension on LV remodeling and hypertrophy in more detail.

Hypertension is a major public health problem associated with a significant and rapidly increasing mortality worldwide (Figure 1.). The bulk of patients who develop HFpEF suffer from persistent hypertension (Steinberg *et al.*, 2012). It is well known that hypertensive heart disease (HHD) is initially characterized by compensated LVH, but there is considerable inter-individual variability in the increase of LV mass and geometry (Drazner, 2011). LV mass can increase from either wall thickening or chamber dilation in hypertensive patients; the ratio of LV wall thickness to diastolic diameter (relative wall thickness, RWT) classifies LVH as concentric (RWT is increased) or eccentric (RWT is not increased), as discussed above (Ganau *et al.*, 1992). A third pattern, termed concentric remodeling, occurs when RWT, but not LV mass, is increased. Interestingly, contrary to the classical view of concentric hypertrophy slowly progressing into eccentric hypertrophy and then to decompensation during the course of the disease, hypertensive patients can have any of these patterns of LV geometry as an initial hypertrophic response (Ganau *et al.*, 1992; Sehgal & Drazner, 2007). What decides whether a patient develops one pattern or another in response to hypertension seems likely to be defined by a multitude of variables, including the extent of hypertension itself (Fagard *et al.*, 1997; Ross, 1997), ethnicity (Drazner *et al.*, 2005; Kizer *et al.*, 2004), sex (Krumholz *et al.*, 1993), age (Chahal *et al.*, 2010; Cheng *et al.*, 2009), neurohumoral activation (Alderman *et al.*, 2004; Brunner *et al.*, 1972; Davila *et al.*, 2008; du Cailar *et al.*, 2000; Muscholl *et al.*, 1998; Nakahara *et al.*, 2007; Olsen *et al.*, 2002; Velagaleti *et al.*, 2008), troponin I variants and thus altered Ca^{2+} sensitivity of the contractile apparatus in cardiomyocytes (Davis *et al.*, 2016) and the presence of comorbidities such as diabetes or obesity (Avelar *et al.*, 2007; de Simone *et al.*, 1994; Gottdiener *et al.*, 1994; Markus *et al.*, 2011; Palmieri *et al.*, 2001; Zabalgoitia *et al.*, 2001). How these factors combine to generate the final phenotype, however, is yet to be discovered. On the molecular level, LVH in response to pathological stimuli such as hypertension is characterized by increased myocardial fibrosis (Villari *et al.*, 1995), injury or loss of cardiomyocytes (Sano *et al.*, 2007; Shimizu *et al.*, 2010) and coronary microvascular rarefaction (Mohammed *et al.*, 2015; Paulus & Tschope, 2013), all of which are ultimately contributing to the transition of LVH to HF. Lastly, there is evidence that excessive LVH in response to pressure overload might not be necessary to evade dilated cardiac failure (Esposito *et al.*, 2002; Hill *et al.*, 2000; Hill *et al.*, 2002),

which suggests that inhibition of the development of concentric LVH might be a potential therapeutic target in pressure overload, such as hypertension (Drazner, 2011; Frey *et al.*, 2004b).

2.2.2. Myocardial dysfunction associated with pathological myocardial hypertrophy

Unlike physiological myocardial hypertrophy that is associated with normal cardiac performance, sustained pathological LVH results in both diastolic and systolic functional deterioration eventually progressing to HF. This transformation, however, might not present itself for extended periods of time, which is termed the compensated phase of pathological LVH. During this period, cardiac performance is normal or only mildly decreased in spite of the pathological structural alterations already existing in the myocardium. Despite the long-known maladaptive nature of pathological myocardial hypertrophy, the mechanisms that determine how longstanding hypertrophy ultimately progresses to overt heart failure are still poorly understood. Again, as a detailed review of the diverse functional consequences of different types of pathological stimuli exceeds the limitations of this dissertation, I will focus on the functional deterioration associated with longstanding hypertension.

The causality between maladaptive concentric LVH and diastolic dysfunction was established more than 30 years ago (Lorell *et al.*, 1990). In HFpEF patients, LVH is the most frequent cardiac structural abnormality, and it is correlated with hospitalization for heart failure, cardiovascular death, and aborted cardiac arrest (Hawkins *et al.*, 2007; Shah *et al.*, 2014), although the exact mechanisms linking pathological LVH to diastolic dysfunction have not been elucidated completely. Nevertheless, HFpEF patients were shown to have more pronounced concentric hypertrophy than patients with HHD but without HFpEF (Melenovsky *et al.*, 2007). Furthermore, pathological LVH is associated with an attenuated increase or even decrease in EF during exercise and reduced exercise capacity, this reduction being worst in patients with a concentric type of LVH (Lam *et al.*, 2010; Meyer *et al.*, 2015; Schnell *et al.*, 2013). There is evidence that this failure to increase EF in response to exercise is not related to an inability to increase LV end-diastolic volume (LVEDV), therefore to a restriction in LV filling, but rather to a failure in the Frank-Starling mechanism in patients with HFpEF (Abudiab *et al.*, 2013; Borlaug, 2014; Shibata *et al.*, 2011). Increased LV stiffness might also play a significant

role in the diastolic dysfunction related to pathological LVH, as τ in HFpEF patients was shown not to decrease during exercise as it normally would in healthy subjects, but even become prolonged (Borlaug *et al.*, 2011).

Many studies have shown that patients with HFpEF display impairments in regional deformation detected by tissue Doppler and strain-based imaging techniques, resulting in subtle but significant abnormalities in chamber and myocardial contractility, despite the overall preservation of EF (Borlaug *et al.*, 2009; Shah & Solomon, 2012; Tan *et al.*, 2009; Wang *et al.*, 2008). Even this subtle impairment of contractility at rest may indicate marked limitations in reserve, which is markedly impaired in HFpEF patients compared with age-matched healthy and hypertensive controls (Borlaug *et al.*, 2010). Systolic dysfunction affects diastolic function as well, as the ability to contract more enhances the recoil and suction forces during early diastole (Opdahl *et al.*, 2009), which have also been shown to be impaired in HFpEF (Ohara *et al.*, 2012).

Animal models are crucially important tools in the discovery of the driving forces behind human pathologies. As such, many small and large animal models have been developed to model the various clinical conditions resulting in the cardiac phenotype discussed above as closely as possible. The most commonly modeled diseases of pressure overload of the LV are aortic stenosis via thoracic aortic constriction (Huss *et al.*, 2007; Tagawa *et al.*, 1998) and hypertension via renovascular constriction (Cangiano *et al.*, 1979; Goldblatt *et al.*, 1934), compression of renal parenchyma (Grollman, 1955; Hart *et al.*, 2001), reduction of renal mass (Anderson *et al.*, 1985; Li *et al.*, 2009), increased salt intake (Coleman *et al.*, 1975), genetic modifications (Molkentin *et al.*, 1998; Okamoto & Aoki, 1963; Pfeffer *et al.*, 1982; Rapp & Dene, 1985), endocrine stimulation (Bois & Selye, 1957; Krege *et al.*, 1995) and aortic banding (Silver *et al.*, 1990; Thiedemann *et al.*, 1983).

2.2.3. Molecular pathways implicated in pathological myocardial hypertrophy

During pathological conditions, increased mechanical stress imposed on cardiomyocytes is accompanied by modulating factors that eventually shepherd actuated hypertrophic signaling pathways in the direction of generating pathological myocardial hypertrophy. Regarding the immense complexity of hypertrophic signaling, elucidation of the exact mechanism how activated pathways combine to create pathologic LVH is still in progress. The result of the processes discovered so far is generally referred to as

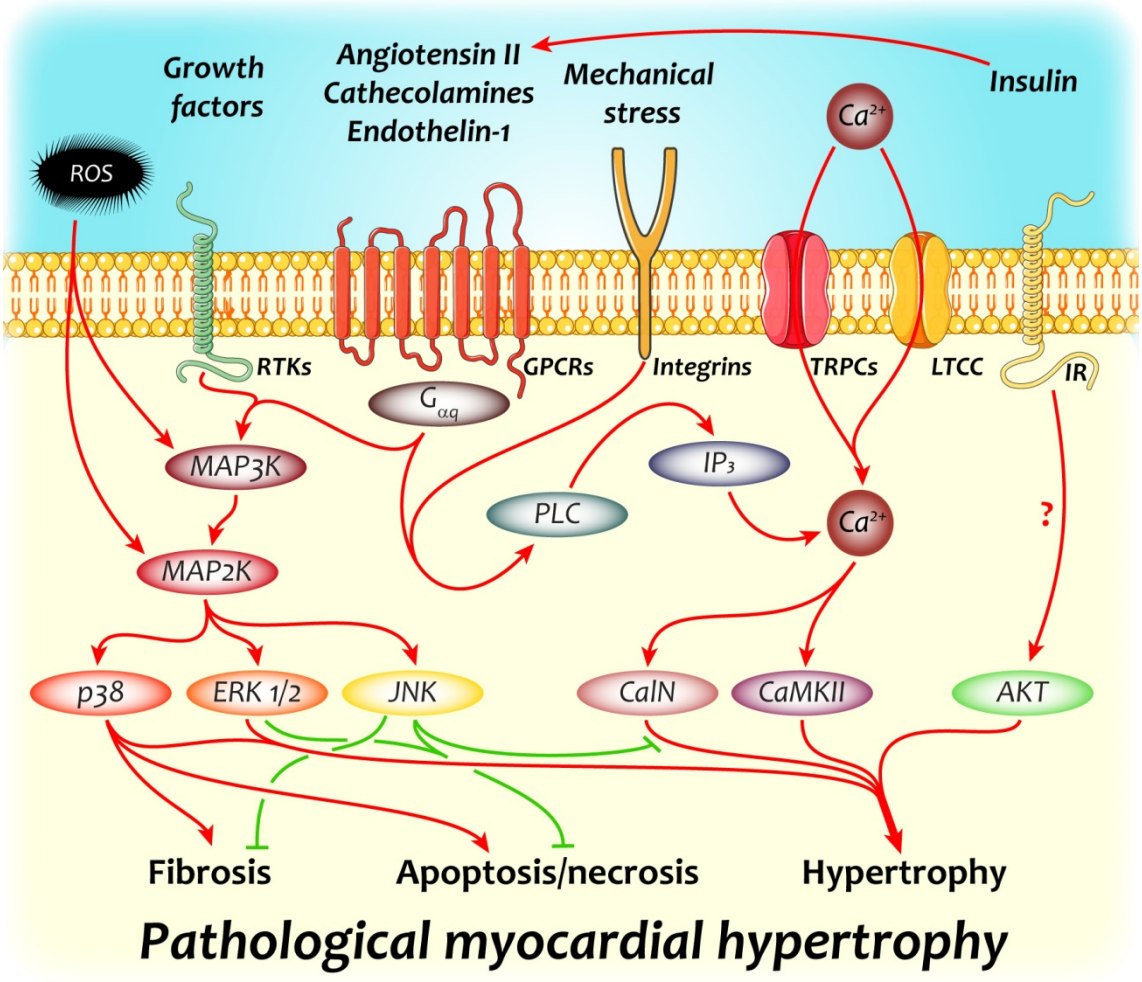

Figure 4. Key molecular pathways implicated in the development of pathological myocardial hypertrophy

Neurohumoral and growth factors together with the increased mechanical stress imposed on cardiomyocytes and other cellular components of the myocardium trigger multiple signaling pathways that bring about the characteristic phenotypical changes associated with pathological left ventricular hypertrophy. The two most important signaling cascades involved are Ca^{2+}-related and mitogen activated protein kinase signaling, members of which can potently induce gene expression changes generating all major hallmarks of pathological myocardial hypertrophy: fibrosis, apoptosis/necrosis and cardiomyocyte hypertrophy.

CalN – calcineurin; CaMKII – Ca^{2+}/calmodulin dependent kinase II; ERK1/2 – extracellular signal-regulated kinase 1/2; GPCR – G protein coupled receptor; IP3 – inositol-1,4,5-triphosphate; IR – insulin receptor; JNK – c-Jun N-terminal kinase; LTCC – L-type Ca^{2+} channel; MAP3K – MAP2K kinase; MAP2K – mitogen activated protein kinase kinase; PLC – phospholipase C; ROS – reactive oxygen species; RTK – receptor tyrosine kinase; TRPC – transient receptor cation channel

"reactivation of the fetal gene program", which covers re-expression of a wide array of molecular markers that are characteristic to the fetal period of ontogeny. Among others, such marker is the isotype-switch of myosin heavy chains (MHCs), significant overexpression of atrial natriuretic peptide (ANP), or the increased expression of endothelial nitric oxide synthase (NOS3). This altered gene expression profile is the driving force in the background of pathological LVH, and in the following section, I will shortly summarize the most important pathways initiating it.

2.2.3.1. Hypertrophy-inducing signals converging on Ca^{2+}-dependent pathways

Neurohumoral mediators such as catecholamines, angiotensin II or endothelin-1 have all been implicated in the development of pathological LVH and in the long term, HF. β-blockers and angiotensin converting enzyme inhibitors (ACEi) were shown to reduce the mortality of HF patients, hence becoming first line pharmacotherapeutic agents in HF (AIRE Study Investigators, 1993; Packer *et al.*, 2001; Poole-Wilson *et al.*, 2003). These mediators bind to G protein-coupled receptors (GPCRs) that comprise seven transmembrane domains. The G_{α} proteins involved can either be $G_{\alpha s}$, $G_{\alpha i}$, $G_{\alpha q}$ or $G_{\alpha 12/13}$, $G_{\alpha q}$ being the most important for the mediators listed above. $G_{\alpha q}$ signaling activates PLC, which catalyzes the synthesis of IP_3, thereby inducing intracellular Ca^{2+} release and thus an increase in $[Ca^{2+}]_i$. The excess Ca^{2+} can also originate from the extracellular space, e.g. through transient receptor potential cation (TRPC) channels. TRPCs regulate Ca^{2+} and Na^{+} movement in specific microdomains, and were shown to be upregulated in pathological myocardial hypertrophy and heart failure (Kuwahara *et al.*, 2006; Wu *et al.*, 2010). Regardless of its origin, Ca^{2+} modulates the activity of various Ca^{2+}-dependent signaling pathways, the two most important of which within cardiomyocytes being calcineurin/nuclear factor of activated T cells (NFAT) signaling and Ca^{2+}/calmodulin-dependent kinase II (CaMKII) signaling. Either of these pathways is sufficient to induce pathological LVH alone (Hoch *et al.*, 1999; Kirchhefer *et al.*, 1999; Molkentin *et al.*, 1998), but interplay between them is highly likely in various pathological conditions [Figure 4., (Zarain-Herzberg *et al.*, 2011)].

Calcineurin is a Ca^{2+}-activated serine/threonine protein phosphatase that induces translocation of NFAT into the nucleus by dephosphorylating it in the cytoplasm, thus increasing the expression of genes involved in pathological LVH (Figure 4.). Although cardiac-specific disruption of calcineurin expression revealed that it is necessary for

normal postnatal cardiac growth (Schaeffer *et al.*, 2009), calcineurin/NFAT signaling does not seem to be involved in physiological hypertrophy (Wilkins *et al.*, 2004).

The serine/threonine kinase CaMKII has been known to be involved in heart failure based on animal models and clinical data (Ai *et al.*, 2005; Kirchhefer *et al.*, 1999), and more recently was implicated in the progression of pressure overload-induced pathologic LVH to HF (Ling *et al.*, 2009).

Forced expression or activation of CaMKII mediates cardiac hypertrophy that is phenotypically similar to that of induced by norepinephrine, phenylephrine, or endothelin-1, while inhibition of its function prevents pathological LVH and improves HF [Figure 4., (Bossuyt *et al.*, 2008; Hoch *et al.*, 1999; Zhu *et al.*, 2000)]. Furthermore, class II histone deacetylase (HDAC) phosphorylation by CaMKII was shown to induce hypertrophic growth via myocyte enhancer factor-2 (MEF-2) dependent gene expression upregulation (Backs *et al.*, 2006; Passier *et al.*, 2000).

2.2.3.2. Mitogen activated protein kinase (MAPK) pathways in pathological hypertrophy

MAPKs are highly conserved kinases among eukaryotes that are implicated in a wide array of cellular processes. In the cardiovascular system, these include cell proliferation, cell growth, fibrotic remodeling and cellular response to different stressors. MAPK activation involves a three-tiered, phosphorylation based amplification system, during which signals originating from GPCRs, receptor tyrosine kinases, ion channels or oxidative and other types of stress, including pressure overload, activate the three main branches of MAPK signaling: ERK1/2, p38 MAPKs and c-Jun N-terminal kinases (JNKs, Figure 4.). All three branches play a role in the development of pathological hypertrophy and HF (Gutkind & Offermanns, 2009; Haq *et al.*, 2001; Toischer *et al.*, 2010), albeit reports so far on these roles are contradictory (Javadov *et al.*, 2014).

ERK1/2 is implicated in promoting cardiac hypertrophy in response to activation of GPCRs by catecholamines, angiotensin II or endothelin-1 and also to increased oxidative stress (Figure 4.). Although pro-hypertrophic, ERK1/2 and its downstream signaling does not seem to be essential in cardiac hypertrophy, since the deletion of its gene ($ERK1^{-/-}$ and $ERK2^{+/-}$) did not prevent development of LVH (Purcell *et al.*, 2007). It does, however, seem to play a role in determining the phenotype (i.e., eccentric or concentric) of LVH developed in response to various stimuli (Kehat *et al.*, 2011).

Potential downstream targets of ERK1/2-mediated hypertrophy include members of Ca^{2+} homeostasis and activation of the transcription factor GATA4 [Figure 4., (Zheng *et al.*, 2004)]. Furthermore, activation of ERK1/2 was shown to play a role in resistance to apoptosis (Yamaguchi *et al.*, 2004).

The role of p38 in the development of pathological hypertrophy is still controversial. Although it was shown to promote LVH in some studies (Liang & Molkentin, 2003), others concluded that even dramatic down-regulation of the kinase left cardiac hypertrophic growth unaffected (Nishida *et al.*, 2004). This discrepancy in the results published might be related to methodological differences, such as the use of different cell types, animal models, inhibitors or agonists, and also the temporal design of a specific study (Javadov *et al.*, 2014). Demonstration of the participation of p38 in fibrotic remodeling was more consistent: its activation (Koivisto *et al.*, 2011; Liao *et al.*, 2001; Wang *et al.*, 1998) or inhibition (Liu *et al.*, 2005; Yin *et al.*, 2008; Zhang *et al.*, 2003) resulted in enhanced or reduced myocardial fibrosis, respectively (Figure 4.). Furthermore, p38 activation is associated with increased apoptosis (Kaiser *et al.*, 2004; Ren *et al.*, 2005), thereby promoting the transition of pathologic LVH to overt HF.

There is, similarly to p38, contradiction in what role JNK plays in the development of pathologic LVH. Neonatal cardiomyocytes were shown to respond with hypertrophy to targeted activation of JNK signaling (Wang *et al.*, 1998), whereas adult hearts exhibited increased hypertrophy, fibrosis and apoptosis when JNK or members of its signaling were inhibited (Hilfiker-Kleiner *et al.*, 2005; Liang *et al.*, 2003), suggesting an anti-hypertrophic role for JNK in adult hearts via interference with calcineurin/NFAT signaling (Figure 4.). On the other hand, JNK was shown to induce cardiac dysfunction as well via (1) decreasing intercellular communication within the myocardium due to the downregulation of connexin-43, and thus loss of gap junctions (Petrich *et al.*, 2002), and (2) the activation of matrix metalloproteinase-2 resulting in detrimental cardiac remodeling (Krishnamurthy *et al.*, 2007).

An endogenous negative regulator of MAPK cascades is MAPK phosphatase 1 (MKP-1), constitutive expression of which in the heart downregulates all three major pathways discussed above, and also prevents induction of hypertrophy by catecholamines or aortic banding (Bueno *et al.*, 2001). MKP-1 and MKP-4 were shown to have a cardioprotective role; MKP-1 and -4 knockout mice express elevated amounts of

p38MAPK with no change of JNK or ERK1/2 levels, and have a low survival rate associated with systolic dysfunction and cardiac dilatation (Auger-Messier *et al.*, 2013).

2.2.3.3. Excessive activation of insulin signaling contributes to pathological myocardial hypertrophy

Although insulin/IR/Akt signaling is widely accepted to promote physiological myocardial hypertrophy, neither animal studies nor large clinical trials have provided conclusive evidence whether insulin signaling is cardioprotective in adults. Instead, insulin resistance, and thus hyperinsulinemia, has been reported to increase the risk of developing heart failure in patients with systolic dysfunction, which observation gains epidemiological importance if one considers the high prevalence of this condition (Ashrafian *et al.*, 2007; Ingelsson *et al.*, 2005; Witteles *et al.*, 2004). Also, contrary to what might be expected, intensive glycemic control with insulin increased cardiovascular events in diabetic patients instead of reducing these complications (Action to Control Cardiovascular Risk in Diabetes Study Group, 2008).

Experimental evidence shows that chronic hyperinsulinemia might induce pathological hypertrophy via an angiotensin II-dependent manner [Figure 4., (Samuelsson *et al.*, 2006)], and that excessive insulin signaling exacerbates the transition of hypertrophy to overt HF (Shimizu *et al.*, 2010). Furthermore, pressure overload was shown to induce adipose tissue inflammation and lipolysis, resulting in insulin resistance (Shimizu *et al.*, 2012). Suppression of adipose tissue inflammation in the same study decreased insulin resistance, therefore, possibly, hyperinsulinemia, and lead to improved systolic function in mice subjected to chronic pressure overload (Shimizu *et al.*, 2012).

2.3. Redox and nitric oxide/cGMP signaling in cardiovascular physiology and pathology

Redox signaling, like many other signaling pathways implicated in cardiovascular physiology, is Janus-faced. Whether physiological processes or detrimental effects are mediated by reactive oxygen (ROS) and nitrogen species (RNS), depends on the local concentration and compartmentation of the reactive species involved, and also on the capacity of antioxidant mechanisms present. Oxidative and nitrosative stress, in fact, cannot be meaningfully separated, as generation of either ROS or RNS will bring about the genesis of the other, hence the term nitro-oxidative stress.

Previously known as the elusive endothelial-derived relaxing factor [EDRF, (Furchgott & Zawadzki, 1980)], the discovery of nitric oxide (NO) and its involvement in many physiological processes and virtually all cardiovascular pathologies reestablished our thinking concerning cardiovascular health and disease. NO, though often referred to as a toxic agent when present in higher concentrations and thus considered a major player in nitrosative stress, is not particularly reactive. There is, however, one reactive species that seems to stand out from the rest, especially in terms of biological importance: peroxynitrite, a powerful oxidant that is formed in a spontaneous reaction between NO and superoxide (Pacher *et al.*, 2007).

The cardioprotective effects of NO, mediated intracellularly via cGMP signaling, are severely reduced in disease states, including hypertension, associated with increased nitro-oxidative stress. Therefore, novel pharmacological approaches specifically targeting the upregulation of this physiologically important pathway are increasingly investigated. In the following section, I will briefly review the most important aspects of redox- and NO signaling in cardiovascular homeostasis and pathology, and also give a short introduction into the concept of sGC activation as a novel pharmacological interventional option.

2.3.1. The role of redox signaling in cardiac (patho)physiology

2.3.1.1. Forms, sources, targets and elimination of reactive oxygen species in the heart

ROS are powerful oxidants that contain at least one oxygen atom with an unpaired electron. The most important ROS *in vivo* are superoxide anion (O_2^-) and hydrogen peroxide (H_2O_2), but other species such as the highly reactive hydroxyl radical or

singlet oxygen also play a significant role. ROS can either be generated by nicotinamide adenine dinucleotide phosphate (NADPH) oxidases (Noxs) that are specialized enzymes having no known biological role other than forming ROS, or can originate from the functioning of the mitochondrial electron transport chain, oxidases involved in metabolism (e.g. xanthine oxidase and monoamine oxidases) and uncoupled NO synthases as by-products [Figures 5. and 6., (Burgoyne *et al.*, 2012)]. The compartmentation and local concentration of ROS produced have a significant role in their effect, as these define the targets they can reach; in cardiomyocytes, these redox sensitive targets include CaMKII (Erickson *et al.*, 2008), cAMP-dependent protein kinase (PKA, Brennan *et al.*, 2006), cGMP-dependent protein kinase (PKG, Burgoyne *et al.*, 2007), MAPKs (Valko *et al.*, 2007) and members of Ca^{2+} homeostasis such as ryanodine receptor 2 (RyR2) and sarcoplasmic and endoplasmic reticulum Ca^{2+}-ATPase 2a (SERCA2a, Zima & Blatter, 2006). An efficient endogenous antioxidant system comprising enzymatic and non-enzymatic components exists to scavenge and thus limit the effects of ROS both spatially and temporally. Superoxide dismutase (SOD) catalyzes the conversion of O_2^- to H_2O_2, which is then further converted by catalase (Cat) and glutathione peroxidase to water and molecular oxygen. Furthermore, non-enzymatic defense is represented by ascorbic acid (vitamin C), α-tocopherol (vitamin E), glutathione, carotenoids, flavonoids and other antioxidants such as thioredoxin (Burgoyne *et al.*, 2012; Valko *et al.*, 2007).

2.3.1.2. Oxidative stress and its role in pathological myocardial hypertrophy

Reviewing all the known ROS-related mechanisms in the background of cardiovascular pathologies would significantly exceed the possibilities of this dissertation; therefore, I will focus on pathological myocardial hypertrophy and relevant mechanisms including alterations in Ca^{2+} handling and induction of apoptosis/necrosis.

Oxidative modification of CaMKII (Wagner *et al.*, 2011), RyR2 (Terentyev *et al.*, 2008) and SERCA2a (Lancel *et al.*, 2010) all contribute to the imbalance of cellular Ca^{2+} homeostasis in pathological LVH (Figure 5.). Diastolic Ca^{2+} leakage through oxidized RyR2 and SERCA2a results in increased $[Ca^{2+}]_i$ and thus impaired relaxation, contractile dysfunction and increased probability of arrhythmias. Oxidation-enhanced activation of PKA could also potentially contribute to Ryr2 dysfunction via hyper-phosphorylation.

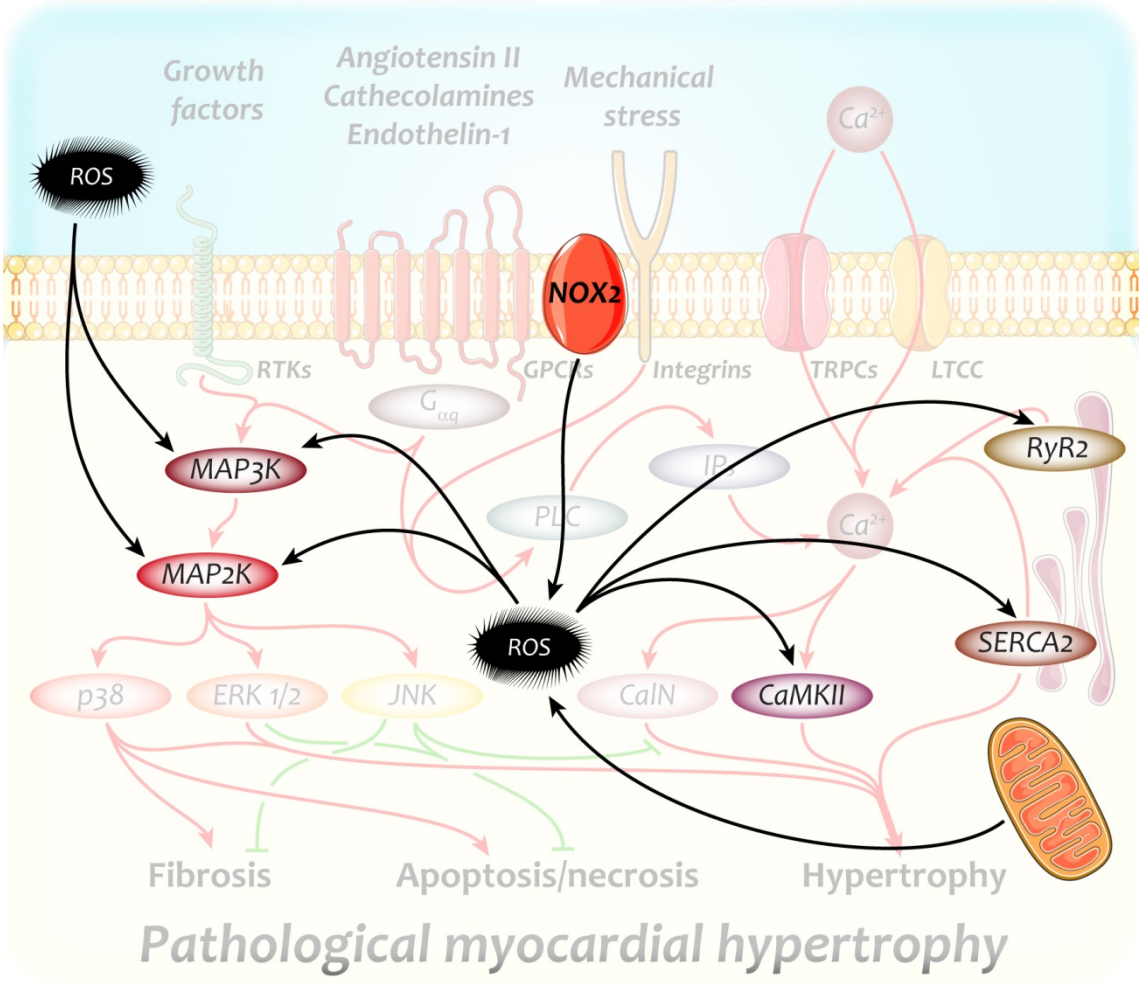

Figure 5. Major redox-sensitive targets with a significant role in the development of pathological myocardial hypertrophy

Reactive oxygen species are capable of activating key players of pathological hypertrophic growth independently of their original activators. ROS, therefore, further enhance the over-activation of hypertrophic signaling, resulting in an aggravated hypertrophic phenotype. CaMKII – Ca^{2+}/calmodulin dependent kinase II; MAP2K – mitogen activated kinase kinase; MAP3K – MAP2K kinase; NOX2 – nicotinamide adenine dinucleotide phosphate oxidase 2; ROS – reactive oxygen species; RyR2 – ryanodine receptor 2; SERCA2 – sarcoplasmic and endoplasmic reticulum Ca^{2+}-ATPase isoform 2

Mitochondria play a central role in orchestrating apoptotic/necrotic cell death in response to ROS and Ca^{2+} overload (Sack *et al.*, 2017). Mitochondrial permeability transition pore opening or translocation of pro-apoptotic proteins Bax/Bad to the mitochondria are both central processes in the intrinsic pathway of apoptotic cell death

facilitated by ROS (Donath *et al.*, 2006). Excessive GPCR activation also leads to ROS production and activation of JNK and p38 MAPK, leading to activation of apoptotic pathways (Yamaguchi *et al.*, 2003).

As discussed above, both Ca^{2+}-dependent and MAPK signaling involved in cardiac hypertrophy might also be activated by ROS; in fact, due to the interdependence of the effects of vasoactive mediators and ROS, they cannot meaningfully be separated in pressure overload-induced LVH. Nox2 is of central importance in generating the reactive species activating/interfering with hypertrophic signaling actuated by other factors [Figure 5., (Bendall *et al.*, 2002; Grieve *et al.*, 2006)], but activation of Nox2 is certainly not obligatory for the development of pressure overload-induced LVH (Maytin *et al.*, 2004; Touyz *et al.*, 2005). Furthermore, mechanical stretch has also been associated with ROS-mediated induction of hypertrophy, also via the activation of Nox2 (Pimentel *et al.*, 2001).

2.3.2. Nitric oxide and cGMP signaling in cardiovascular health and disease

NO, despite its simple structure comprising only two atoms, is among the most important intercellular messengers in all vertebrates, playing a significant role in the modulation of thrombosis, neural activity and cardiovascular homeostasis (Pacher *et al.*, 2007). NO mediates its effects mainly through increasing the generation of cGMP, but also has cGMP-independent effects via protein nitrosylation (Lima *et al.*, 2010), here not discussed in more detail. Certain disease conditions, especially those associated with oxidative stress result in the dysfunction of this important pathway, which will be reviewed briefly in this section.

2.3.2.1. cGMP generation and degradation

NO in the cardiovascular system is predominantly produced by NOS3 located in the endothelium, but cardiac myocytes are also capable of producing it – mainly for tightly localized regulatory purposes – by neuronal NOS (NOS1). NOS3-derived NO then diffuses to its target cells, including cardiomyocytes, to activate sGC. The enzyme binds NO with its heme moiety (Derbyshire & Marletta, 2009), resulting in an up to 800-fold increase in its activity and a production of cGMP from GTP in a similar magnitude.

sGC, however, is not the only source of cGMP within the cell. Membrane-bound enzymes, particulate GCs (pGCs) also produce it in response to natriuretic peptides ANP, B-type (BNP) and C-type NP (CNP) (Kuhn, 2009). Compartmentation of the

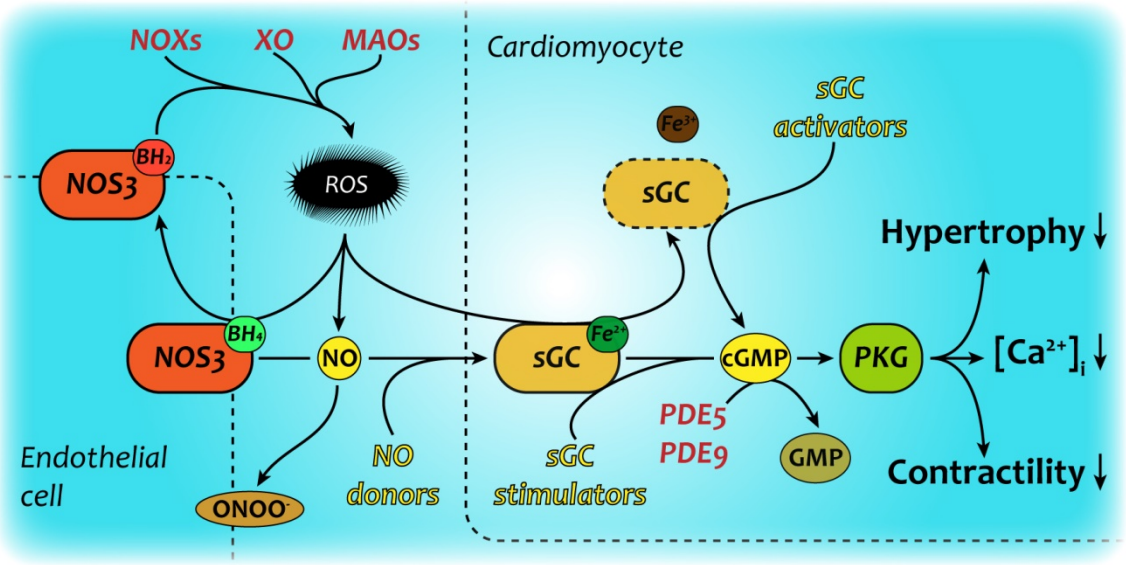

Figure 6. NO-cGMP signaling in health and disease

Physiological signaling through the NO/cGMP/PKG pathway deteriorates at multiple levels under pathological conditions. Oxidative stress decreases the generation, amount and sensing of nitric oxide by target cells, therefore disrupting cGMP generation and signaling within these cells as well. There have been various attempts at restoring cGMP signaling in cardiovascular pathologies, these are marked with yellow color. The novel sGC stimulators require reduced, functional sGC to mediate their effects, while sGC activators are capable of inducing cGMP production of dysfunctional sGC in absence of its heme prosthetic group (Evgenov et al., 2006)

$BH_{4/2}$ – reduced/oxidized tetrahydrobiopterin; cGMP – cyclic GMP; GMP – guanosine monophosphate; MAO – monoamine oxidase; NO – nitric oxide; NOS3 – endothelial NO synthase; NOX – nicotinamide adenine dinucleotide phosphate oxidase; $ONOO^-$ – peroxynitrite; PDE5/9 – phosphodiesterase 5/9; PKG – cGMP dependent kinase; ROS; reactive oxygen species; sGC – soluble guanylate cyclase; XO – xanthine oxidase

cGMP generated in response to these peptides differ from that of derived from sGC, therefore cardiomyocytes exhibit distinct responses as well (Castro *et al.*, 2006; Fischmeister *et al.*, 2006); ANP has anti-hypertrophic properties (Patel *et al.*, 2005), while BNP mediates anti-fibrotic effects (Tamura *et al.*, 2000). CNP does not play a significant role in the cGMP-generation of cardiomyocytes (Yasoda *et al.*, 2004).

cGMP is removed from the cell by either enzymatic degradation or extrusion via multi drug resistance proteins. Enzymatic degradation is responsible for the bulk of cGMP elimination, and is catalyzed by cyclic nucleotide-specific phosphodiesterases (PDEs),

which are members of a superfamily comprising eleven smaller families (PDE1-11). PDEs have distinct specificities for cAMP and cGMP, among which PDE5 and PDE9 are significant in the cardiovascular system regarding the hydrolysis of cGMP (Lee *et al.*, 2015; Takimoto *et al.*, 2005a).

2.3.2.2. cGMP-dependent effects of nitric oxide signaling

cGMP mediates its effects through a number of mechanisms. Predominantly it activates PKGs and thus regulates phosphorylation state of various protein targets, but it can also modulate the activity of distinct PDEs and cAMP-dependent protein kinases either directly or indirectly (termed as cAMP-cGMP crosstalk). Most cells contain at least one of three PKGs: PKGIα, PKGIβ, or PKGII that are targeted by their distinct amino termini to different substrates (Hofmann *et al.*, 2009). Cardiomyocytes express PKGIα, which resides within the cell in a soluble form. PKGIα has been established to be a powerful brake on the cellular stress response signaling [Figure 6., (Hofmann, 2018; Rainer & Kass, 2016)]: it can suppress selective GPCR agonism through regulator of G protein signaling subtypes (Takimoto *et al.*, 2009), phosphorylate titin and troponin I (Kruger *et al.*, 2009; Lee *et al.*, 2010), increase the activity of late rectifier K^+-channels (Bai *et al.*, 2005) and antagonize members of the TRPC channel family (Koitabashi *et al.*, 2010; Wu *et al.*, 2010). More recently it was discovered that PKG might also modulate mechanosensing (Seo *et al.*, 2014) and protein quality control (Ranek *et al.*, 2013). In addition, as described above, oxidation of the PKG1α isoform in cardiomyocytes impairs its brake-like function; therefore oxidative stress adversely impacts stress-response signaling (Nakamura *et al.*, 2015).

2.3.2.3. Oxidative stress results in an imbalance in NO-cGMP signaling

Oxidative stress impairs NO signaling at multiple levels (Figure 6.). Tetrahydrobiopterin, which serves as a prosthetic group in NOS3, becomes oxidized, which results in uncoupling of the enzyme. Uncoupled NOS3 cease to produce NO, and instead, starts production of O_2^-, thereby aggravating oxidative stress [Figure 6., (Stasch *et al.*, 2011)]. NO bioavailability is further reduced by its instantaneous conversion to peroxynitrite by O_2^-. Peroxynitrite is a strong oxidant itself, mediating nitro-oxidative stress by nitrating tyrosine residues of various proteins and damaging other targets (Pacher *et al.*, 2007). Oxidative stress results in damaged sGC via the oxidation of its heme group (Figure 6.). Oxidized heme of sGC is unable to bind NO, therefore

rendering sGC incapable of generating cGMP (Evgenov *et al.*, 2006). Furthermore, cGMP degradation is increased in oxidative stress mainly because of upregulation of PDE5 (Das *et al.*, 2015). As a result, cGMP level within cardiomyocytes becomes significantly decreased, resulting in the loss of its cardioprotective effects.

2.3.3. Modulation of sGC activity – a novel pharmacotherapeutic concept

Long before any knowledge regarding the mechanism of their action, glyceryl trinitrate and other organic nitrates, as well as nitro-vasodilators had been in clinical use to treat angina pectoris and hypertensive crises for decades (Megson & Miller, 2009). Most of these drugs, however, have an important limitation: they lose their efficacy during prolonged use, termed as nitrate tolerance (Munzel *et al.*, 2005). Furthermore, NO resistance is an important feature of ischemic heart disease and hypertension, and is also present in a significant portion of patients with pulmonary hypertension. The discovery that cGMP generated by sGC, as discussed above, mediates the cardioprotective effects associated with NO, provided rationale for development of new pharmaceuticals acting at different steps of the NOS3-NO-sGC-cGMP-PKG axis, potentially downstream of NO (Figure 6.).

sGC stimulation and activation as a highly effective method to increase intracellular cGMP-production, have been subject to extensive preclinical and clinical research (Boerrigter *et al.*, 2007; Schmidt *et al.*, 2009; Stasch *et al.*, 2015; Stasch & Hobbs, 2009). sGC stimulators require sGC to be functional (i.e., sGC having an intact, reduced heme prosthetic group) to increase cGMP production, and synergize with NO in activation of the enzyme [Figure 6., (Evgenov *et al.*, 2006)]. A sGC stimulator, riociguat under the trade name Adempas®, has recently been approved by the Food and Drug Administration for clinical use in pulmonary hypertension based on data from a large, randomized, Phase III clinical trial (Ghofrani *et al.*, 2013). sGC activators, in contrast, are capable of activating sGC independently of both NO and heme, therefore might be more potent in cardiovascular conditions with oxidative stress where sGC activity is severely diminished (Figure 6.).

Cinaciguat (also known as BAY 58-2667) was the first sGC activator to be developed, and remains the most potent such drug to this day. Due to its strong and selective binding to heme-free and thus inactive sGC (Figure 7.) prevalent mainly in conditions associated with oxidative stress, makes this drug especially interesting because of the

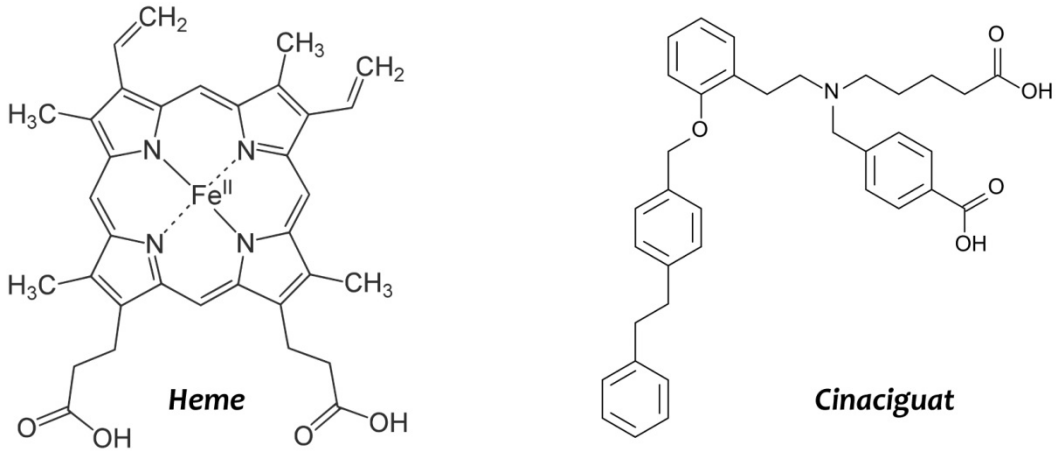

Figure 7. Structural similarity of heme and cinaciguat

Heme serves as the nitric oxide sensor in soluble guanylate cyclase. Under pathological conditions that are associated with increased oxidative stress, the ferrous ion in the center of heme becomes oxidized, and the resulting conformational change leads to the dissociation of the prosthetic group from the enzyme. Due to its structural homology, cinaciguat binds into the empty heme pocket of soluble guanylate cyclase, thus restoring its ability to generate cGMP.

potentially disease-selective mode of action. It has been shown to have beneficial effects in various cardiovascular disorders, such as myocardial infarction (Korkmaz *et al.*, 2009), ischemia/reperfusion injury (Radovits *et al.*, 2011), endothelial dysfunction induced by nitro-oxidative stress (Korkmaz *et al.*, 2013), vascular neointima formation (Hirschberg *et al.*, 2013) and diabetic cardiomyopathy (Matyas *et al.*, 2015), as well as preservation of the donor organ during heart transplantation (Loganathan *et al.*, 2015). Clinical trials in which the drug was used in acute heart failure patients intravenously, however, have not been successful so far (Erdmann *et al.*, 2013). Alternative temporal and drug delivery designs in other patient populations, such as chronic oral administration in HFpEF patients, as well as development of short-acting sGC activators (Sawabe *et al.*, 2019), however, might still be feasible, and need further investigation.

3. Objectives

Although both physiological and pathological myocardial hypertrophy have been extensively studied from molecular viewpoints, functional data regarding the differences between these hypertrophic phenotypes is limited in terms of reliability, given the non-invasive and thus less accurate modalities used to describe them. Therefore, there is a need to provide a deeper insight into the functional alterations characterizing these distinct forms of cardiac hypertrophy. Furthermore, the incidence of heart failure is continuously rising, largely because of the growing incidence of its preceding conditions such as longstanding hypertension.

Our aims for the experimental investigations discussed in this thesis were as follows:

(1) Compare the functional characteristics of physiological and pathological myocardial hypertrophy utilizing P-V analysis, the current gold standard method for in vivo cardiac functional measurements

(2) Explore the morphological and molecular background of the functional differences observed in physiological and pathological myocardial hypertrophy

(3) Characterize the effect of the sGC activator cinaciguat in pathological myocardial hypertrophy from morphological, functional and molecular points of view as well.

4. Materials and Methods

All animals received humane care in compliance with the "Principles of Laboratory Animal Care", formulated by the National Society for Medical Research and the Guide for the Care and Use of Laboratory Animals, prepared by the Institute of Laboratory Animal Resources and published by the National Institutes of Health (NIH Publication No. 85-23, Revised 1996). All procedures and handling of the animals during the studies were reviewed and approved by the Ethical Committee of Hungary for Animal Experimentation.

Young adult (body weight=200–250 g) male Wistar rats (n=58) (Toxi-Coop, Dunakeszi, Hungary) were housed in a room with constant temperature of 22±2°C with a 12h light-dark cycle, were fed a standard laboratory rat chow ad libitum and had free access to water.

4.1. Experimental protocols, treatment groups

4.1.1. Differences between physiological and pathological myocardial hypertrophy

4.1.1.1. Exercise training

To induce physiological hypertrophy, we used swimming to train our animals, utilizing a swimming apparatus designed specifically for rats. A suitable water tank 40 cm in depth was divided into 6 lanes with a surface area of approximately 20x25cm to prevent rats from reclining on the walls, and filled with tap water (30-32°C) to allow for individual training. Based on literature data (Evangelista *et al.*, 2003) and on results of preliminary pilot studies of our own, long-term (a total of 12 weeks) exercise training in the exercised (Ex; n=12) group consisted of 200 minutes/day of swimming 5 days a week, gradually built up in 15-minute blocks every other training session (Figure 8., A). Untrained sedentary (Sed; n=11) rats were placed into the water for 5 minutes every training day during the training program to control for the possibility of stress resulting from exposure to water.

4.1.1.2. Aortic banding procedure

After acclimation, pathological myocardial hypertrophy was induced by banding of the abdominal aorta (AAB, n=10) between the renal arteries and the superior mesenteric artery, or sham operation (n=8) was performed in pentobarbital sodium (60mg/kg i.p.)

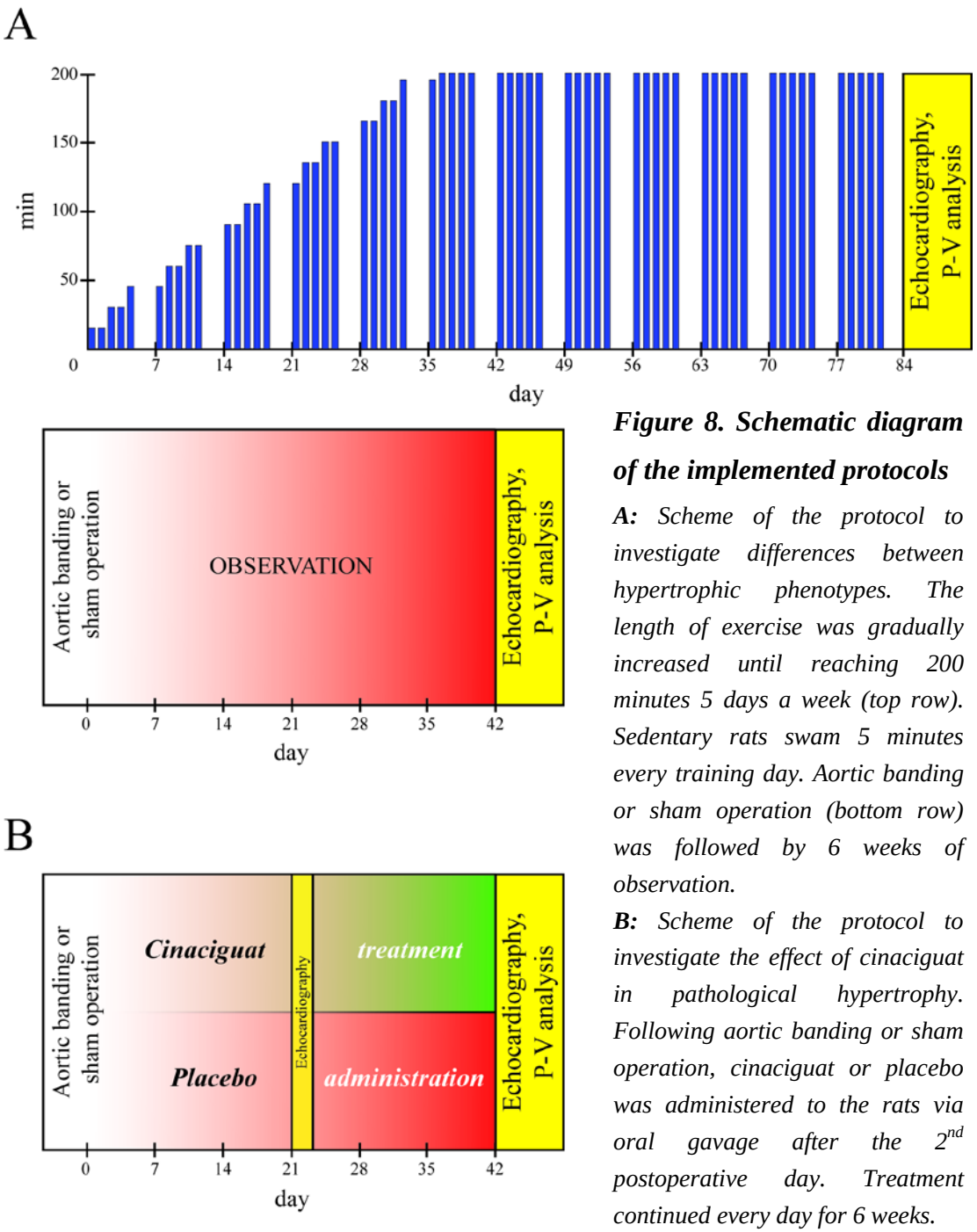

Figure 8. Schematic diagram of the implemented protocols

A: *Scheme of the protocol to investigate differences between hypertrophic phenotypes. The length of exercise was gradually increased until reaching 200 minutes 5 days a week (top row). Sedentary rats swam 5 minutes every training day. Aortic banding or sham operation (bottom row) was followed by 6 weeks of observation.*

B: *Scheme of the protocol to investigate the effect of cinaciguat in pathological hypertrophy. Following aortic banding or sham operation, cinaciguat or placebo was administered to the rats via oral gavage after the 2nd postoperative day. Treatment continued every day for 6 weeks.*

anesthesia. In order to achieve a standard degree of stenosis in our aortic banded animals, a blunted needle with an outer diameter of 20 Gauge (G, 0.9mm) was placed in parallel with the aorta, around which a 2-0 surgical suture was tightened in all cases. Then, the needle was removed, leaving a standard 20G stenosis behind. Sham operation comprised all steps excluding the banding procedure, which was replaced by a 1 min occlusion at the same level of the aorta. After recovering from anesthesia and on the

first and second postoperative day, all animals received meloxicam (1.5mg/kg p.o.) for postoperative analgesia. At the end of the 6 weeks of observation, all animals were subjected to functional measurements, as described below (Figure 8. A).

4.1.2. Effects of cinaciguat in pathological myocardial hypertrophy

The AAB procedure or sham operation was executed as described above.
5 days after the operation, sham and AAB animals were randomized into control or treatment groups [ShamCo, n=8; ShamCin, n=8; AABCo, n=10; AABCin, n=9, (Figure 8. B)]. Treated animals received cinaciguat (10mg/kg p.o.) suspended in 0.5% methylcellulose solution via oral gavage, while control rats were given only the vehicle every day for 6 weeks. The dosage was adjusted to body weight, which was measured three times a week during the whole study period.

4.2. Echocardiography

Echocardiographic measurements were performed at the end of the training program (Ex and Sed rats) and on the 3rd and 6th week (AAB and Sham animals). The rats were anesthetized with pentobarbital sodium (60mg/kg i.p.), and were placed on controlled heating pads. Core temperature of the animals, measured via rectal probe, was maintained at 37°C. After the anterior chest was shaved, transthoracic echocardiography was performed in the supine position by an investigator blinded to the experimental groups. Two-dimensional and M-mode echocardiographic images of long- and short-axis were recorded using a 13-MHz linear transducer (GE 12L-RS, GE Healthcare, Waukesha, WI, USA) connected to a commercially available echocardiographic imaging unit (Vivid i, GE Healthcare). Digital images were analyzed by an investigator in blinded fashion using an image analysis software (EchoPac, GE Healthcare). On two-dimensional recordings of the short-axis at the mid-papillary muscle level, left ventricular anterior wall thickness (AWT), posterior wall thickness (PWT) in diastole (index: d) and systole (index: s), and LV end-diastolic (LVEDD) and end-systolic (LVESD) diameters were measured. In addition, end-diastolic and end-systolic LV areas were planimetered from short- and long-axis two-dimensional recordings. End systole was defined as the time point of minimal LV dimensions, and end diastole as the time point of maximal dimensions. All values were averaged over three consecutive

cycles. The following parameters were derived from these measurements: FS was calculated as [(LVEDD-LVESD)/LVEDD]*100. End-diastolic and end-systolic (LVESV) LV volumes were estimated according to a validated geometrical model, the biplane ellipsoid model (van de Weijer *et al.*, 2012). Stroke volume (SV) was calculated as LVEDV-LVESV. EF was determined as (SV/LVEDV)*100. LV mass (LVM) was calculated according to a cubic formula, suggested by Devereux et al. (Devereux *et al.*, 1986): LV mass = ([(LVEDD+AWTd+PWTd)^3-LVEDD^3]*1.04)*0.8+0.14. To calculate LVM index (LVMi), we normalized the LVM values to the body weight of the animal.

4.3. Hemodynamic Measurements: LV Pressure-Volume (P-V) Analysis

Rats were anesthetized with pentobarbital sodium (60mg/kg i.p.), tracheotomized, intubated and ventilated with a tidal volume and frequency adjusted to body weight, using an Inspira Advanced Safety Ventilator (MA1 557058, Harvard Apparatus, Holliston, MA, USA). Animals were placed on controlled heating pads, and the core temperature, measured via rectal probe, was maintained at 37°C. A polyethylene catheter was inserted into the left external jugular vein for fluid administration. A 2-Fr micro tip pressure-conductance catheter (SPR-838, Millar Instruments, Houston, TX, USA) was inserted into the right carotid artery and advanced into the ascending aorta. After stabilization for 5 minutes, arterial blood pressure and heart rate (HR) were recorded. Then, the catheter was advanced into the LV under pressure control (Figure 9.). After stabilization for another 5 minutes, signals were continuously recorded at a sampling rate of 1,000 samples/s using a P-V conductance system (MPVS-Ultra, Millar Instruments) connected to the PowerLab 16/30 data acquisition system (AD Instruments, Colorado Springs, CO, USA), stored, and displayed on a personal computer by the LabChart7 Software System (AD Instruments). LV end-systolic pressure and volume (LVESP and LVESV), LV end-diastolic pressure and volume (LVEDP and LVEDV), the maximum rate of LV pressure increment (dP/dt_{max}), time constant of LV pressure decay (τ, according to the Glantz method), EF and stroke work (SW) were computed and calculated using a special P-V analysis program (PVAN, Millar Instruments). SV and cardiac output (CO) were calculated and corrected according to *in vitro* and *in vivo* volume calibrations using the PVAN software. In

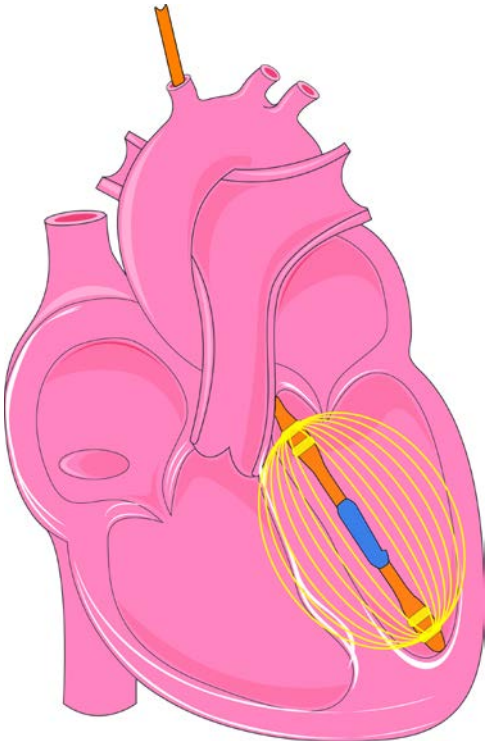

Figure 9. Schematic figure on the principle of operation and localization of the pressure-conductance micro tip catheter within the rat heart

The catheter must be in the axis of the ventricle in order to accurately measure LV pressures and volumes. The pressure sensor (blue) continuously measures pressure changes in the LV utilizing a piezoresistive semiconductor. Volume is measured using 4 electrodes (gold); the electric field generated by the outer electrode pair is attenuated depending on the size of the current blood volume (i.e., contraction and relaxation during the cardiac cycle) within the LV. This fluctuation in the electric field and the resulting voltage potentials are measured by the inner – sensing – pair of electrodes. Since this method measures LV volumes indirectly, blood conductance calibration has to be performed in order to convert the measured relative volume units into standard units of volume.

addition to the above parameters, P-V loops recorded at different preloads can be used to derive other useful indices of systolic function that are less influenced by loading conditions and cardiac mass (Oláh *et al.*, 2015). Therefore, LV P-V relations were measured during transiently decreasing preload, which was achieved by the compression of the inferior vena cava proximal to the diaphragm with a cotton-tipped applicator. The slope [end-systolic elastance (E_{es})] of the LV end-systolic P-V relationship [ESPVR, Figure 10.; according to the parabolic curvilinear model (Kass *et al.*, 1989)], preload recruitable SW (PRSW), and the slope of the dP/dt_{max}-end-diastolic volume relationship (dP/dt_{max}-EDV) were calculated as load-independent indices of LV

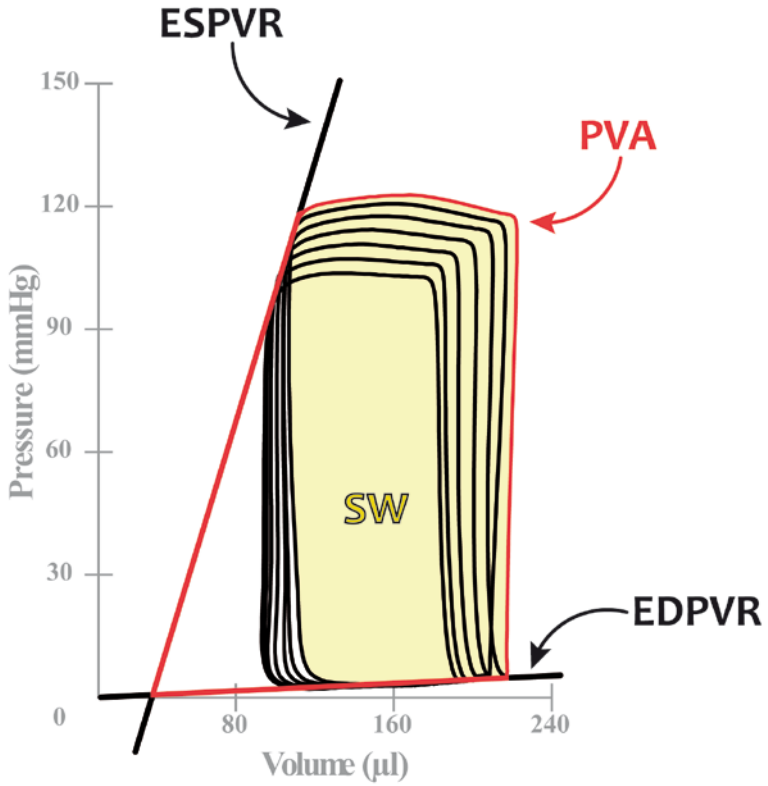

Figure 10. Representative P-V recording during the inferior vena cava occlusion maneuver, and the parameters directly derivable from the acquired loops

Occlusion of the inferior vena cava results in the left- and downward shift of the P-V loops. End-systolic pressure-volume relationship (ESPVR) and end-diastolic pressure-volume relationship (EDPVR) are the lines defined by the end-systolic and end-diastolic points, respectively. Stroke work (SW, yellow fill) can be calculated as the area enclosed by the baseline P-V loop, while pressure-volume area (PVA, marked with red) is bound by the systolic half of the baseline P-V loop and the appropriate segments of ESPVR and EDPVR.

contractility. LV compliance was investigated by calculating the slope of end-diastolic pressure-volume relationship (EDPVR, Figure 10.). Pressure-volume area (PVA) was also calculated utilizing the lines of ESPVR, EDPVR, and the systolic segment of the steady state P-V loop (Figure 10.). At the end of each experiment, 100 µl of hypertonic saline was injected intravenously to calculate parallel conductance volume from the shift of P-V relations. Parallel conductance was calculated by the PVAN software and used to correct for the cardiac mass volume. The volume calibration of the conductance system was performed using a block with nine, 1 cm deep cylindrical holes, which had known diameters (and thus known volume) ranging from 2 to 11 mm. Each hole was

filled with fresh heparinized whole rat blood. In this calibration, the linear volume-conductance regression of the absolute volume in each cylinder versus the raw signal acquired by the conductance catheter was used as the volume calibration formula. After completion of the hemodynamic measurements all animals were euthanized by exsanguination.

4.4. Measurement of organ weights and tibia length

After euthanasia, the heart, the lung and the liver of the animals were immediately placed into ice-cold saline and wet weight of the organs was measured on a scale. This was followed by the sampling of the organs, as described below. To exclude the natural variability between the bodyweight of the animals, the right tibia of every rat was also prepared and its length measured (Yin *et al.*, 1982).

4.5. Histology and immunohistochemistry

Heart samples were placed in 4% buffered paraformaldehyde solution. Transverse transmural slices of the ventricles were sectioned (5 µm) and conventionally processed for histological examination. Heart sections were stained with hematoxylin and eosin (H&E) and Picrosirius red. Light microscopic examination was performed with a Zeiss microscope (Axio Observer.Z1, Carl Zeiss, Jena, Germany), and digital images were captured using an imaging software (QCapture Pro 6.0, QImaging, Surrey, BC, Canada).

4.5.1. Cardiomyocyte diameter measurement

The transverse transnuclear widths of randomly selected, longitudinally oriented cardiomyocytes were measured on H&E-stained sections by a single investigator after calibration of the system. The mean value of 100 LV cardiomyocytes represents each sample.

4.5.2. Assessment of LV collagen content

The amount of myocardial collagen was determined by measuring the area fraction of the Picrosirius red-stained areas of heart sections with ImageJ software. The mean value

of five randomly selected visual fields (magnification, 200x) of free LV wall represents each sample.

4.5.3. cGMP immunostaining

5µm thick sections of formalin-fixed, paraffin-embedded heart samples were deparaffinized with xylene, and rehydrated through descending concentrations of ethanol. After blocking unspecific binding sites with 5% goat serum for 30 minutes at room temperature, immunohistochemical staining for cGMP was performed using the avidin-biotin method. An anti-cGMP rabbit monoclonal primary antibody (dilution: 1:2000, Abcam, Cambridge, UK) was applied for 60 minutes at room temperature. A biotinylated secondary anti-rabbit antibody (BioGenex, Fremont, CA, USA) was applied for 20 minutes, after which the slides were exposed to streptavidin-conjugated alkaline phosphatase (BioGenex). Between each step, all slides were subjected to two 5-minute rinses with Tris-buffered saline. The DAKO® Fast Red Substrate System (Dako, Santa Clara, CA, USA) was used for antigen visualization. Color development was stopped by addition of distilled water, which was followed by counterstaining with hematoxylin. Negative control staining comprised all steps save the primary antibody. Immunohistochemical reactivity was examined with light microscopy at a magnification of 400x. Semi-quantitative scoring (scores 0–4; 0: no staining, 1: weak, 2: mild, 3: strong, 4: very strong staining) was performed by two people blinded to the groups.

4.5.4. Terminal deoxynucleotidyl transferase dUTP nick end labeling (TUNEL) assay

Paraffin embedded, 5µm thick heart tissue sections were used to detect DNA strand breaks in LV myocardium. TUNEL assay was performed using a commercially available kit (DeadEnd™ Colorimetric TUNEL System, Promega, Mannheim, Germany) according to the manufacturer's protocol. Briefly, fragmented DNA of apoptotic cells were end-labeled using a modified TUNEL assay. Biotinylated nucleotides were incorporated at the 3´-OH DNA ends using a recombinant terminal deoxynucleotidyl transferase (rTDT) enzyme. Horseradish peroxidase-labeled streptavidin (Streptavidin HRP) was then bound to these biotinylated nucleotides, which were detected using the peroxidase substrate, hydrogen peroxide, and the stable

chromogen, diaminobenzidine (DAB). TUNEL positive cell nuclei were counted by two blinded observers in 10 fields of each section at 200x magnification. Data were normalized to the mean value of the ShamCo group and were used to perform statistical analysis.

4.6. Biochemical Measurements

After hemodynamic measurements were completed, blood samples from the inferior vena cava were collected in tubes rinsed with ethylenediamine-tetraacetic acid (EDTA). The blood samples were centrifuged at 3,000 RPM for 15 min at 4°C, and then separated plasma was stored in aliquots at -80°C. Plasma level of cGMP was determined using an enzyme immunoassay (EIA) kit as per manufacturer's protocol (Amersham cGMP EIA Biotrak System, GE Healthcare, Little Chalfont, Buckinghamshire, UK).

4.7. Cardiac mRNA Analysis

LV myocardial tissue samples were snap frozen in liquid nitrogen, and stored at -80°C. LV tissue was homogenized in RLT buffer, and RNA was isolated from the ventricular samples using the RNeasy Fibrous Tissue Mini Kit (Qiagen, Hilden, Germany) according to the manufacturer's instructions and quantified by measuring optical density at 260nm. RNA purity was ensured by obtaining a 260/280nm optical density ratio of >2.0. Reverse transcription reaction (1μg total RNA of each sample) was completed using the QuantiTect Reverse Transcription Kit (Qiagen). Quantitative real-time PCR was performed with the StepOne-Plus Real-Time PCR System (Applied Biosystems, Foster City, CA, USA) in triplicates of each sample in a volume of 10μl in each well containing cDNA (1μl), TaqMan Universal PCR MasterMix (5μl), and a TaqMan Gene Expression Assay for the following targets (0.5μl, Table 1.): MHCα, MHCβ, NOS3, ANP, B cell lymphoma 2 (Bcl-2), 70kDa heat shock protein (HSP70), SERCA2a and Pln, endogenous antioxidants, such as catalase, superoxide dismutase-2

(SOD-2), and thioredoxin-1 (Trx1); inflammatory markers, such as interleukin-1β (IL-1β), tumor necrosis factor α (TNFα), and transforming growth factor β (TGFβ); and markers related to mitochondrial function, such as peroxisome proliferator activated

Table 1. TaqMan® Gene Expression Assays used for qRT-PCR

Target gene	*Abbreviation*	*Assay ID*
B-cell CLL/lymphoma 2	Bcl-2	Rn99999125_m1
catalase	Cat	Rn00560930_m1
cytochrome-c	CytC	Rn00470541_g1
endothelial nitric oxide synthase	NOS3	Rn02132634_s1
estrogen-related receptor α	ERRα	Rn00433142_m1
glyceraldehyde-3-phosphate dehydrogenase	GAPDH	Rn01775763_g1
heat shock 70kD protein 1A	HSP70	Rn04224718_u1
interleukine-1β	IL-1β	Rn00580432_m1
myosin heavy chain α	MHCα	Rn00568304_m1
myosin heavy chain β	MHCβ	Rn00568328_m1
natriuretic peptide A	ANP	Rn00561661_m1
nuclear respiratory factor 1	Nrf1	Rn01455958_m1
peroxisome proliferator-activated receptor γ coactivator-1α	PGC1α	Rn00580241_m1
peroxisome proliferator-activated receptor α	PPARα	Rn00566193_m1
phospholamban	Pln	Rn01434045_m1
sarcoplasmic and endoplasmic reticulum Ca^{2+}-ATPase isoform 2a	SERCA2a	Rn00568762_m1
superoxide dismutase-2	SOD-2	Rn00690587_g1
thioredoxin-1	Trx1	Rn00587437_m1
transforming growth factor β	TGFβ	Rn00572010_m1
tumor necrosis factor α	TNFα	Rn99999017_m1

receptor γ coactivator 1α (PGC1α), nuclear respiratory factor 1 (Nrf1), estrogen-related receptor α (ERRα), peroxisome proliferator-activated receptor α (PPAR α), and cytochrome c (CytC), all purchased from Applied Biosystems. Gene expression data were normalized to glyceraldehyde-3-phosphate dehydrogenase (GAPDH; reference gene), and expression levels were calculated using the CT comparative method ($2^{-\Delta CT}$). All results are expressed as values normalized to a positive calibrator, which was a pool of cDNAs from all samples of the Sed and Sham, as well as the ShamCo group in the respective experiments.

4.8. Immunoblot analysis

LV tissue samples were homogenized in radio-immunoprecipitation assay lysis buffer (RIPA; 50mM Tris HCl at pH 8.0, 150mM NaCl, 1% NP-40, 0.5% sodium deoxycholate, 0.1% sodium dodecyl sulphate [SDS]) containing Complete Protease Inhibitor Cocktail (Roche, Mannheim, Germany). Protein concentration was determined using the Pierce® BCA Protein Assay Kit (Thermo Scientific, Rockford, IL, USA). Samples were mixed with 2× Laemmli buffer and boiled at 95ºC for 5 min. Equal amounts of protein (30 µg) were loaded and separated on commercially available, precast 4–12% SDS-PAGE gels (NuPAGE® Novex® Bis-Tris Mini Gel, Invitrogen, Carlsbad, CA, USA). Afterwards, proteins were transferred to nitrocellulose membranes by using a semi-dry electroblotting system (iBlot™ Gel Transfer Device, Invitrogen). Membranes were blocked in 5% non-fat milk in Tris-buffered saline containing 0.1% Tween-20 (TTBS) for 1 h. After blocking, membranes were incubated overnight at 4ºC with primary antibodies (diluted in 1% bovine serum albumin in TTBS, all purchased from Cell Signaling, Danvers, MA, USA, unless noted otherwise) against various target proteins as follows (Table 2): the main effector of NO signaling, PKG (Enzo Life Sciences, Plymouth Meeting, PA, USA), and its targets such as vasodilator-stimulated phosphoprotein (VASP) and Pln, as well as phospho-VASP (p-VASP) and phospho-Pln (p-Pln). After washing, membranes were incubated in horseradish peroxidase (HRP) – conjugated secondary antibody dilutions at room temperature for 1 h (anti-rabbit IgG or anti-mouse IgG as appropriate, 1:2000). Immunoblots were developed using Pierce® ECL Western Blotting Substrate Kit (Thermo Scientific). Protein band densities were quantified using the GeneTools software (Syngene, Frederick, MD, USA). GAPDH

Table 2. Antibodies used for immunoblot analysis

Target protein	*Abbreviation*	*Primary antibody (Manufacturer)*	*Dilution*	*Target molecular mass*
glyceraldehyde-3-phosphate dehydrogenase	GAPDH	MAB374 (Millipore, Billerica, MA, USA)	1:10000	38 kDa
phospholamban	Pln	8495 (Cell Signaling, Danvers, MA, USA)	1:5000	24 kDa
phospho-Pln	p-Pln	8496 (Cell Signaling)	1:5000	24 kDa
phospho-VASP	p-VASP	3114 (Cell Signaling)	1:500	50 kDa
protein kinase G	PKG	ADI-KAP-PK005-F (Enzo Life Sciences, Plymouth Meeting, PA, USA)	1:1000	75 kDa
vasodilator-stimulated phosphoprotein	VASP	3112 (Cell Signaling)	1:1000	50 kDa

The table shows the primary antibodies used against various protein targets and reference protein glyceraldehyde-3-phosphate dehydrogenase in Western blot experiments.

(primary antibody purchased from Millipore, Billerica, MA, USA) was used to assess equal protein loading. Values of protein band densities (after adjusting to GAPDH band densities) were normalized to the average value of the ShamCo group and were used to perform statistical analysis. Representative original immunoblots are shown in Figure 20.

4.9. Drugs

All drugs listed were purchased from Sigma-Aldrich (St. Louis, MO, USA) except for cinaciguat, which is a kind gift of Bayer AG (Leverkusen, Germany).

4.10. Statistical Analysis

Statistical analysis was performed on a personal computer with commercially available software (GraphPad Prism 7, La Jolla, CA, USA). All data are expressed as mean ± standard error of the mean. After testing normal distribution of the data using the Shapiro-Wilk test, Student's *t*-testing or two-factorial analysis of variance (ANOVA,

with ’aortic banding’ and ’cinaciguat treatment’ as factors) was carried out as appropriate. The two-factorial ANOVA was used to detect independent effects of the factors (p_{band}, p_{treat}) and significant banding×treatment interactions (p_{int}). Tukey’s *post hoc* testing was performed to evaluate differences between the groups. Data that did not show normal distribution were transformed logarithmically before performing two-factorial ANOVA in order to reach normal distribution. A paired Student’s *t*-test was performed for comparing data of the echocardiographic measurements at 2 time points within a group. Furthermore, to test for the effect of the different hypertrophic stimuli in the models used (p_{diff}), a two-tailed Student’s *t*-test was performed using Ex and AAB values that were normalized to their respective controls. Differences were considered statistically significant when $p<0.05$.

5. Results

5.1. Differences between physiological and pathological myocardial hypertrophy

5.1.1. Morphological assessment

Heart weight in both Ex and AAB animals increased significantly compared with their respective controls (Table 3.). Normalization to tibia length revealed that although the difference in body weight might mask the difference in relative heart weight between the models, the increase in heart weight was more pronounced in the AAB group than in Ex animals (Table 3.).

Table 3. Exercise and pathological stimuli result in similar degree of hypertrophy

	Sed	***Ex***	***Sham***	***AAB***	p_{diff}
HW (g)	1.32±0.03	1.46±0.03*	1.29±0.03	1.61±0.06$^{\#}$	**0.011**
BW (g)	469±10	402±10*	421±14	435±16	**<0.001**
HW/BW (mg/g)	2.85±0.06	3.64±0.10*	3.07±0.10	3.69±0.10$^{\#}$	0.112
HW/TL (mg/mm)	30.0±0.8	33.5±1.0*	29.3±0.7	37.3±1.2$^{\#}$	**0.017**

AAB: abdominal aortic banding; Ex: exercised; Sed: sedentary; Sham: sham operated; HW: heart weight; /BW: normalization to body weight; /TL: normalization to tibia length; p_{diff}: p value of the difference between the models
*: $p<0.05$ vs. Sed; #: $p<0.05$ vs. Sham

5.1.2. Echocardiographic parameters

Heart rate was comparable among the groups. Anterior and posterior wall thickness was increased in both hypertrophy models both in systole and diastole (Table 4.). Estimated LVM and LVMi was also increased in Ex and AAB rats compared with their respective controls. Diastolic LV chamber size was similar in the two models, while end-systolic diameter significantly decreased in the Ex group, resulting in significantly increased EF and FS in these animals (Table 4.). A differential effect of the hypertrophic stimulus on phenotypic changes was observed in LVESD, LVM, FS and EF (Table 4.).

Table 4. Exercise and pathological stimuli result in similar degree of hypertrophy – echocardiographic measurements

	Sed	***Ex***	***Sham***	***AAB***	p_{diff}
HR (beats/min)	357±15	351±10	378±24	382±11	0.500
LVEDD (mm)	6.85±0.05	6.89±0.03	6.79±0.08	6.95±0.08	0.532
LVESD (mm)	4.06±0.08	3.45±0.09*	3.99±0.17	4.22±0.11	**<0.0001**
AWTd (mm)	1.96±0.02	2.17±0.02*	1.95±0.02	2.19±0.03#	0.452
AWTs (mm)	3.02±0.05	3.37±0.06*	2.94±0.10	3.32±0.07#	0.731
PWTd (mm)	1.82±0.03	1.93±0.02*	1.78±0.01	2.06±0.04#	**0.002**
PWTs (mm)	2.91±0.04	3.09±0.04*	2.84±0.06	3.09±0.04#	0.356
LVM (mg)	872±14	976±11*	849±17	1031±23#	**0.012**
LVMi (mg/mm)	20.2±0.4	24.6±0.3*	20.2±0.3	26.0±0.7#	0.264
FS (%)	41.4±0.7	50.0±1.1*	41.3±2.3	40.5±1.3	**<0.0001**
EF (%)	65.5±1.3	73.0±1.3*	65.1±1.5	62.4±1.3	**<0.0001**

AAB: abdominal aortic banding; Ex: exercised; Sed: sedentary; Sham: sham operated; HR: heart rate; LVEDD: LV end-diastolic diameter; LVESD: LV end-systolic diameter; AWTd/s: anterior wall thickness in diastole/systole; PWTd/s: posterior wall thickness in diastole/systole; LVM: left ventricular mass; LVMi: LVM index (LVM normalized to tibia length); FS: fractional shortening; EF: ejection fraction; p_{diff}: p value of the difference between the models
*: $p<0.05$ vs. Sed; #: $p<0.05$ vs. Sham

5.1.3. Pressure-volume analysis

The baseline hemodynamic characteristics of physiological and pathological hypertrophy are summarized in Table 5. Ex rats displayed decreased LVESV compared with the sedentary animals, which accompanied by unchanged HR and LVEDV, resulted in increased SV, EF, CO and SW (Table 5.). LV pressures, dP/dt_{max} and dP/dt_{min} were unaltered, while E_a decreased in our exercised rats. In contrast, LV volumes and thus SV,

Table 5. Hemodynamic characteristics of physiological and pathological myocardial hypertrophy

	Sed	***Ex***	***Sham***	***AAB***	p_{diff}
HR (beats/min)	412±9	400±8	429±15	434±11	0.378
MAP (mmHg)	145.3±2.8	142.1±5.2	142.0±2.0	182.3±7.9$^{\#}$	**0.001**
LVEDP (mmHg)	3.0±0.2	3.7±0.4	3.9±0.7	4.4±0.4	0.131
LVESP (mmHg)	154.8±3.4	152.2±8.2	150.8±2.0	213.4±6.8$^{\#}$	**<0.0001**
dP/dt_{max} (mmHg/s)	9237±397	9847±659	9103±424	12185±399$^{\#}$	**0.012**
dP/dt_{min} (mmHg/s)	-12191±443	-12213±670	-12390±261	-12506±676	0.780
τ (ms)	12.1±0.3	11.2±0.3*	11.7±0.6	16.6±1.3$^{\#}$	**0.001**
EDPVR (mmHg/μl)	0.036±0.003	0.042±0.003	0.034±0.004	0.042±0.006	0.680
LVEDV (μl)	234±5	239±6	240±7	262±9	0.239
LVESV (μl)	112±2	99±2*	106±5	114±5	**0.002**
SV (μl)	123±6	141±5*	134±7	147±6	0.247
EF (%)	52±1	58±1*	56±2	56±1	**0.001**
CO (ml/min)	50.6±2.0	56.2±1.5*	58.5±3.9	63.7±2.8	0.263
*SW (mmHg*ml)*	14.7±0.8	18.0±0.8*	15.6±1.2	22.7±1.2$^{\#}$	**0.046**
*PVA (mmHg*ml)*	25.6±1.6	25.4±1.8	26.8±1.6	37.3±3.9$^{\#}$	**0.017**
E_a (mmHg/μl)	1.33±0.05	1.09±0.08*	1.07±0.05	1.48±0.07$^{\#}$	**<0.0001**
Eff (%)	58±3	71±3*	58±3	63±4	0.173
VAC	0.53±0.03	0.32±0.03*	0.42±0.02	0.37±0.03	**0.006**

AAB: abdominal aortic banding; Ex: exercised; Sed: sedentary; Sham: sham operated; HR: heart rate; MAP: mean arterial pressure; LVEDP: LV end-diastolic pressure; LVESP: LV end-systolic pressure; dP/dt_{max}: maximal increment of pressure change; dP/dt_{min}: maximal decrement of pressure change; τ: time constant of active LV relaxation; LVEDV: LV end-diastolic volume; LVESV: LV end-systolic volume; SV: stroke volume; EF: ejection fraction; CO: cardiac output; CI: cardiac index (CO normalized to body weight); SW: stroke work; PVA: pressure-volume area; E_a: arterial elastance; Eff: mechanical efficiency; VAC: ventriculo-arterial coupling; p_{diff}: p value of the difference between the models

*: $p<0.05$ vs. Sed; #: $p<0.05$ vs. Sham

EF and CO did not change significantly in the AAB animals compared with Sham rats. In this model, however, LVESP and, consequently, MAP significantly increased in the AAB group, leading to increased values of dP/dt_{max}, SW and E_a (Table 5.).

Representative PV loops and vena cava occlusions from all groups are shown in Figure 11. Load-independent indices of systolic cardiac function calculated from occlusions (E_{es}, PRSW and dP/dt_{max}-EDV) all showed increased contractility in both hypertrophy models (Figure 11.). With respect to diastolic function, τ was significantly decreased in the Ex group compared with Sed animals, while it was significantly increased in the AAB rats compared with the Sham group (Table 5.).

Cardiac mechanoenergetics were also differentially influenced by the two types of hypertrophic stimuli. SW was elevated in both physiological and pathological hypertrophies, although it was increased significantly more following AAB than exercise (Table 5.). Furthermore, mechanical efficiency (Eff) was significantly better following exercise, while remained unchanged after AAB (Table 5.). Compared with their respective controls, ventriculo-arterial coupling (VAC) was also improved in the Ex group, while it was mitigated in the AAB animals (Table 5.).

5.1.4. Histology

Cardiac hypertrophy was observed on the microscopic level as well (Figure 12. A, C): average cardiomyocyte diameter was increased in both hypertrophy models. In contrast, while myocardial collagen content did not increase in physiological hypertrophy, pathological hypertrophy was characterized by a significant increase of subendocardial collagen deposition (Figure 12. B, C).

5.1.5. Cardiac mRNA analysis

Physical exercise did not result in significant changes regarding cardiac gene expression (Figures 13. and 14.). In contrast, mRNA expression of genes involved in reactivation of the fetal gene program, such as ANP, MHCα and MHCβ (Figure 13. A), or expression of effectors important in mitochondrial function, such as CytC, Nrf1 and PGC1α (Figure 14.) was altered following pressure overload of the LV. Investigated markers of antioxidant defense and inflammatory processes were found to be unchanged in both physiological and pathological hypertrophies (Figure 13. B, C).

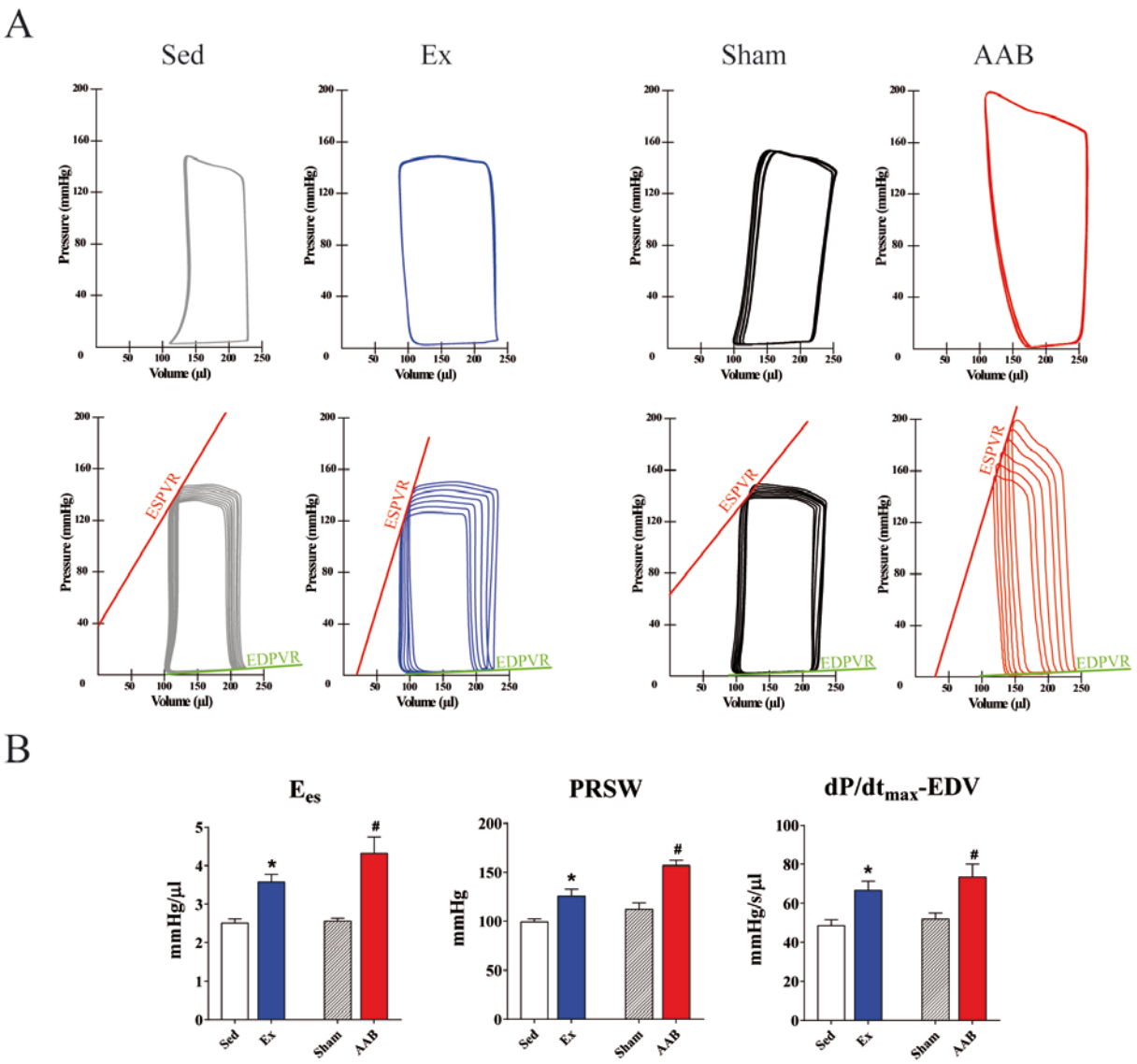

Figure 11. Both physiological and pathological hypertrophies are associated with increased contractility

A: *representative PV-loops recorded during baseline (top row) and occlusion of the inferior vena cava (bottom row). The difference between the slope of ESPVR among the groups clearly demonstrates increased contractility both in Ex and AAB groups.*

B: *contractility parameters calculated from the PV-loops acquired during occlusion of the vena cava. All three parameters indicate similarly increased contractility in the hypertrophy models.*

E_{es}: end-systolic elastance; ESPVR: end-systolic pressure-volume relationship; PRSW: preload recruitable stroke work; dP/dt_{max}-EDV: maximal dP/dt – end-diastolic volume relationship.

**: p<0.05 vs. Sed; #: p<0.05 vs. Sham*

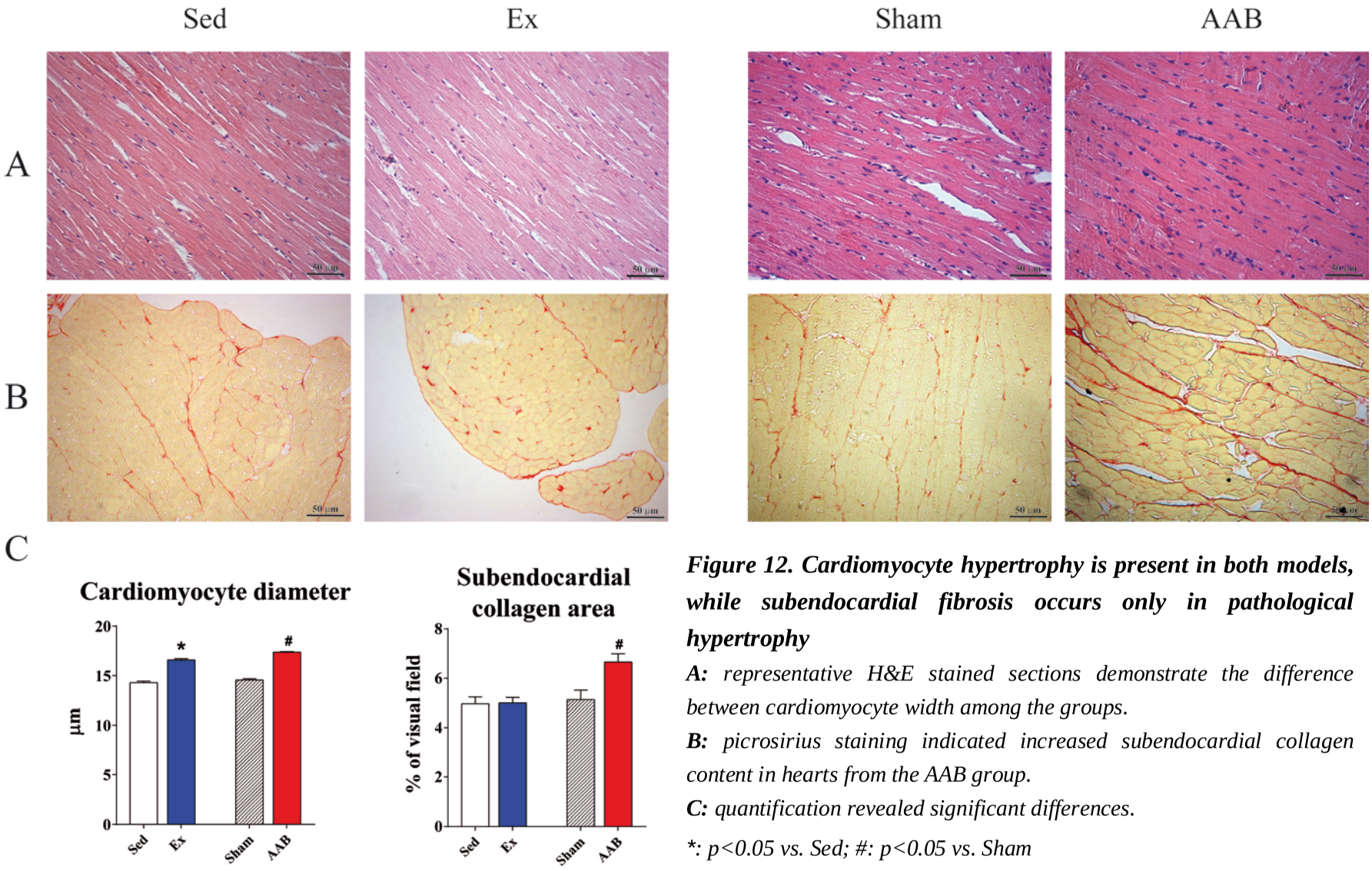

Figure 12. Cardiomyocyte hypertrophy is present in both models, while subendocardial fibrosis occurs only in pathological hypertrophy

A: *representative H&E stained sections demonstrate the difference between cardiomyocyte width among the groups.*

B: *picrosirius staining indicated increased subendocardial collagen content in hearts from the AAB group.*

C: *quantification revealed significant differences.*

**: p<0.05 vs. Sed; #: p<0.05 vs. Sham*

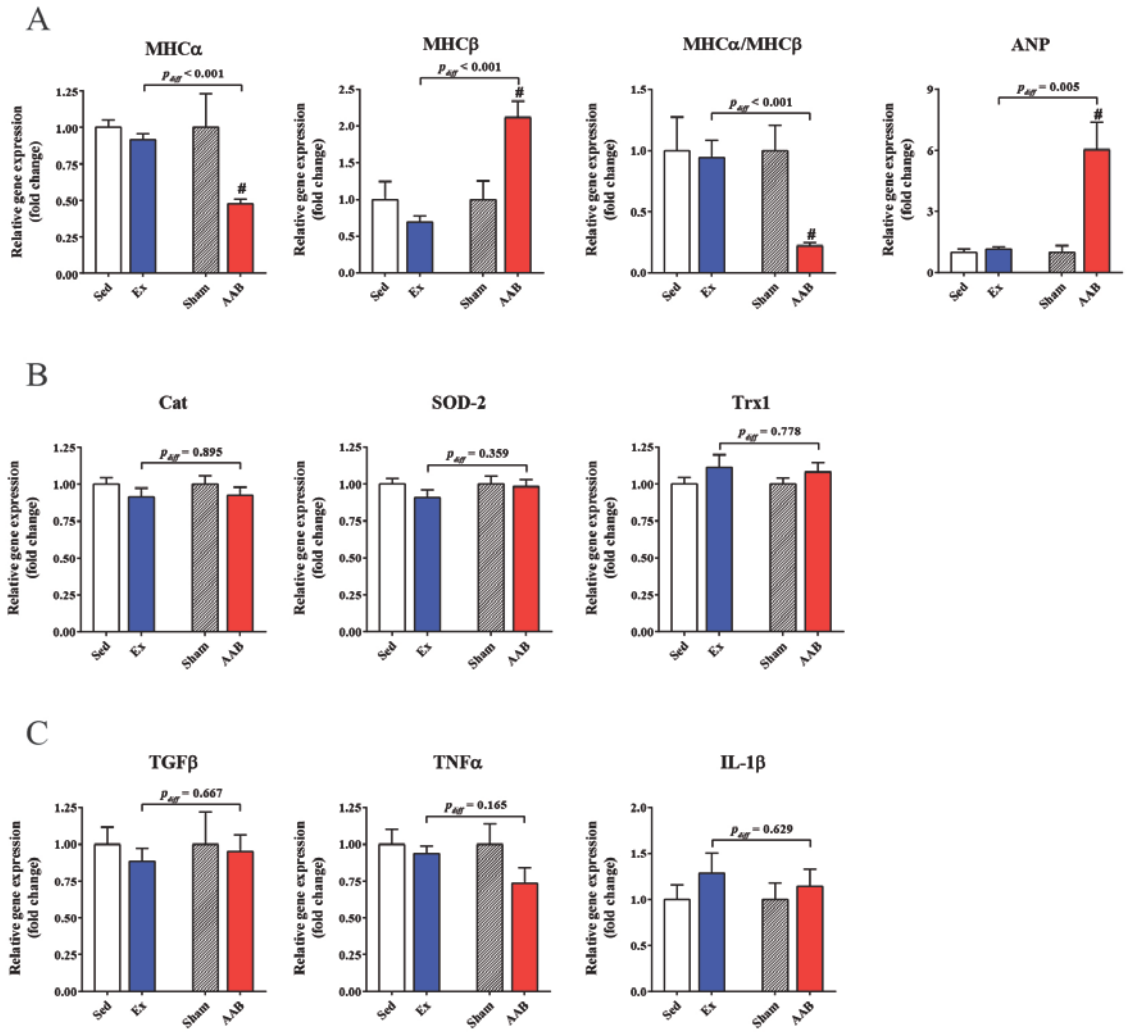

Figure 13. Elements of the fetal gene program are reactivated in pathological, but not in physiological hypertrophy, while expression of antioxidants and inflammatory markers are left unchanged in both hypertrophy models

*A characteristic alteration under pathologic conditions is the reactivation of the fetal gene program, a prominent marker of which is the myosin heavy chain isoform switch (**A**). A significant increase in LV wall stretch in the AAB group was confirmed by the elevation of ANP expression (**A**). No significant alterations were observed in antioxidant (**B**) or inflammatory (**C**) markers among the groups. Neither of these changes was present in physiological hypertrophy (**A-C**).*

ANP: atrial natriuretic peptide; Cat: catalase; IL-1β: interleukin 1β; MHCα/β: myosin heavy chain α/β; SOD-2: superoxide dismutase 2; TGFβ: transforming growth factor β; TNFα: tumor necrosis factor α; Trx1: thioredoxin 1.

**: p<0.05 vs. Sed; #: p<0.05 vs. Sham*

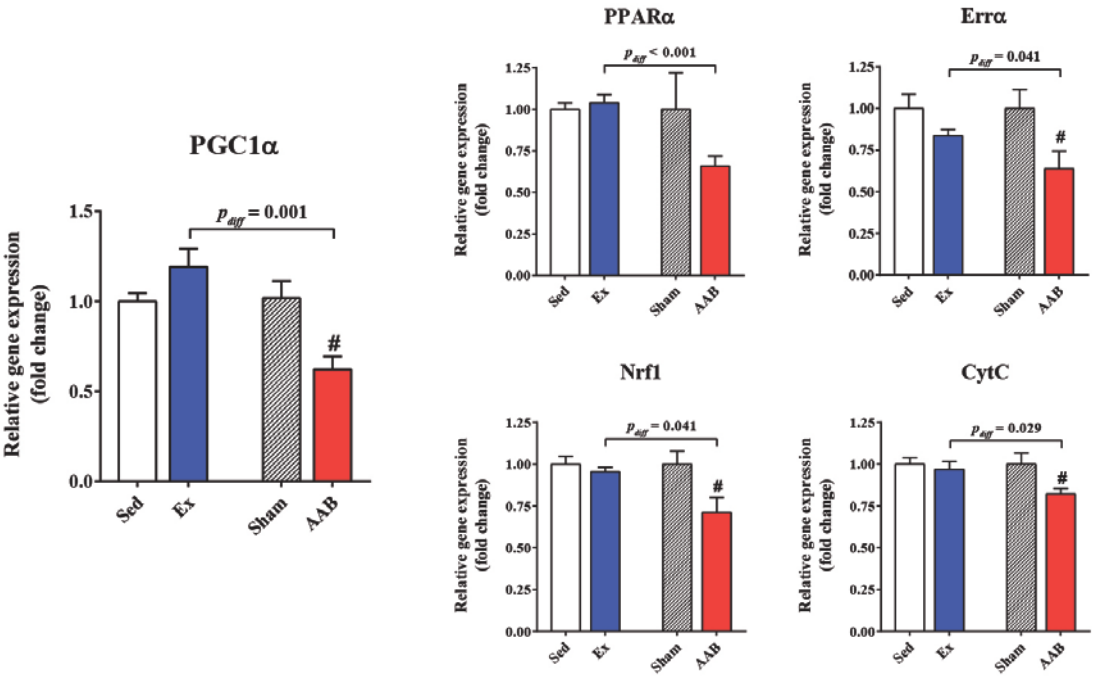

Figure 14. Myocardial mRNA expression of markers involved in metabolic processes are changed in pathological, but not in physiological hypertrophy

Several markers of mitochondrial function were found to be significantly less expressed in myocardial samples of the AAB group than that of the Sham animals, suggesting a pathological shift of energy source from fatty acids to glucose in the AAB group. Neither of these changes was present in physiological hypertrophy.

CytC: cytochrome C; Errα: estrogen-related receptor α; Nrf1: nuclear respiratory factor 1; PGC1α: peroxisome proliferator activated receptor γ coactivator 1α; PPARα: peroxisome proliferator activated receptor α.

**: p<0.05 vs. Sed; #: p<0.05 vs. Sham*

5.2. Effects of cinaciguat in pathological myocardial hypertrophy

5.2.1. Morphological assessment

There was no significant difference among the groups in body weight (Table 6.). Heart weight normalized to tibia length (HW/TL) was significantly higher in the AABCo rats than in the ShamCo or ShamCin animals (Table 6.). HW/TL was significantly reduced in the AABCin animals compared with the AABCo rats. Relative lung weight (LuW/TL) was significantly increased in the AABCo group compared with ShamCo. This parameter did not differ from ShamCo in the AABCin animals (Table 6.).

5.2.2. Echocardiographic parameters

The echocardiographic measurement performed on the 3rd postoperative week verified significantly elevated LV wall thickness values, RWT and estimated LVM in the AABCo group compared with ShamCo without significant changes in chamber dimensions (Figure 15. A). LVH increased over the second half of the treatment period in the AABCo animals (Figures 15. and 16.), which was accompanied by significantly elevated LVESD compared with ShamCo. Treatment with cinaciguat in aortic banded rats resulted in significantly decreased LV diastolic wall thicknesses, LVM and LVM index (LVMi) compared with AABCo at both time points (Figure 15. A). Systolic posterior wall thickness at the 6th week of the treatment was also significantly decreased in the AABCin animals compared with the AABCo group, while EF and FS remained unchanged during the whole study (Figure 15. B).

5.2.3. Invasive hemodynamic measurements and P-V analysis

Basic hemodynamic parameters, such as HR, EF, SV, CO, or LVESV, and also parameters of preload, such as LVEDV and LVEDP were not significantly different among the groups (Table 7.).

LVESP and mean arterial pressure (MAP) proximal to the site of stenosis were significantly higher in both AAB groups than in the Sham groups, and neither of these parameters was affected by Cinaciguat (Table 7.). dP/dt_{max} was significantly higher in AABCo animals than in ShamCo rats (Table 7.).

Table 6. Cinaciguat reverses the excess in myocardial hypertrophy in response to pressure overload

	ShamCo	***ShamCin***	***AABCo***	***AABCin***	p_{band}	p_{treat}	p_{int}
BW (g)	421±39	416±32	435±49	404±51	0.939	0.258	0.392
HW (g)	1.29±0.03	1.21±0.03	1.65±0.07*	1.47±0.05*	**<0.0001**	**0.019**	0.346
LuW (g)	1.72±0.05	1.70±0.06	1.88±0.03	1.81±0.09	**0.029**	0.493	0.708
LiW (g)	12.72±0.70	13.39±0.61	13.38±0.48	12.06±0.74	0.832	0.878	**0.011**
HW/BW (mg/g)	3.07±0.10	2.91±0.08	3.81±0.16*	3.66±0.12*	**<0.0001**	0.207	0.941
HW/TL (mg/mm)	29.3±0.8	28.1±0.9	38.4±1.5*	33.5±0.7*#	**<0.0001**	**0.008**	0.094
LuW/TL (mg/mm)	39.2±1.1	39.5±1.3	43.9±0.9*	41.9±1.8	**0.007**	0.733	0.278
LiW/TL (mg/mm)	289.5±14.3	312.0±15.7	311.7±9.2	278.7±15.6#	0.627	0.645	**0.002**

AAB: abdominal aortic banding; Sham: sham operated; /Co: placebo treated; /Cin: cinaciguat treated; BW: body weight; HW: heart weight; LuW: lung weight; LiW: liver weight; /BW: normalization to body weight; /TL: normalization to tibia length; p_{band}: *p* value of 'aortic banding' main effect; p_{treat}: *p* value of 'Cinaciguat treatment' main effect; p_{int}: interaction *p* value
*: $p<0.05$ vs. ShamCo; #: $p<0.05$ vs. AABCo

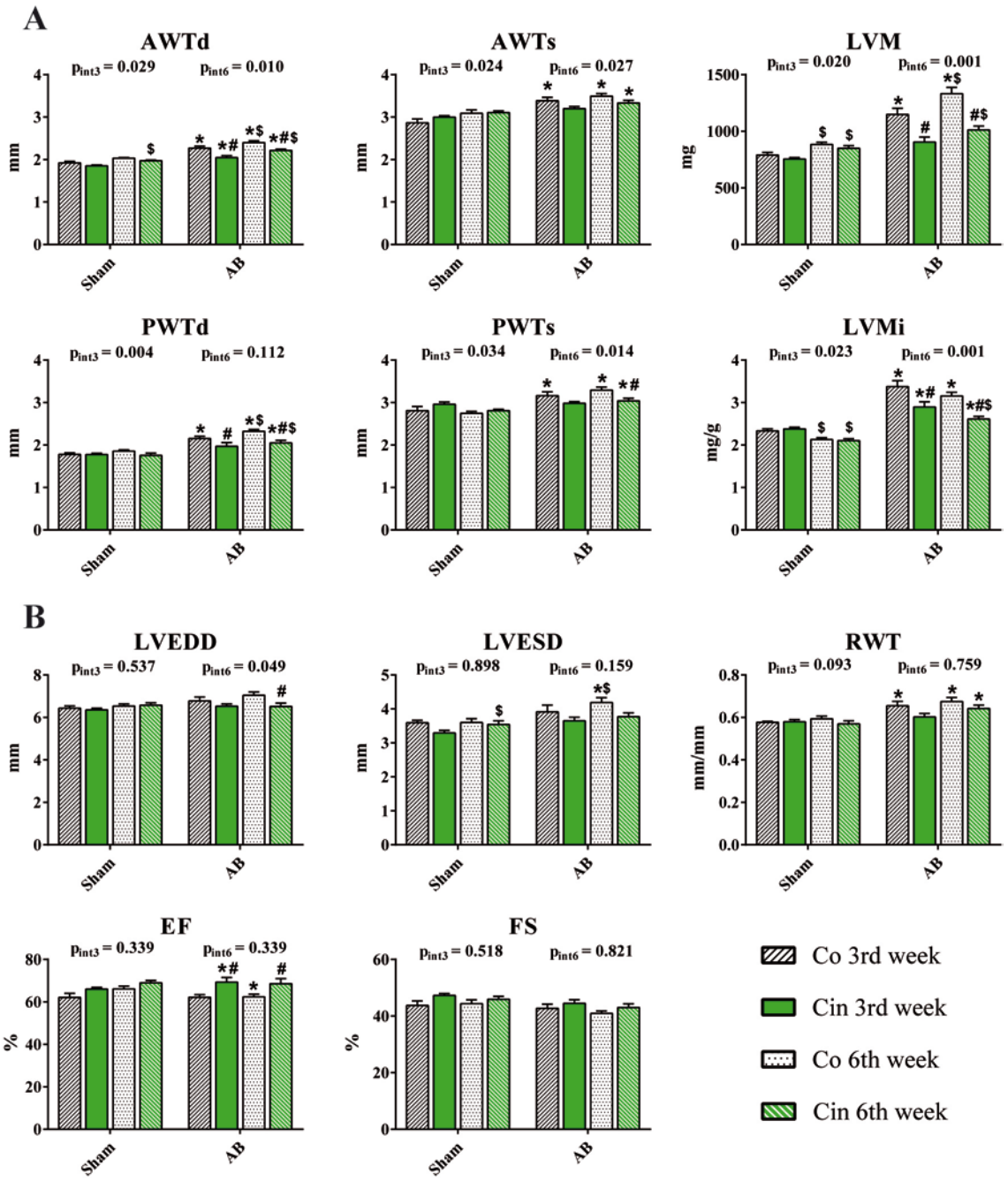

Figure 15. Cinaciguat significantly decreases the extent of myocardial hypertrophy induced by pressure overload

A: *wall thickness and LV mass continuously increased in pressure overload during the six-week protocol. The cinaciguat treatment significantly decreased the thickening of LV walls and, consequently, ameliorated the increase in LVM at both time points.*

B: *chamber dimensions did not change dramatically during the study period. Accordingly, relative wall thickness systolic parameters, such as EF or FS also remained unchanged.*

AWTd/s: anterior wall thickness in diastole/systole; PWTd/s: posterior wall thickness in diastole/systole; LVM: left ventricular mass; LVMi: LVM index; LVEDD: LV end-diastolic diameter; LVESD: LV end-systolic diameter; EF: ejection fraction; FS: fractional shortening; RWT: relative wall thickness.

**: p<0.05 vs. ShamCo; #: p<0.05 vs. AABCo; $: p<0.05 vs. 3rd week*

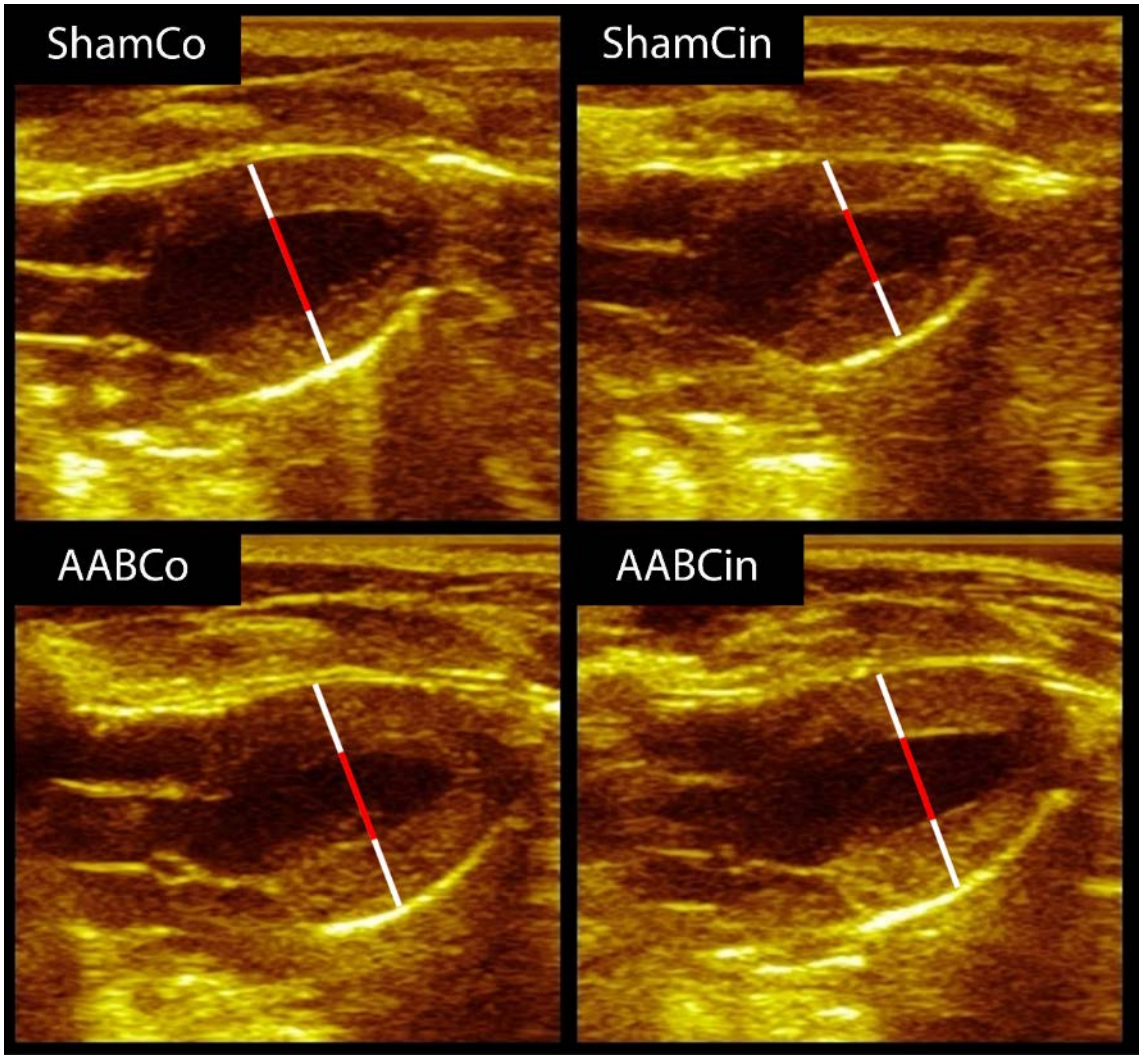

Figure 16. Representative echocardiographic images from the 6th week in diastole

White bars represent walls, and red bars show cavities. Note the difference among groups in the length of the bars.

Load independent indices of contractility, such as E_{es} and PRSW (Figure 17. B), also showed that AABCo animals had significantly elevated LV contractility compared with ShamCo. These parameters, however, indicated a significant decrease of contractility in AABCin compared with AABCo rats. dP/dt_{max}-EDV had a similar trend (Figure 17. B). Active relaxation was impaired in the AABCo rats compared with ShamCo, as evidenced by τ, while it was similar to ShamCo in the AABCin animals (Table 7.).

Table 7. Cinaciguat does not alter baseline hemodynamic parameters

	ShamCo	***ShamCin***	***AABCo***	***AABCin***	p_{band}	p_{treat}	p_{int}
HR (beats/min)	433±15	412±17	435±11	444±17	0.255	0.679	0.309
MAP (mmHg)	134±5	127±5	183±7*	177±5*	**<0.0001**	0.218	0.902
LVEDP (mmHg)	4.7±0.5	4.1±0.4	4.5±0.3	4.9±0.6	0.248	0.741	0.484
LVESP (mmHg)	140±4	138±3	191±14*	185±6*	**<0.0001**	0.610	0.903
dP/dt_{max} (mmHg/s)	8589±460	8200±543	10999±430*	10374±648	**0.0001**	0.338	0.822
τ (ms)	11.21±0.49	11.33±0.75	16.30±1.65*	13.65±0.66	**0.001**	0.225	0.185
LVEDV (μl)	221±19	190±13	233±11	199±16	0.790	0.094	0.728
LVESV (μl)	103±8	91±8	97±7	96±8	0.959	0.400	0.436
SV (μl)	145±14	128±7	156±10	135±7	0.390	0.066	0.857
EF (%)	60±1	61±2	61±1	61±1	0.489	0.685	0.854
CO (μl/min)	63273±6714	52417±3103	67575±4575	59680±3507	0.373	**0.025**	0.984
SW (mmHgμl)*	16492±1756	14290±1189	20921±1641	17666±1401	**0.017**	0.088	0.736
Ea (mmHg/μl)	1.03±0.10	1.06±0.07	1.28±0.13	1.39±0.07	**0.008**	0.479	0.668

AAB: abdominal aortic banding; Sham: sham operated; /Co: placebo treated; /Cin: cinaciguat treated; HR: heart rate; MAP: mean arterial pressure; LVEDP: LV end-diastolic pressure; LVESP: LV systolic pressure; dP/dt_{max}: maximal increment of pressure change; τ: time constant of active LV relaxation; LVEDV: LV end-diastolic volume; LVESV: LV end-systolic volume; SV: stroke volume; EF: ejection fraction; CO: cardiac output; SW: stroke work; E_a: arterial elastance; p_{band}: *p* value of 'aortic banding' main effect; p_{treat}: *p* value of 'Cinaciguat treatment' main effect; p_{int}: interaction *p* value
*: $p<0.05$ vs. ShamCo; #: $p<0.05$ vs. AABCo

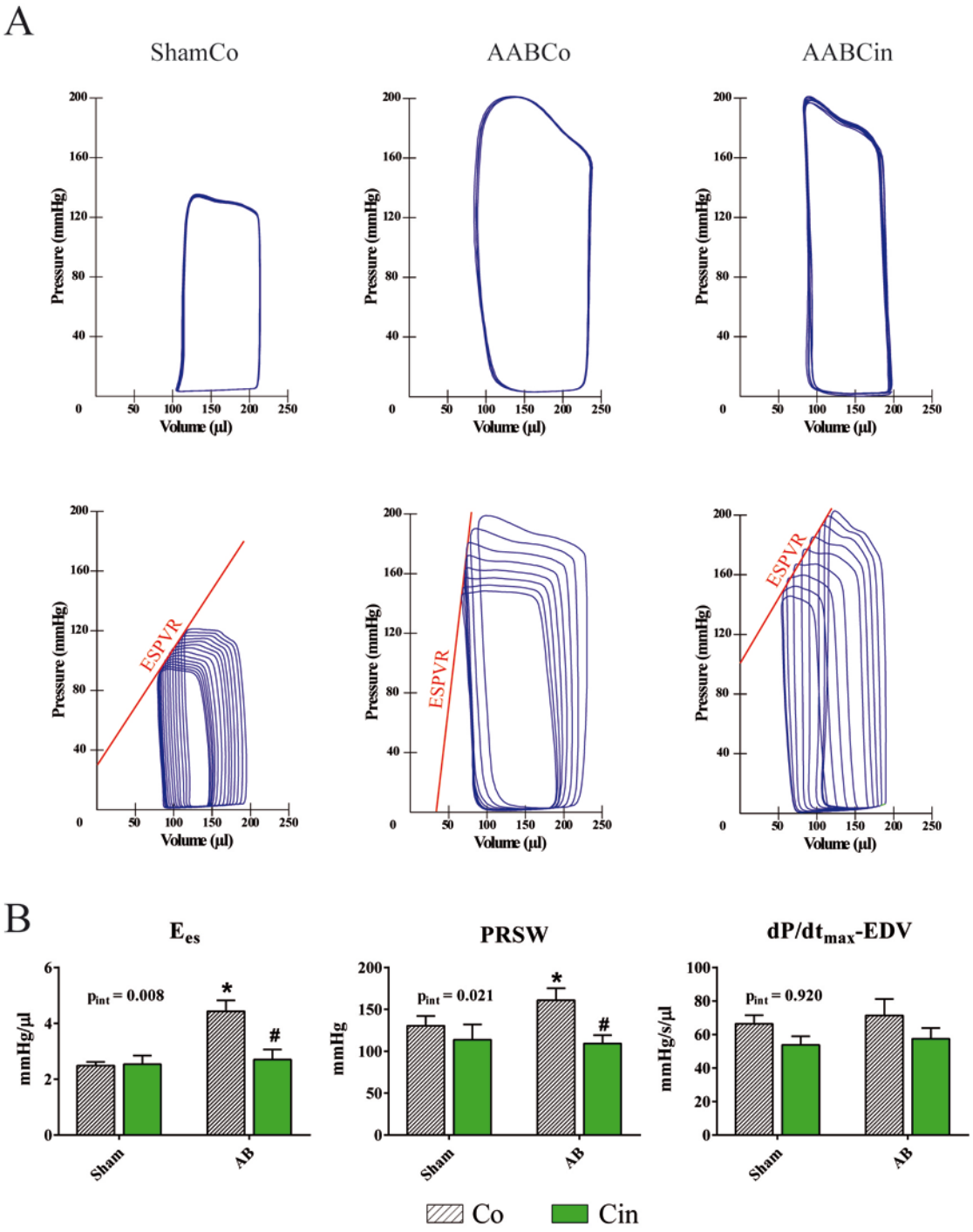

Figure 17. Cinaciguat normalises increased contractility in pressure overload

*Baseline characteristics of pressure-volume relations did not differ in the AABCo and AABCin groups (**A**, top row). PV loops recorded during occlusion of the inferior vena cava (**A**, bottom row) and the load independent indices of contractility derived from these measurements (**B**) show, however, that cinaciguat significantly decreased the increase in contractility following abdominal aortic banding.*
E_{es}: end systolic elastance; PRSW: preload recruitable stroke work; dP/dt_{max}-EDV: maximum rate of pressure change – end diastolic volume relationship; p_{int}: interaction p value
**: $p<0.05$ vs. ShamCo; #: $p<0.05$ vs. AABCo*

5.2.4. Histology

Morphological changes were present on the microscopic level as well. Average cardiomyocyte width was significantly increased in the AABCo group compared with ShamCo (Figure 18. A, E), and was significantly lower in AABCin rats than in AABCo animals. Quantitative analysis of heart sections stained with Picrosirius red showed that the collagen area of subendocardial LV myocardium was significantly increased in the AABCo group compared with ShamCo, which was significantly decreased in the AABCin rats compared with AABCo (Figure 18. B, F). TUNEL staining revealed a significant increase in DNA fragmentation, which implies an increase in the number of possibly apoptotic cell nuclei in the AABCo group compared with ShamCo and AABCin (Figure 18. C, G).

Analyzing immunohistochemical staining on myocardial sections for cGMP resulted in significantly higher score in AABCin rats than either in ShamCo or AABCo animals (Figure 18. D, H).

5.2.5. Molecular and biochemical measurements

5.2.5.1. Cardiac mRNA analysis

Pressure overload of the left ventricle resulted in elevated myocardial expression of ANP and NOS3 (Figure 19. A) as well as decreased ratio of MHCα/MHCβ expression (Figure 19. A), indicating the reactivation of the fetal gene program in the AABCo animals. Treatment with cinaciguat normalized the relative expression of NOS3 and the ratio of MHCα/MHCβ expression (Figure 19. A), while ANP expression was unaltered by the treatment (Figure 19. A). Expression ratio of SERCA2a and Pln was significantly elevated in the AABCin rats (Figure 19. A).

Anti-apoptotic signaling was reinforced by Cinaciguat, as evidenced by the significant increase in Bcl-2 expression and the strong tendency towards higher expression of HSP70 in the AABCin animals (Figure 19. B).

5.2.5.2. Plasma cGMP measurement

Plasma level of cGMP was significantly elevated in the AABCin animals compared with both ShamCo and AABCo groups (Figure 20.).

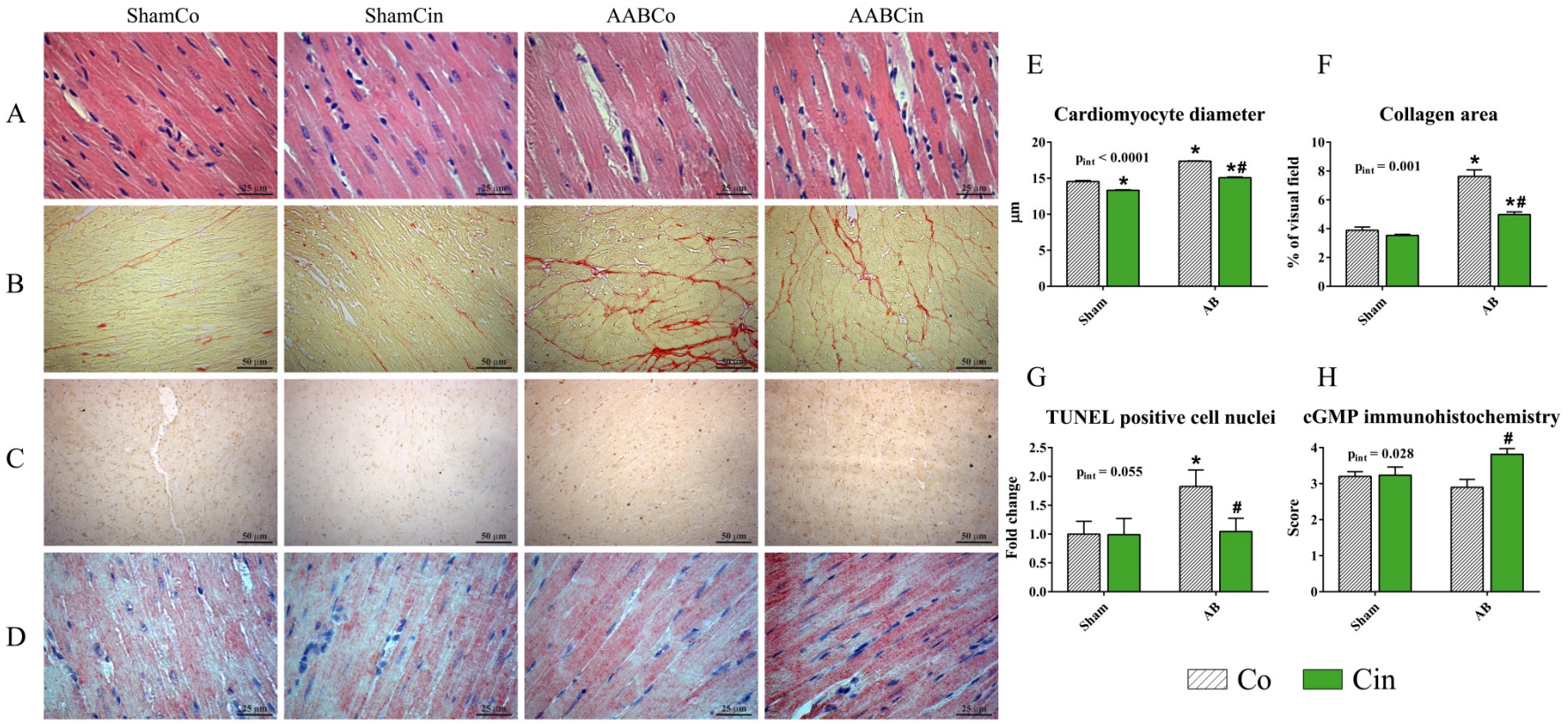

Figure 18. Histological alterations in pressure overload are blunted by Cinaciguat

Differences between the groups are illustrated in representative photomicrographs of left ventricular (LV) myocardial sections with haematoxylin-eosin (A) and Picrosirius red staining (B), TUNEL (C) and cGMP immunohistochemistry (D). Average cardiomyocyte diameter (E) and collagen area of subendocardial LV myocardium (F) was significantly elevated in the AABCo group compared with ShamCo, both of which alterations were significantly decreased following Cinaciguat treatment. TUNEL staining revealed a significant increase in the number of apoptotic cell nuclei in the AABCo group compared with ShamCo and AABCin (G). cGMP score (H) was significantly higher in the AABCin group than in the AABCo animals. p_{int}: interaction p value

**: p<0.05 vs. ShamCo; #: p<0.05 vs. AABCo*

Figure 19. Cinaciguat treatment favourably alters gene expression profile in pressure overloaded hearts

A: *Aortic banding resulted in reactivation of the foetal gene program, as evidenced by elevated expression of ANP, MHCβ, and NOS3, as well as the decreased expression of MHCα. Expression of NOS3 and MHCα along with the MHC isoform expression ratio was normalised by the cinaciguat treatment following aortic banding. The SERCA2a/Pln expression ratio was significantly increased in the AABCin rats compared with the AABCo animals.*

B: *both HSP70 and Bcl-2 expression was markedly elevated in the AABCin group, indicating reinforced anti-apoptotic signalling in these animals.*

ANP: atrial natriuretic peptide; Bcl-2: B-cell lymphoma 2; HSP70: 70 kDa heat shock protein; MHCα/β: α and β isoform of myosin heavy chain; NOS3: endothelial nitric oxide synthase; Pln: phospholamban; SERCA2a: sarcoplasmic and endoplasmic reticulum Ca^{2+} *ATPase isoform 2a;* p_{int}*: interaction p value*

**: p<0.05 vs. ShamCo; #: p<0.05 vs. AABCo*

5.2.5.3. Immunoblot analysis

Protein density of PKG was significantly elevated in myocardial homogenates of AABCo rats, while it was comparable to ShamCo in the AABCin group (Figure 20.). Phosphorylation ratio of VASP and Pln are widely used indicators of PKG activity, both of which were elevated following cinaciguat treatment (Figure 20.). Representative images showing original blots are displayed in Figure 21.

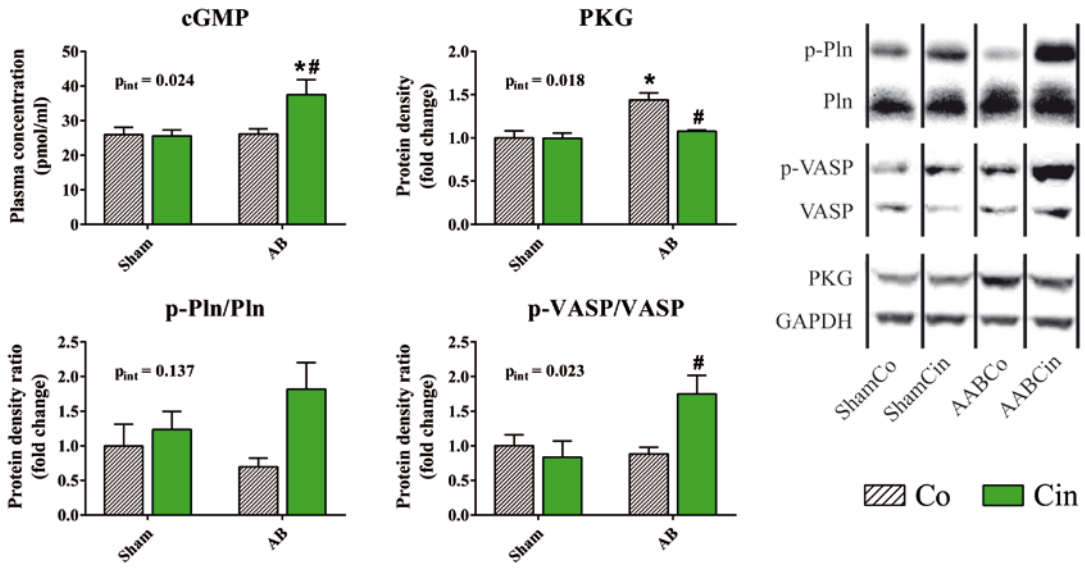

Figure 20. Effects of Cinaciguat on cGMP signalling in pressure overload

The strong sGC activating effect of Cinaciguat during pathologic conditions was confirmed by measuring plasma level of cGMP, which was significantly elevated in AABCin rats. cGMP activates PKG, which then phosphorylates VASP and Pln, phosphorylation ratio of which are widely used markers of PKG activity. Both of these were markedly increased despite the unchanged amount of PKG in the AABCin group, indicating increased PKG activity in these animals. Representative Western blot bands are shown for each group and investigated protein on the right.

PKG: protein kinase G; Pln: phospholamban; VASP: vasodilator stimulated phosphoprotein; p_{int}: interaction p value

**: p<0.05 vs. ShamCo; #: p<0.05 vs. AABCo*

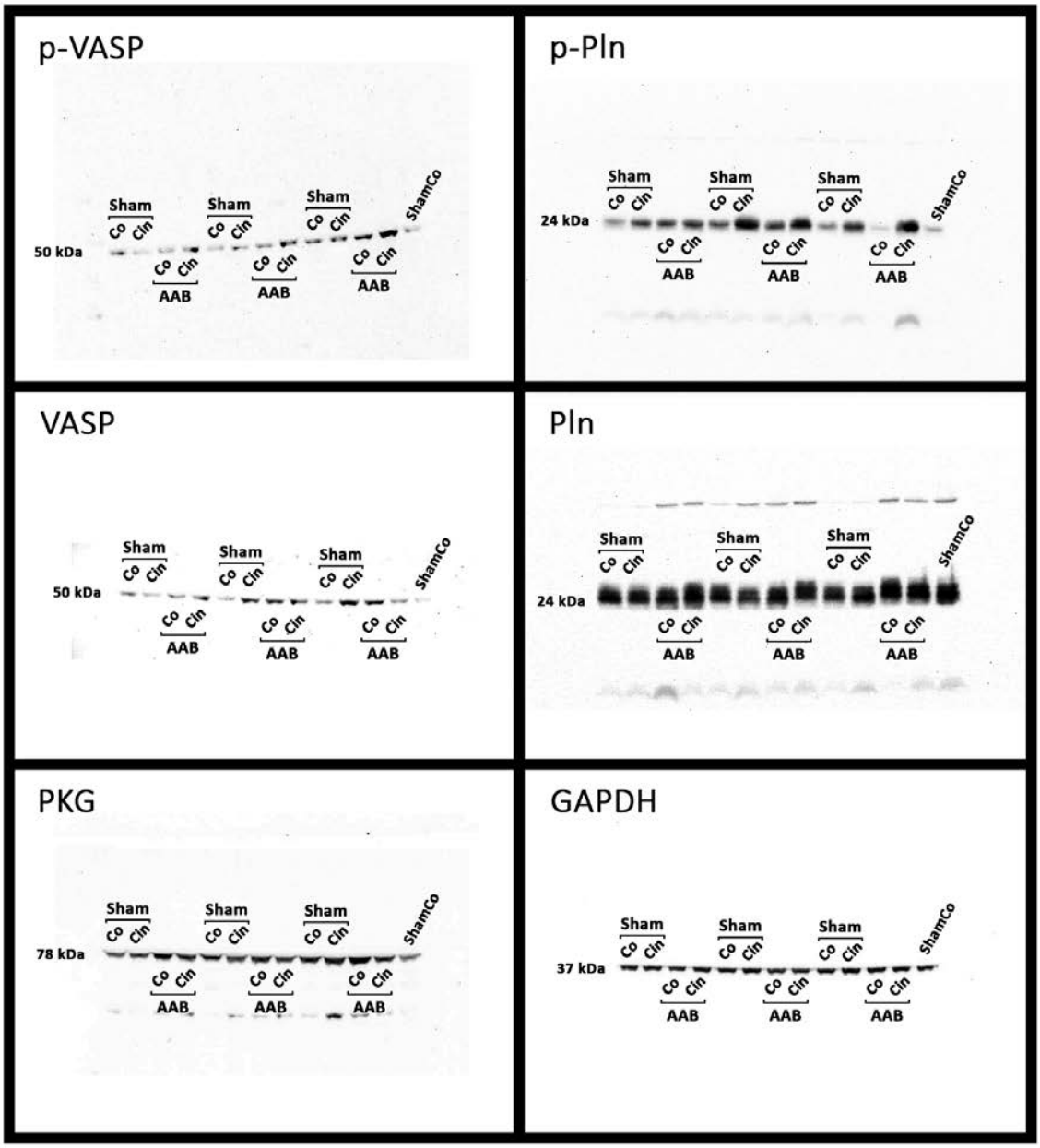

Figure 21. Representative immunoblots showing antibody specificity

The last ShamCo band on every blot was used to normalize differences in chemiluminescence between blots incubated with the same antibody.

GAPDH: glyceraldehyde 3-phosphate dehydrogenase; PKG: protein kinase G; Pln: phospholamban; p-Pln: phospho-Pln; VASP: vasodilator stimulated phosphoprotein; p-VASP: phospho-VASP

6. Discussion

6.1. Differences between physiological and pathological myocardial hypertrophy

We gave direct hemodynamic comparison of physiological and pathological LVH in this study for the first time using a pressure-conductance catheter system in relevant small animal models. Characteristics of energy-dependent LV performance in these models were found to be distinctly different despite the comparable degree of LVH. According to our data, a possible underlying mechanism might be the alteration of mitochondrial regulation, appearing in the form of differential myocardial expression of mitochondrial markers.

Cardiac hypertrophy is described as the response of the heart to a variety of stimuli that impose increased biomechanical stress on it. The hypertrophic phenotype is characterized by an increase in cardiomyocyte size, enhanced protein synthesis, and a better organization of the sarcomere (Frey & Olson, 2003). In line with these observations, both chronic pressure overload and exercise training led to significantly increased heart weight (Table 3.) and LV wall thickness values (Table 4.) in rats. LV mass index data revealed that the extent of LV mass increase compared with control is ~20–25% after exercise training and ~25–30% after the stimulus of chronic pressure overload (Table 4.). These results are comparable with the findings of our previous study (Oláh *et al.*, 2015) and other experimental investigations (McMullen *et al.*, 2003; Wang *et al.*, 2010; Wilkins *et al.*, 2004). Histological evaluation of average LV cardiomyocyte diameter on H&E-stained sections confirmed comparable hypertrophy of cardiomyocytes in both Ex and AAB animals (Figure 12.), providing further evidence for a corresponding LVH in our models. Despite the similar extent of LV mass increase, there is a major difference between physiological and pathological hypertrophy. While regular exercise did not induce collagen deposition, pressure overload resulted in subendocardial accumulation of collagen (Figure 12.), which is in line with previous results with AAB (Derumeaux *et al.*, 2002). Interestingly, despite excess collagen was deposited in the LV of our AAB animals, TGF-β expression was left unchanged after 6 weeks of pressure overload (Figure 13. C). This discrepancy, however, might be explained by previous findings regarding attenuation of the initial surge of TGF-β expression during sustained pressure overload (Li & Brooks, 1997). The absence of

fibrotic remodeling in our Ex animals provides further evidence for the physiological nature of LVH after long-term exercise training (Wilkins *et al.*, 2004). On the molecular level, reactivation of the fetal gene program in the heart is a hallmark of pathological hypertrophy (Frey & Olson, 2003), during which, as a major change, a shift from the normal expression of the α isoform of myosin heavy chain toward the less efficient, but less energy consuming β isoform occurs. Such alterations in the gene expression profile are not present in exercise training-induced LV enlargement (Figure 13. A). In line with this, altered myocardial expression of markers of this gene program, such as MHCα, MHCβ and ANP clearly demonstrated the pathological nature of LVH following AAB (Figure 13. A), while the absence of these changes after 12 weeks of training (Figure 13. A) supports our observation of physiological LVH in Ex animals (Iemitsu *et al.*, 2001; McMullen *et al.*, 2003).

The transition of pathological hypertrophy to overt heart failure is associated with myocardial oxidative stress and activated inflammatory processes (Bernardo *et al.*, 2010). Intensive oxidative stress and the consecutive inflammatory response, however, might not play a significant role in our 6-week long model of pathological hypertrophy, which is evidenced by unaltered myocardial expression of endogenous antioxidants and inflammatory cytokines (Figure 13. B, C). These results support the notion of the observed pathological hypertrophy being compensated in nature, and are in line with results comparing compensated myocardial hypertrophy with the failing heart in a model of pressure overload (Brooks *et al.*, 2010). We did not expect nor found any alterations in the expression of oxidative stress- and inflammation-related markers in exercise-induced hypertrophy, which is in alignment with literature data [Figure 13. B, C, (Iemitsu *et al.*, 2001)].

Exercise did not influence pressure conditions within the LV (Table 5.). Concerning volume relations, contrary to what is observed in human athletes – i.e., physiological hypertrophy induced by aerobic training is associated with increased end-diastolic volume and decreased heart rate compared with sedentary individuals (Maron, 1986) –, our exercised animals under anesthesia displayed unaltered end-diastolic, but smaller end-systolic dimensions together with similar heart rate compared with control rats (Figure 11. A and Table 4.). Heart rate, although might be expected to show a decrease in exercised rats, was found similar among the groups (Table 3.). This finding was most

probably the consequence of all functional measurements being completed on animals under appropriate anesthesia, which affects the vegetative nervous system significantly enough to dampen the potential differences in this parameter observable in awake animals. These changes in baseline hemodynamics, however, led to a net increase in stroke volume, cardiac output, ejection fraction and fractional shortening in our exercised rats, similarly to what is characteristic to athlete's heart, as shown in human studies using noninvasive methods (Scharhag *et al.*, 2002; Spirito *et al.*, 1994), excluding ejection fraction that is unchanged or may even be decreased at rest in humans (Prior & La Gerche, 2012). The increase in ejection fraction observed in our Ex rats, an alteration that does not correlate with what is characteristic to human athlete's heart, is most probably the consequence of the enormous difference in resting heart rate between humans and rats. The heart rate of rats is 6-8-fold higher than that of humans, which shortens the time available for diastole at rest to an extent that significantly increasing diastolic volume is unachievable. Therefore, the rat heart adapts to exercise by increasing contractility (Figure 11.) and ejection fraction (Tables 4. and 5.), the latter through decreasing end-systolic volume (Table 5.).

Abdominal aortic banding, on the other hand, was associated with a marked increase in MAP (~40 mmHg), peak LV systolic pressure (~60 mmHg) and unchanged LV end-diastolic pressure, while LV volumes were only slightly shifted toward higher values – leading to relatively unchanged stroke volume, cardiac output, fractional shortening and ejection fraction –, a phenomenon corresponding to results from other groups investigating pressure overload-induced cardiac hypertrophy [Figure 15. B and Table 7., (Derumeaux *et al.*, 2002; Moens *et al.*, 2008)]. Furthermore, these data confirm the lack of chamber dilatation in AAB rats, also corresponding to experiments using abdominal aortic banding (Figure 15. B) (Derumeaux *et al.*, 2002; Juric *et al.*, 2007). The extent of hypertension in our animals is comparable with the findings of other studies using this method to induce pathological hypertrophy in rodents (Kompa *et al.*, 2010; McMullen *et al.*, 2003). These data imply preserved systolic function, which altogether suggest that our animals were in the compensated phase of pathological hypertrophy after 6 weeks of pressure overload.

In summary, concerning baseline LV P-V relations, physiological hypertrophy is characterized by volume changes resulting in increased stroke volume and cardiac

output, while the pathological stimulus-induced hypertrophy presents itself mainly as – a pathological – adaptation to increased systolic pressure with relatively unaltered volume conditions. Furthermore, conventional parameters describing systolic function, such as ejection fraction and fractional shortening, are increased in physiological, while, at the stage we investigated, maintained in pathological hypertrophy, clearly reflecting the difference between the underlying stimuli.

LV contractility is traditionally approximated using the peak rate of systolic pressure increment, dP/dt_{max}. This parameter, however, is influenced mainly by preload, but heart rate or extremely increased afterload also deteriorates its value (Cingolani & Kass, 2011). As such, this parameter might be especially unreliable in our AAB rats. Pressure-volume analysis provides precise and reliable parameters of LV contractility utilizing the P-V relations recorded during occlusion of the inferior vena cava, a transient preload reduction maneuver. Thus, load-independent indicators of ventricular contractility can be calculated. The most widely used such sensitive contractility index, E_{es} was significantly increased in both swim-trained and AAB rats (Figure 11. A, B). Preload dependence of stroke work and dP/dt_{max}, both being load-dependent indices, can effectively be reduced by using linear regression to end-diastolic volume when measured during the preload-reducing maneuver (Cingolani & Kass, 2011). The resulting load-independent indices, PRSW and dP/dt_{max}-EDV were also increased in both hypertrophy models, confirming the increase in contractility in both exercise training- and pressure overload-induced LVH. These observations are in line with our previous results in physiological hypertrophy (Radovits *et al.*, 2013) and with formerly published data of pressure overload-induced pathological hypertrophy in rodents (Chen *et al.*, 2013; Takimoto *et al.*, 2005b). Control animals of our models showed similar contractility (Figure 11. A, B).

Ventricular diastole comprises two main phases: active relaxation followed by passive filling. The first phase of diastole, LV relaxation is considered an active, energy-consuming process and depends mostly on Ca^{2+} reuptake by the sarcoplasmic reticulum during early diastole (Zhao *et al.*, 2008). dP/dt_{min} was unchanged in both types of LVH, but the utility of this parameter under conditions that differ from physiological – much like dP/dt_{max} – is very limited due to its dependence on various hemodynamic factors, mostly loading conditions (Garrido *et al.*, 1993). Again, P-V analysis provided a more

reliable index, τ, which has been described as a relatively load-independent index of active relaxation of the LV (Zhao *et al.*, 2008). τ was decreased in physiological hypertrophy, which suggests a shorter isovolumetric relaxation period and thus enhanced relaxation in our trained rats (Table 5.). This is in line with previously published data from our workgroup in this model of athlete's heart (Radovits *et al.*, 2013). In contrast, we observed a markedly lengthened relaxation in pathological hypertrophy (Table 5.). This is in accordance with investigations aiming at functional characterization of LVH induced by pressure overload; these studies utilized animal models including aortic constriction (Kompa *et al.*, 2010; Takimoto *et al.*, 2005b) or spontaneously hypertensive rats (Cingolani & Kass, 2011), and have yielded similar results regarding active relaxation. This discrepancy in active relaxation might be the most characteristic difference between the two types of investigated cardiac hypertrophies (Figure 12. B, C and Table 5.). Our findings are consistent with recent human echocardiographic studies, where hypertrophic cardiomyopathy and athlete's heart could be distinguished by early diastolic components (Caselli *et al.*, 2014; Kovacs *et al.*, 2014).

Passive filling during diastole is mainly defined by ventricular compliance. Although ventricular compliance is influenced by multiple factors, it is affected predominantly by alterations in myocardial intracellular and extracellular structural components [e.g., fibrosis or edema, (Pacher *et al.*, 2008)]. The passive viscoelastic property – or stiffness – of the myocardium can be quantified by examination of the relationship between diastolic pressure and volume (Zile & Brutsaert, 2002a). Our protocols did not result in any significant alteration in EDPVR, and there was no difference between the hypertrophy models (Figure 11. A). These data are in good agreement with the lack of collagen deposition observed in the hearts of exercised animals (Figure 12. B, C). Furthermore, the slight increase of subendocardial fibrosis in AAB rats might not be extensive enough to result in characteristic functional consequences (Figure 12. B, C). LVEDP, another index of LV stiffness, was consistent with our observation concerning EDPVR, providing further support to the notion of unchanged LV stiffness in these models (Table 5.).

SW describes the effective external mechanical work of the LV in one cardiac cycle, and can be calculated as the area enclosed by the resting P-V loop (Figure 10). Both

exercise training and pressure overload resulted in increased mechanical work due to increased stroke volume and elevated systolic pressure values, respectively (Figure 11. A and Table 5.). SW increased significantly more in pressure overload compared with exercise training, clearly reflecting the severe hypertension in these animals (Table 5.). PVA is the area in the P-V plane that is bound by the end-systolic and end-diastolic P-V relationship lines and the systolic segment of the P-V loop (Figure 10). It serves as a reliable index of total mechanical work, and is directly proportional to myocardial oxygen consumption (Suga *et al.*, 1981). While this parameter was similar in control animals and exercised rats with physiological hypertrophy, pressure overload and the resulting pathological hypertrophy was associated with a marked increase in PVA, suggesting markedly increased energy consumption of the LV myocardium compared with sham operated animals (Table 5.). Taking a closer look at these results revealed that a greater proportion of the total work of the LV (PVA) manifested as effective work (SW) in exercised animals than in pressure-overloaded rat hearts. Therefore, mechanical efficiency (Eff) of LV performance was better in animals with exercise training-induced hypertrophy than in any other group (Table 5.). In other words, and in good agreement with our expectations, while increased work was achieved through an adaptive increase in LV mass and improvement of efficiency in training-induced physiological hypertrophy, matching the need for increased work induced by extreme afterload was only sustainable through an excessive increase in contractile mass without any improvement of efficiency in pathological hypertrophy resulting from pressure overload. The observed differences in efficiency, however, most probably do not originate from the LV alone. Other components of the cardiovascular system, such as the compliance of the arterial system connected to the LV, might play a significant role as well. The interaction between the LV and the arterial system is described by another important factor of cardiac mechanoenergetics, ventricular-arterial coupling (VAC), which can be calculated as the ratio of arterial elastance (E_a) and E_{es} (Sunagawa *et al.*, 1983). E_a is an integrative index of afterload that includes, among others, peripheral vascular resistance, arterial compliance, and characteristic impedance of the vasculature, giving an overall characterization of the total resistance of the arterial system. Decreased E_a in exercised rats revealed a better compliance of the arteries in our physiological hypertrophy model, whereas – as expected – E_a was increased in pressure

overload, clearly reflecting the increased afterload in our pathological hypertrophy model originating from the banding on the abdominal aorta (Table 5.). As E_{es} is similarly increased in both hypertrophy models, it is evident that the difference in E_a is responsible for the difference in VAC between physiological and pathological hypertrophy (Table 5.). Therefore, improved VAC in exercise-trained animals is most probably attributable to decreased arterial impedance, while the value of VAC in pressure overload-induced pathological hypertrophy indicates that the increased arterial load is merely compensated by the increased systolic LV performance (Table 5.). These observations are in accordance with human investigations describing ventriculo-arterial relations in athletes and in patients with hypertension-induced LVH (Florescu *et al.*, 2010; Nitenberg *et al.*, 2001).

In addition to what I discussed above, there might be a difference in metabolic efficiency between physiological and pathological myocardial conditions: exercise training is associated with enhanced fatty acid and glucose oxidation, whereas pathological hypertrophy is related to a decrease in fatty acid oxidation and increase in glucose metabolism (Bernardo *et al.*, 2010; Gibb &Hill, 2018). Some of the most important investigated cardiac functional parameters, such as active relaxation, SW or mechanical efficiency, have each been referred to as energy-dependent indices; intact mitochondrial function, therefore, is vital for efficient cardiac functioning. Thus, we examined the myocardial expression of the master regulator of myocardial energy metabolism, the mitochondrial transcriptional coactivator PGC1α, which regulates mitochondrial biogenesis and function (Finck & Kelly, 2007). In line with literature data (Rimbaud *et al.*, 2009), PGC1α and some of its important downstream coactivators and targets (ERRα, NRF1, PPARα, and CytC) were downregulated in pathological hypertrophy, suggesting mitochondrial dysfunction and a shift from lipid to glucose utilization (Figure 14.). In contrast, physiological cardiac hypertrophy was shown to be associated with normal or enhanced mitochondrial biogenesis (Rimbaud *et al.*, 2009). Our data is in accordance with previous findings – there was no significant upregulation of these genes in our swim training model of athlete's heart (Figure 14.). This difference in metabolism between our cardiac hypertrophy models supports the concept that targeting regulator molecules of mitochondrial biogenesis and function might play an important role in the treatment of pathological hypertrophy.

6.2. Effects of cinaciguat in pathological myocardial hypertrophy

In this project we demonstrated for the first time that the chronic activation of sGC by cinaciguat and the subsequent rise in cGMP levels efficiently reduce pressure overload-induced pathologic myocardial hypertrophy *in vivo* despite the unchanged loading of the LV. In parallel with the significant morphological changes, functional alterations were normalized by the cinaciguat treatment following AAB.

In vivo, the major drive in the background of the hypertrophic response of cardiomyocytes to chronically increased afterload is stretching of the cell membrane (Seymour *et al.*, 2015; Zhang *et al.*, 2013). Recently published *in vitro* studies have shown that cinaciguat has anti-hypertrophic effects in cultured neonatal rat cardiomyocytes (Irvine *et al.*, 2012), suggesting that chronic activation of the NO-cGMP-PKG pathway is capable of decreasing cardiomyocyte hypertrophy irrespective of the mechanical stress inflicted on cardiomyocytes by hemodynamic load. The significance of NO-cGMP-PKG signaling in this protective effect might be that it regulates a plethora of important mechanisms including Ca^{2+}-related signaling pathways, as well as phosphorylation of troponin I (Kaye *et al.*, 1999) and various ion channels (Bai *et al.*, 2005). Our present results are in line with the above mentioned anti-hypertrophic properties of sGC-activation. *In vivo* myocardial anti-hypertrophic effect of cinaciguat in previously published works, however, was suggested to be secondary to amelioration of the primary disease [pulmonary hypertension (Dumitrascu *et al.*, 2006) and uremia (Kalk *et al.*, 2006)] by the drug. In contrast, banding on the abdominal aorta and thus the pathological stimulus in our model cannot be resolved by the drug, therefore we showed with this project for the first time that cinaciguat exerts a primary anti-hypertrophic effect *in vivo*, irrespective of the hemodynamic loading of the LV. The observed effect might be the result of increased activity of PKG brought about by the elevation of intracellular cGMP levels in response to cinaciguat. This conclusion is supported by myocardial and plasma cGMP-levels (Figures 18. D, H and 20.), and increased phosphorylation ratio of VASP and Pln (Figure 20.), both of which are widely used as markers of PKG activity (Gorbe *et al.*, 2010; Sartoretto *et al.*, 2009).

Although oxidation and thus inactivation of sGC has been reported to contribute to the development of LVH (Tsai *et al.*, 2012), plasma cGMP levels were found to be unaltered in the AABCo group when compared with ShamCo. This finding might be

explained by the overexpression of natriuretic peptides (such as ANP, Figure 19. A) and subsequent cGMP-production by particulate GC (Kuhn, 2003) in our AABCo rats, and could be interpreted as an ineffective compensatory reaction to sGC inactivation. Furthermore, pGC seems to be improbable to directly replace the function of sGC in the cell; the different subcellular compartmentalization of sGC versus pGC derived cGMP should be taken into account (Castro *et al.*, 2006).

Similarly to the previous setting, significant concentric LVH was present in the AABCo group by the 6th week, as shown by RWT values. AWTd, PWTd and LVEDD were significantly decreased in the AABCin group compared with AABCo (Figure 15. A). Indeed, LVMi estimated from our echocardiographic measurements showed that cinaciguat significantly decreased the extent of LVH (Figure 15. A). Our finding correlates with data about the PDE-5 inhibitor sildenafil, which also increases the amount of intracellular cGMP, and was shown to reduce LVH significantly (Takimoto *et al.*, 2005a). Post mortem organ weight measurements correlated with these results: AABCo rats developed a significant increase both in absolute and relative heart weight compared with ShamCo, which is similar to previous data in this model (Schunkert *et al.*, 1990). The gain of heart weight was significantly decreased by cinaciguat treatment (Table 6.), which clearly reflects the anti-hypertrophic properties of the compound.

Chronically increased afterload induces compensatory remodeling of the myocardium. Unlike physiological myocardial hypertrophy, as it has been described above, pathologic stimuli such as hypertension, lead to maladaptive changes in the cellular structure of cardiomyocytes (McMullen & Jennings, 2007). On the microscopic level, we found a significant increase in average cardiomyocyte width and subendocardial collagen area in the AABCo group compared with ShamCo (Figure 18. A, B, E, F), confirming our previous results (Figure 12. B, C). Treatment with cinaciguat significantly reduced both average cardiomyocyte width and subendocardial collagen area in our aortic banded rats (Figure 18. A, B, E, F), which correlates well with the decrease observed in LVMi and heart weight (Figure 14. A and Table 6.) both within this study and with previous results (Derumeaux *et al.*, 2002; Takimoto *et al.*, 2005a).

A major change in the subcellular phenotype characteristic to pathologic LVH is the reactivation of the fetal gene program (Swynghedauw, 2006). Indeed, we observed the previously discussed characteristic switch in myosin heavy chain isotypes (Figure 19.

A) in AABCo animals, a well-known change (Izumo *et al.*, 1987) that was completely normalized by cinaciguat treatment, as observed in the AABCin group (Figure 19. A). This result is especially remarkable considering that loading of the LV was similar, as MAP was comparable in the aortic banding groups (Table 7.). It must again be noted here that cinaciguat has been critically discussed in a number of publications due to its hypotensive effect in human clinical trials utilizing the drug intravenously (Erdmann *et al.*, 2013; Gheorghiade *et al.*, 2012). It is very important to emphasize, however, that consistently with other pharmacological agents, pharmacokinetics of cinaciguat is significantly different when administered orally. In line with this, according to previous reports, a single oral dose of 10mg/kg cinaciguat only mildly and transiently lowers blood pressure (Stasch *et al.*, 2002). Furthermore, chronic oral administration of the drug in this dose did not significantly alter arterial blood pressure in the systemic circulation neither in murine models of pulmonary hypertension (Dumitrascu *et al.*, 2006) nor in a rat model of diabetic cardiomyopathy (Matyas *et al.*, 2015). Similar results with oral ataciguat and GSK2181236A, two further sGC activators have recently been reported in a rat myocardial infarction model and in spontaneously hypertensive stroke prone rats (Costell *et al.*, 2012; Fraccarollo *et al.*, 2014). Conforming to these data, we did not observe any changes in MAP of the rats in response to orally administered cinaciguat at the time of hemodynamic assessment, 24h after last application of the drug. Nevertheless, the observed robust overexpression of ANP in both AAB groups (Figure 18. A) provided evidence for unchanged loading, similar LV wall stretch and thus mechanical hypertrophic stimulus in the AABCo and AABCin animals. Similar results have been published regarding mTOR signaling (Boluyt *et al.*, 2004; Shioi *et al.*, 2003), where a significant reduction in LVH was observed without any change in pressure overload; whether there is an interplay between cGMP and mTOR signaling, however, is yet to be elucidated.

Excessive stretching of the plasma membrane of cardiac myocytes could also induce programmed cell death (Cheng *et al.*, 1995). Our results correspond with previous data, because we observed a significant increase in DNA fragmentation, and thus in the number of possibly apoptotic cell nuclei in the AABCo group compared with ShamCo with TUNEL staining (Figure 18. C, G). This alteration was normalized by the cinaciguat treatment, which improvement could be explained by reinforced anti-

apoptotic signaling, as evidenced by the increased expression of Bcl-2 and HSP70 (Figure 19. B).

Thus, we observed a significant improvement of the detrimental changes occurring during pathologic LVH on all three observable (i.e., macroscopic, microscopic and molecular) levels in response to cinaciguat treatment.

As described above in more detail, chronic overload of the LV results in pathologic morphological changes of the myocardium, which initially result in a functionally compensated phase with hypertrophy and an increase in contractility, eventually leading to decompensation with LV dilatation, systolic dysfunction and overt HF (Litwin *et al.*, 1995). We found maintained systolic performance in our animals with echocardiography both on the 3rd and 6th week (Figure 15. B), which finding confirms our previous results in this model. The significantly increased LVESD in the AABCo animals, however, might anticipate LV dilatation and systolic dysfunction, while cinaciguat effectively prevented this alteration as well (Figure 15. B).

Analysis of P-V data acquired during invasive hemodynamic measurements provides more precise assessment of cardiac performance. E_{es} was proposed as a fairly load-insensitive index of ventricular contractility, while PRSW has been described to be a parameter independent of chamber size and mass in addition to load-insensitivity (Radovits *et al.*, 2013). These indices showed an increase in LV contractility in the AABCo group, which was not present following cinaciguat treatment (Figure 17. B and Table 7.). These results are partially explained by the anti-hypertrophic effects of cinaciguat, as described above and in previous studies (Heineke & Molkentin, 2006; Takimoto *et al.*, 2009). Further important contributors to these results might be functional changes induced by activation of PKG: inactivation of L-type Ca^{2+}-channels and activation of late rectifier K^{+}-channels by PKG might both decrease intracellular Ca^{2+} concentration (Bai *et al.*, 2005). What is more, phosphorylation of troponin I by PKG could ameliorate Ca^{2+}-sensitivity of cardiomyocytes (Kaye *et al.*, 1999). Therefore, while not completely preventing adaptive compensatory hypertrophy (Figures 15. A, 16., 18. A, E and Table 6.), cinaciguat appears to attenuate the excess in hypertrophic response that might not be required for the LV to withstand increased afterload (Esposito *et al.*, 2002), in parallel with ameliorating all characteristic changes

of pathological hypertrophy including fibrosis (Figure 18. B, F), apoptosis (Figure 18. C, G) and reactivation of the fetal gene program (Figure 19. A).

A hallmark of HHD is the impairment of LV diastolic function long before systolic dysfunction occurs, resulting clinically in the HFpEF phenotype. Both decrease of passive compliance and impaired active relaxation of the LV can be in the background of diastolic dysfunction (Zile & Brutsaert, 2002b). Conforming to our previous results discussed above, LVEDP did not change compared with ShamCo (Table 7.) despite the elevated subendocardial collagen area in the AABCo animals (Figure 18. B, F), which suggests that passive compliance of the LV was unaltered at this early stage of HHD. We confirmed in this study as well that increased collagen area was present only in the subendocardial region of the LV wall following 6 weeks of pressure overload, as shown on Picrosirius red stained sections (Figure 18. B). Collagen deposition, as observed by Derumeaux et al., expanded to the complete width of the LV wall when the duration of pressure overload was increased (Derumeaux *et al.*, 2002). τ, on the other hand, which characterizes active relaxation, was significantly increased in the AABCo group, suggesting impaired active relaxation (Table 7.). There was no sign of diastolic dysfunction in the AABCin animals, which could be explained by the elevated ratio of expression of SERCA2a and Pln (Figure 18. A) and increased phosphorylation ratio of Pln (Figure 20.) compared with AABCo. Both of these changes could contribute to the facilitation of cytoplasmic Ca^{2+}-clearance in the early phase of diastole, resulting in maintained active relaxation (del Monte *et al.*, 1999; Tsuji *et al.*, 2009), although further investigation is needed to elucidate the mechanisms underlying this phenomenon.

Diastolic dysfunction causes backward failure initially in the pulmonary circulation (Lorell & Carabello, 2000). In accordance with this, we found significantly elevated relative lung weight in our AABCo rats, while it was comparable to ShamCo in the AABCin animals (Table 6.).

6.3. Limitations

The most important and perhaps obvious limitation of these investigations is the use of small animals. The significant phylogenetic distance between humans and rats alone limits comparability, which is further aggravated by the vast difference in corporeal dimensions. Thus, all results discussed herein should be interpreted to human clinical situations with caution.

7. Conclusions

Our current experiments provided the first detailed hemodynamic comparison of physiological and compensated pathological hypertrophy in relevant rodent models. Although the investigated types of myocardial hypertrophies were phenotypically similar, distinctive functional and molecular differences were present. Active relaxation during diastole was differentially affected: physiological hypertrophy was associated with a significant improvement, while pathological hypertrophy resulted in a significant deterioration. Furthermore, efficiency of the work of the LV and coupling to the arterial system was improved only in physiological hypertrophy. Altered myocardial expression of markers related to mitochondrial function and biogenesis, such as the master regulator PGC1α might explain the described energy-dependent functional differences.

We showed for the first time in our second set of experiments that chronic activation of sGC by cinaciguat potently prevents the development of excessive myocardial hypertrophy induced by pressure overload *in vivo*. We observed this beneficial effect of sGC activation on morphological, functional and molecular levels as well.

8. Summary

With respect to its minimal proliferative capacity, the response of adult myocardium to increased load is hypertrophy. Depending on the factors leading to its development, this hypertrophic response varies significantly in either its molecular, morphological or functional characteristics. Based on these observations, physiological and pathological myocardial hypertrophy are traditionally distinguished, which, from a clinical point of view, differ most significantly in their prognosis. Thus, research on effective new pharmacological options inhibiting the development of pathological myocardial hypertrophy is of prime importance.

Our aim with the current investigations was to discover functional, morphological and molecular differences between physiological and pathological myocardial hypertrophy in animal models, as well as to study the effects of pharmacological activation of the NO-cGMP signaling pathway, gaining prominence recently, in a rat model of pathological myocardial hypertrophy.

We showed in our experiments that the most important difference between physiological and pathological myocardial hypertrophy at their early stage is found in diastolic function: while physiological hypertrophy is associated with a significant improvement, pathological hypertrophy leads to a marked deterioration of active relaxation compared with control. Changes in the metabolism of cardiomyocytes and energy production of their mitochondria might play an important role in the background of functional differences, while morphological alterations are not significant.

We also revealed that pharmacological activation of the NO-cGMP signaling pathway effectively reduces extreme hypertrophic response of the myocardium to pressure overload, which includes reduction of futilely increased contractility and improvement of diastolic dysfunction, decrease of subendocardial collagen accumulation and DNA-strand breaks in cardiomyocytes, as well as normalization of expression of pathologically reactivated genes characteristic to the fetal period of ontogeny.

Based on our results we can conclude that the sGC activator cinaciguat might be an effective new therapeutic option in the prevention of pressure overload-induced pathological myocardial hypertrophy.

9. Összefoglalás

A felnőtt szívizomzatot érő fokozott terhelés, tekintettel a miokardium minimális proliferációs képességére, hipertrófiás válasz kialakulásához vezet. A hipertrófia, függően a létrejöttéhez vezető okoktól, molekuláris, morfológiai és funkcionális szempontból is igen eltérő tulajdonságokkal rendelkezik. Ezek alapján tradicionálisan két nagy csoportot: fiziológiás, valamint patológiás miokardiális hipertrófiát különítünk el, melyek klinikai szemszögből legfontosabb különbsége a prognózisban rejlik, ezért a patológiás miokardiális hipertrófia kialakulását gátló új, hatékony gyógyszeres terápiák kutatása elsőrendű feladat.

Jelen vizsgálatainkban célul tűztük ki, hogy a fiziológiás, valamint patológiás miokardiális hipertrófia állatmodelljein e két állapot funkcionális, morfológiai és molekuláris különbségeit feltárjuk, továbbá hogy a patológiás miokardiális hipertrófia patkánymodelljében a közelmúltban egyre nagyobb jelentőséget kapott NO-cGMP jelátvitel farmakológiai aktiválásának hatásait vizsgáljuk.

Kísérleteink során igazoltuk, hogy a fiziológiás és patológiás miokardiális hipertrófia kezdeti szakaszában legfontosabb funkcionális különbség a diasztolé során jelentkezik: az aktív relaxáció fiziológiás hipertrófia esetén lényegesen javul, míg patológiás szívizom-megnagyobbodás alkalmával lényegesen romlik a kontrollhoz viszonyítva. Ennek hátterében a szívizomsejtek anyagcseréjében, illetve mitokondriumaik energiatermelésében beálló változások játszhatnak szerepet, miközben a morfológiai különbségek nem jelentősek.

Kimutattuk továbbá, hogy a NO-cGMP jelátvitel gyógyszeres aktiválásával a nyomástúlterhelés hatására kialakuló szélsőséges hipertrófiás válasz mértéke hatékonyan csökkenthető. Ennek jeleként megfigyelhető volt a túlzott kontraktilitás csökkenése és a diasztolés diszfunkció mérséklése, a szubendokardiális kollagén mennyiségének, valamint a szívizomsejtekben megfigyelhető DNS-károsodás mértékének csökkenése, továbbá a magzati korra jellemző, kórosan újfent kifejeződő gének expressziójának normalizálódása.

Eredményeink alapján kijelenthetjük, hogy a sGC aktivátor cinaciguat hatékony új terápiás opció lehet a nyomás indukálta patológiás miokardiális hipertrófia kialakulásának megelőzésében.

10. References

Abudiab MM, Redfield MM, Melenovsky V, Olson TP, Kass DA, Johnson BD, Borlaug BA. (2013) Cardiac output response to exercise in relation to metabolic demand in heart failure with preserved ejection fraction. Eur J Heart Fail, 15**:** 776-785.

Action to Control Cardiovascular Risk in Diabetes Study Group, Gerstein HC, Miller ME, Byington RP, Goff DC, Jr., Bigger JT, Buse JB, Cushman WC, Genuth S, Ismail-Beigi F, Grimm RH, Jr., Probstfield JL, Simons-Morton DG, Friedewald WT. (2008) Effects of intensive glucose lowering in type 2 diabetes. N Engl J Med, 358**:** 2545-2559.

Acute Infarction Ramipril Efficacy (AIRE) Study Investigators. (1993) Effect of ramipril on mortality and morbidity of survivors of acute myocardial infarction with clinical evidence of heart failure. Lancet, 342**:** 821-828.

Ai X, Curran JW, Shannon TR, Bers DM, Pogwizd SM. (2005) Ca^{2+}/calmodulin-dependent protein kinase modulates cardiac ryanodine receptor phosphorylation and sarcoplasmic reticulum Ca^{2+} leak in heart failure. Circ Res, 97**:** 1314-1322.

Alderman MH, Cohen HW, Sealey JE, Laragh JH. (2004) Plasma renin activity levels in hypertensive persons: their wide range and lack of suppression in diabetic and in most elderly patients. Am J Hypertens, 17**:** 1-7.

Anderson S, Meyer TW, Rennke HG, Brenner BM. (1985) Control of glomerular hypertension limits glomerular injury in rats with reduced renal mass. J Clin Invest, 76**:** 612-619.

Ashrafian H, Frenneaux MP, Opie LH. (2007) Metabolic mechanisms in heart failure. Circulation, 116**:** 434-448.

Auger-Messier M, Accornero F, Goonasekera SA, Bueno OF, Lorenz JN, van Berlo JH, Willette RN, Molkentin JD. (2013) Unrestrained p38 MAPK activation in Dusp1/4 double-null mice induces cardiomyopathy. Circ Res, 112**:** 48-56.

Avelar E, Cloward TV, Walker JM, Farney RJ, Strong M, Pendleton RC, Segerson N, Adams TD, Gress RE, Hunt SC, Litwin SE. (2007) Left ventricular hypertrophy in severe obesity: interactions among blood pressure, nocturnal hypoxemia, and body mass. Hypertension, 49**:** 34-39.

Backs J, Song K, Bezprozvannaya S, Chang S, Olson EN. (2006) CaM kinase II selectively signals to histone deacetylase 4 during cardiomyocyte hypertrophy. J Clin Invest, 116**:** 1853-1864.

Bai CX, Namekata I, Kurokawa J, Tanaka H, Shigenobu K, Furukawa T. (2005) Role of nitric oxide in Ca^{2+} sensitivity of the slowly activating delayed rectifier K^{+} current in cardiac myocytes. Circ Res, 96**:** 64-72.

Barbier J, Ville N, Kervio G, Walther G, Carre F. (2006) Sports-specific features of athlete's heart and their relation to echocardiographic parameters. Herz, 31**:** 531-543.

Beaumont A, Grace F, Richards J, Hough J, Oxborough D, Sculthorpe N. (2017) Left Ventricular Speckle Tracking-Derived Cardiac Strain and Cardiac Twist Mechanics in Athletes: A Systematic Review and Meta-Analysis of Controlled Studies. Sports Med, 47**:** 1145-1170.

Belke DD, Betuing S, Tuttle MJ, Graveleau C, Young ME, Pham M, Zhang D, Cooksey RC, McClain DA, Litwin SE, Taegtmeyer H, Severson D, Kahn CR, Abel ED. (2002) Insulin signaling coordinately regulates cardiac size, metabolism, and contractile protein isoform expression. J Clin Invest, 109**:** 629-639.

Bendall JK, Cave AC, Heymes C, Gall N, Shah AM. (2002) Pivotal role of a gp91(phox)-containing NADPH oxidase in angiotensin II-induced cardiac hypertrophy in mice. Circulation, 105**:** 293-296.

Berk BC, Fujiwara K, Lehoux S. (2007) ECM remodeling in hypertensive heart disease. J Clin Invest, 117**:** 568-575.

Bernardo BC, Weeks KL, Pretorius L, McMullen JR. (2010) Molecular distinction between physiological and pathological cardiac hypertrophy: experimental findings and therapeutic strategies. Pharmacol Ther, 128**:** 191-227.

Boerrigter G, Costello-Boerrigter LC, Cataliotti A, Lapp H, Stasch JP, Burnett JC. (2007) Targeting heme-oxidized soluble guanylate cyclase in experimental heart failure. Hypertension, 49**:** 1128-1133.

Bois P, Selye H. (1957) The hormonal production of nephrosclerosis and periarteritis nodosa in the primate. Br Med J, 1**:** 183-186.

Boluyt MO, Li ZB, Loyd AM, Scalia AF, Cirrincione GM, Jackson RR. (2004) The mTOR/p70S6K signal transduction pathway plays a role in cardiac hypertrophy and influences expression of myosin heavy chain genes in vivo. Cardiovasc Drugs Ther, 18**:** 257-267.

Borlaug BA. (2014) Mechanisms of exercise intolerance in heart failure with preserved ejection fraction. Circ J, 78**:** 20-32.

Borlaug BA, Jaber WA, Ommen SR, Lam CS, Redfield MM, Nishimura RA. (2011) Diastolic relaxation and compliance reserve during dynamic exercise in heart failure with preserved ejection fraction. Heart, 97**:** 964-969.

Borlaug BA, Lam CS, Roger VL, Rodeheffer RJ, Redfield MM. (2009) Contractility and ventricular systolic stiffening in hypertensive heart disease insights into the pathogenesis of heart failure with preserved ejection fraction. J Am Coll Cardiol, 54**:** 410-418.

Borlaug BA, Olson TP, Lam CS, Flood KS, Lerman A, Johnson BD, Redfield MM. (2010) Global cardiovascular reserve dysfunction in heart failure with preserved ejection fraction. J Am Coll Cardiol, 56**:** 845-854.

Bossuyt J, Helmstadter K, Wu X, Clements-Jewery H, Haworth RS, Avkiran M, Martin JL, Pogwizd SM, Bers DM. (2008) Ca^{2+}/calmodulin-dependent protein kinase IIdelta and protein kinase D overexpression reinforce the histone deacetylase 5 redistribution in heart failure. Circ Res, 102**:** 695-702.

Boudina S, Bugger H, Sena S, O'Neill BT, Zaha VG, Ilkun O, Wright JJ, Mazumder PK, Palfreyman E, Tidwell TJ, Theobald H, Khalimonchuk O, Wayment B, Sheng X, Rodnick KJ, Centini R, Chen D, Litwin SE, Weimer BE, Abel ED. (2009) Contribution of impaired myocardial insulin signaling to mitochondrial dysfunction and oxidative stress in the heart. Circulation, 119**:** 1272-1283.

Brennan JP, Bardswell SC, Burgoyne JR, Fuller W, Schroder E, Wait R, Begum S, Kentish JC, Eaton P. (2006) Oxidant-induced activation of type I protein kinase A is mediated by RI subunit interprotein disulfide bond formation. J Biol Chem, 281**:** 21827-21836.

Brooks WW, Shen SS, Conrad CH, Goldstein RH, Bing OH. (2010) Transition from compensated hypertrophy to systolic heart failure in the spontaneously hypertensive rat: Structure, function, and transcript analysis. Genomics, 95**:** 84-92.

Brunner HR, Laragh JH, Baer L, Newton MA, Goodwin FT, Krakoff LR, Bard RH, Buhler FR. (1972) Essential hypertension: renin and aldosterone, heart attack and stroke. N Engl J Med, 286**:** 441-449.

Bueno OF, De Windt LJ, Lim HW, Tymitz KM, Witt SA, Kimball TR, Molkentin JD. (2001) The dual-specificity phosphatase MKP-1 limits the cardiac hypertrophic response in vitro and in vivo. Circ Res, 88**:** 88-96.

Burgoyne JR, Madhani M, Cuello F, Charles RL, Brennan JP, Schroder E, Browning DD, Eaton P. (2007) Cysteine redox sensor in PKGIa enables oxidant-induced activation. Science, 317**:** 1393-1397.

Burgoyne JR, Mongue-Din H, Eaton P, Shah AM. (2012) Redox signaling in cardiac physiology and pathology. Circ Res, 111**:** 1091-1106.

Cangiano JL, Rodriguez-Sargent C, Martinez-Maldonado M. (1979) Effects of antihypertensive treatment on systolic blood pressure and renin in experimental hypertension in rats. J Pharmacol Exp Ther, 208**:** 310-313.

Caselli S, Maron MS, Urbano-Moral JA, Pandian NG, Maron BJ, Pelliccia A. (2014) Differentiating left ventricular hypertrophy in athletes from that in patients with hypertrophic cardiomyopathy. Am J Cardiol, 114**:** 1383-1389.

Castro LRV, Verde I, Cooper DMF, Fischmeister R. (2006) Cyclic guanosine monophosphate compartmentation in rat cardiac myocytes. Circulation, 113**:** 2221-2228.

Catalucci D, Latronico MV, Ceci M, Rusconi F, Young HS, Gallo P, Santonastasi M, Bellacosa A, Brown JH, Condorelli G. (2009a) Akt increases sarcoplasmic reticulum Ca^{2+} cycling by direct phosphorylation of phospholamban at Thr17. J Biol Chem, 284**:** 28180-28187.

Catalucci D, Zhang DH, DeSantiago J, Aimond F, Barbara G, Chemin J, Bonci D, Picht E, Rusconi F, Dalton ND, Peterson KL, Richard S, Bers DM, Brown JH, Condorelli G. (2009b) Akt regulates L-type Ca2+ channel activity by modulating Cavalpha1 protein stability. J Cell Biol, 184**:** 923-933.

Chahal NS, Lim TK, Jain P, Chambers JC, Kooner JS, Senior R. (2010) New insights into the relationship of left ventricular geometry and left ventricular mass with cardiac function: A population study of hypertensive subjects. Eur Heart J, 31**:** 588-594.

Chen H, Hwang H, McKee LA, Perez JN, Regan JA, Constantopoulos E, Lafleur B, Konhilas JP. (2013) Temporal and morphological impact of pressure overload in transgenic FHC mice. Front Physiol, 4**:** 205.

Cheng S, Fernandes VR, Bluemke DA, McClelland RL, Kronmal RA, Lima JA. (2009) Age-related left ventricular remodeling and associated risk for cardiovascular outcomes: the Multi-Ethnic Study of Atherosclerosis. Circ Cardiovasc Imaging, 2**:** 191-198.

Cheng W, Li B, Kajstura J, Li P, Wolin MS, Sonnenblick EH, Hintze TH, Olivetti G, Anversa P. (1995) Stretch-induced programmed myocyte cell death. J Clin Invest, 96**:** 2247-2259.

Chopra A, Tabdanov E, Patel H, Janmey PA, Kresh JY. (2011) Cardiac myocyte remodeling mediated by N-cadherin-dependent mechanosensing. Am J Physiol Heart Circ Physiol, 300**:** H1252-1266.

Cingolani OH, Kass DA. (2011) Pressure-volume relation analysis of mouse ventricular function. Am J Physiol Heart Circ Physiol, 301**:** H2198-2206.

Coleman TG, Guyton AC, Young DB, DeClue JW, Norman RA, Manning J, Manning RD, Jr. (1975) The role of the kidney in essential hypertension. Clin Exp Pharmacol Physiol, 2**:** 571-581.

GBD 2016 Mortality Collaborators (2017). Global, regional, and national under-5 mortality, adult mortality, age-specific mortality, and life expectancy, 1970-2016: a systematic analysis for the Global Burden of Disease Study 2016. Lancet, 390**:** 1084-1150.

Colombo CSSS, Finocchiaro G. (2018). The Female Athlete's Heart: Facts and Fallacies. Curr Treat Options Cardiovasc Med, 20**:** 101.

Condorelli G, Drusco A, Stassi G, Bellacosa A, Roncarati R, Iaccarino G, Russo MA, Gu Y, Dalton N, Chung C, Latronico MV, Napoli C, Sadoshima J, Croce CM, Ross J, Jr. (2002) Akt induces enhanced myocardial contractility and cell size in vivo in transgenic mice. Proc Natl Acad Sci U. S. A., 99**:** 12333-12338.

Costell MH, Ancellin N, Bernard RE, Zhao S, Upson JJ, Morgan LA, Maniscalco K, Olzinski AR, Ballard VL, Herry K, Grondin P, Dodic N, Mirguet O, Bouillot A, Gellibert F, Coatney RW, Lepore JJ, Jucker BM, Jolivette LJ, Willette RN, Schnackenberg CG, Behm DJ. (2012) Comparison of soluble guanylate cyclase stimulators and activators in models of cardiovascular disease associated with oxidative stress. Front Pharmacol, 3**:** 128.

D'Andrea A, D'Andrea L, Caso P, Scherillo M, Zeppilli P, Calabro R. (2006) The usefulness of Doppler myocardial imaging in the study of the athlete's heart and in the differential diagnosis between physiological and pathological ventricular hypertrophy. Echocardiography, 23**:** 149-157.

D'Ascenzi F, Cameli M, Ciccone MM, Maiello M, Modesti PA, Mondillo S, Muiesan ML, Scicchitano P, Novo S, Palmiero P, Saba PS, Pedrinelli R, Gruppo di Studio Ipertensione, Prevenzione e Riabilitazione, Società Italiana di Cardiologia. (2015) The controversial relationship between exercise and atrial fibrillation: clinical studies and pathophysiological mechanisms. J Cardiovasc Med (Hagerstown), 16**:** 802-810.

Das A, Durrant D, Salloum FN, Xi L, Kukreja RC. (2015) PDE5 inhibitors as therapeutics for heart disease, diabetes and cancer. Pharmacol Ther, 147**:** 12-21.

Davila DF, Donis JH, Odreman R, Gonzalez M, Landaeta A. (2008) Patterns of left ventricular hypertrophy in essential hypertension: should echocardiography guide the pharmacological treatment? Int J Cardiol, 124**:** 134-138.

Davis J, Davis LC, Correll RN, Makarewich CA, Schwanekamp JA, Moussavi-Harami F, Wang D, York AJ, Wu H, Houser SR, Seidman CE, Seidman JG, Regnier M,

Metzger JM, Wu JC, Molkentin JD. (2016) A Tension-Based Model Distinguishes Hypertrophic versus Dilated Cardiomyopathy. Cell, 165**:** 1147-1159.

De Innocentiis C, Ricci F, Khanji MY, Aung N, Tana C, Verrengia E, Petersen SE, Gallina S. (2018) Athlete's Heart: Diagnostic Challenges and Future Perspectives. Sports Med, 48**:** 2463-2477.

de Simone G, Devereux RB, Roman MJ, Alderman MH, Laragh JH. (1994) Relation of obesity and gender to left ventricular hypertrophy in normotensive and hypertensive adults. Hypertension, 23**:** 600-606.

del Monte F, Harding SE, Schmidt U, Matsui T, Kang ZB, William Dec G, Gwathmey JK, Rosenzweig A, Hajjar RJ. (1999) Restoration of Contractile Function in Isolated Cardiomyocytes From Failing Human Hearts by Gene Transfer of SERCA2a. Circulation, 100**:** 2308-2311.

Derbyshire ER, Marletta MA. (2009) Biochemistry of soluble guanylate cyclase. Handb Exp Pharmacol**:** 17-31.

Derumeaux G, Mulder P, Richard V, Chagraoui A, Nafeh C, Bauer F, Henry JP, Thuillez C. (2002) Tissue Doppler imaging differentiates physiological from pathological pressure-overload left ventricular hypertrophy in rats. Circulation, 105**:** 1602-1608.

Devereux RB, Alonso DR, Lutas EM, Gottlieb GJ, Campo E, Sachs I, Reichek N. (1986) Echocardiographic assessment of left ventricular hypertrophy: comparison to necropsy findings. Am J Cardiol, 57**:** 450-458.

Donath S, Li P, Willenbockel C, Al-Saadi N, Gross V, Willnow T, Bader M, Martin U, Bauersachs J, Wollert KC, Dietz R, von Harsdorf R, German Heart Failure Network. (2006) Apoptosis repressor with caspase recruitment domain is required for

cardioprotection in response to biomechanical and ischemic stress. Circulation, 113**:** 1203-1212.

Dorn GW, 2nd, Robbins J, Sugden PH. (2003) Phenotyping hypertrophy: eschew obfuscation. Circ Res, 92**:** 1171-1175.

Drazner MH. (2011) The progression of hypertensive heart disease. Circulation, 123**:** 327-334.

Drazner MH, Dries DL, Peshock RM, Cooper RS, Klassen C, Kazi F, Willett D, Victor RG. (2005) Left ventricular hypertrophy is more prevalent in blacks than whites in the general population: the Dallas Heart Study. Hypertension, 46**:** 124-129.

du Cailar G, Pasquie JL, Ribstein J, Mimran A. (2000) Left ventricular adaptation to hypertension and plasma renin activity. J Hum Hypertens, 14**:** 181-188.

Dumitrascu R, Weissmann N, Ghofrani HA, Dony E, Beuerlein K, Schmidt H, Stasch JP, Gnoth MJ, Seeger W, Grimminger F, Schermuly RT. (2006) Activation of soluble guanylate cyclase reverses experimental pulmonary hypertension and vascular remodeling. Circulation, 113**:** 286-295.

Eijsvogels TM, Fernandez AB, Thompson PD. (2016) Are There Deleterious Cardiac Effects of Acute and Chronic Endurance Exercise? Physiol Rev, 96**:** 99-125.

Emdin CA, Callender T, Cao J, McMurray JJ, Rahimi K. (2015) Meta-Analysis of Large-Scale Randomized Trials to Determine the Effectiveness of Inhibition of the Renin-Angiotensin Aldosterone System in Heart Failure. Am J Cardiol, 116**:** 155-161.

Erdmann E, Semigran MJ, Nieminen MS, Gheorghiade M, Agrawal R, Mitrovic V, Mebazaa A. (2013) Cinaciguat, a soluble guanylate cyclase activator, unloads the heart but also causes hypotension in acute decompensated heart failure. Eur Heart J, 34**:** 57-67.

Erickson JR, Joiner ML, Guan X, Kutschke W, Yang J, Oddis CV, Bartlett RK, Lowe JS, O'Donnell SE, Aykin-Burns N, Zimmerman MC, Zimmerman K, Ham AJ, Weiss RM, Spitz DR, Shea MA, Colbran RJ, Mohler PJ, Anderson ME. (2008) A dynamic pathway for calcium-independent activation of CaMKII by methionine oxidation. Cell, 133**:** 462-474.

Esposito G, Rapacciuolo A, Naga Prasad SV, Takaoka H, Thomas SA, Koch WJ, Rockman HA. (2002) Genetic alterations that inhibit in vivo pressure-overload hypertrophy prevent cardiac dysfunction despite increased wall stress. Circulation, 105**:** 85-92.

Evangelista FS, Brum PC, Krieger JE. (2003) Duration-controlled swimming exercise training induces cardiac hypertrophy in mice. Braz J Med Biol Res, 36**:** 1751-1759.

Evgenov OV, Pacher P, Schmidt PM, Hasko G, Schmidt HH, Stasch JP. (2006) NO-independent stimulators and activators of soluble guanylate cyclase: discovery and therapeutic potential. Nat Rev Drug Discov, 5**:** 755-768.

Fagard R. (2003) Athlete's heart. Heart, 89**:** 1455-1461.

Fagard R, Van den Broeke C, Bielen E, Vanhees L, Amery A. (1987) Assessment of stiffness of the hypertrophied left ventricle of bicyclists using left ventricular inflow Doppler velocimetry. J Am Coll Cardiol, 9**:** 1250-1254.

Fagard RH. (1996) Athlete's heart: a meta-analysis of the echocardiographic experience. Int J Sports Med, 17 Suppl 3**:** S140-144.

Fagard RH, Staessen JA, Thijs L. (1997) Prediction of cardiac structure and function by repeated clinic and ambulatory blood pressure. Hypertension, 29**:** 22-29.

Finck BN, Kelly DP. (2007) Peroxisome proliferator-activated receptor gamma coactivator-1 (PGC-1) regulatory cascade in cardiac physiology and disease. Circulation, 115**:** 2540-2548.

Fischmeister R, Castro LR, Abi-Gerges A, Rochais F, Jurevicius J, Leroy J, Vandecasteele G. (2006) Compartmentation of cyclic nucleotide signaling in the heart: the role of cyclic nucleotide phosphodiesterases. Circ Res, 99**:** 816-828.

Florescu M, Stoicescu C, Magda S, Petcu I, Radu M, Palombo C, Cinteza M, Lichiardopol R, Vinereanu D. (2010) "Supranormal" cardiac function in athletes related to better arterial and endothelial function. Echocardiography, 27**:** 659-667.

Fraccarollo D, Galuppo P, Motschenbacher S, Ruetten H, Schafer A, Bauersachs J. (2014) Soluble guanylyl cyclase activation improves progressive cardiac remodeling and failure after myocardial infarction. Cardioprotection over ACE inhibition. Basic Res Cardiol, 109**:** 421.

Francis GS, McDonald KM, Cohn JN. (1993) Neurohumoral activation in preclinical heart failure. Remodeling and the potential for intervention. Circulation, 87**:** IV90-96.

Frankenreiter S, Groneberg D, Kuret A, Krieg T, Ruth P, Friebe A, Lukowski R. (2018) Cardioprotection by ischemic postconditioning and cyclic guanosine monophosphate-elevating agents involves cardiomyocyte nitric oxide-sensitive guanylyl cyclase. Cardiovasc Res, 114**:** 822-829.

Frey N, Barrientos T, Shelton JM, Frank D, Rutten H, Gehring D, Kuhn C, Lutz M, Rothermel B, Bassel-Duby R, Richardson JA, Katus HA, Hill JA, Olson EN. (2004a) Mice lacking calsarcin-1 are sensitized to calcineurin signaling and show accelerated cardiomyopathy in response to pathological biomechanical stress. Nat Med, 10**:** 1336-1343.

Frey N, Katus HA, Olson EN, Hill JA. (2004b) Hypertrophy of the heart: a new therapeutic target? Circulation, 109**:** 1580-1589.

Frey N, Olson EN. (2003) Cardiac hypertrophy: the good, the bad, and the ugly. Annu Rev Physiol, 65**:** 45-79.

Furchgott RF, Zawadzki JV. (1980) The obligatory role of endothelial cells in the relaxation of arterial smooth muscle by acetylcholine. Nature, 288**:** 373-376.

Gabrielli L, Sitges M, Chiong M, Jalil J, Ocaranza M, Llevaneras S, Herrera S, Fernandez R, Saavedra R, Yañez F, Vergara L, Diaz A, Lavandero S, Castro P. (2018) Potential adverse cardiac remodelling in highly trained athletes: still unknown clinical significance. Eur J Sport Sci, 18**:** 1288-1297.

Ganau A, Devereux RB, Roman MJ, de Simone G, Pickering TG, Saba PS, Vargiu P, Simongini I, Laragh JH. (1992) Patterns of left ventricular hypertrophy and geometric remodeling in essential hypertension. J Am Coll Cardiol, 19**:** 1550-1558.

Garrido JM, Gerson MC, Hoit BD, Walsh RA. (1993) Load independence of early diastolic filling parameters in the anesthetized canine model. J Nucl Med, 34**:** 1520-1528.

Gautel M. (2011) Cytoskeletal protein kinases: titin and its relations in mechanosensing. Pflugers Arch, 462**:** 119-134.

George KP, Naylor LH, Whyte GP, Shave RE, Oxborough D, Green DJ. (2010) Diastolic function in healthy humans: non-invasive assessment and the impact of acute and chronic exercise. Eur J Appl Physiol, 108**:** 1-14.

Gheorghiade M, Greene SJ, Filippatos G, Erdmann E, Ferrari R, Levy PD, Maggioni A, Nowack C, Mebazaa A, COMPOSE Investigators Coordinators. (2012) Cinaciguat, a soluble guanylate cyclase activator: results from the randomized, controlled, phase IIb

COMPOSE programme in acute heart failure syndromes. Eur J Heart Fail, 14**:** 1056-1066.

Ghofrani HA, Galie N, Grimminger F, Grunig E, Humbert M, Jing ZC, Keogh AM, Langleben D, Kilama MO, Fritsch A, Neuser D, Rubin LJ, PATENT-1 Study Group. (2013) Riociguat for the treatment of pulmonary arterial hypertension. N Engl J Med, 369**:** 330-340.

Gibb AA, Hill BG. (2018) Metabolic Coordination of Physiological and Pathological Cardiac Remodeling. Circ Res, 123**:** 107-128.

Goldblatt H, Lynch J, Hanzal RF, Summerville WW. (1934) Studies on Experimental Hypertension : I. The Production of Persistent Elevation of Systolic Blood Pressure by Means of Renal Ischemia. J Exp Med, 59**:** 347-379.

Gopalan SM, Flaim C, Bhatia SN, Hoshijima M, Knoell R, Chien KR, Omens JH, McCulloch AD. (2003) Anisotropic stretch-induced hypertrophy in neonatal ventricular myocytes micropatterned on deformable elastomers. Biotechnol Bioeng, 81**:** 578-587.

Gorbe A, Giricz Z, Szunyog A, Csont T, Burley DS, Baxter GF, Ferdinandy P. (2010) Role of cGMP-PKG signaling in the protection of neonatal rat cardiac myocytes subjected to simulated ischemia/reoxygenation. Basic Res Cardiol, 105**:** 643-650.

Gottdiener JS, Reda DJ, Materson BJ, Massie BM, Notargiacomo A, Hamburger RJ, Williams DW, Henderson WG. (1994) Importance of obesity, race and age to the cardiac structural and functional effects of hypertension. The Department of Veterans Affairs Cooperative Study Group on Antihypertensive Agents. J Am Coll Cardiol, 24**:** 1492-1498.

Grieve DJ, Byrne JA, Siva A, Layland J, Johar S, Cave AC, Shah AM. (2006) Involvement of the nicotinamide adenosine dinucleotide phosphate oxidase isoform

Nox2 in cardiac contractile dysfunction occurring in response to pressure overload. J Am Coll Cardiol, 47**:** 817-826.

Grollman A. (1955) The effect of various hypotensive agents on the arterial blood pressure of hypertensive rats and dogs. J Pharmacol Exp Ther, 114**:** 263-270.

Grossman W, Jones D, McLaurin LP. (1975) Wall stress and patterns of hypertrophy in the human left ventricle. J Clin Invest, 56**:** 56-64.

Gutkind JS, Offermanns S. (2009) A new G(q)-initiated MAPK signaling pathway in the heart. Dev Cell, 16**:** 163-164.

Haq S, Choukroun G, Lim H, Tymitz KM, del Monte F, Gwathmey J, Grazette L, Michael A, Hajjar R, Force T, Molkentin JD. (2001) Differential activation of signal transduction pathways in human hearts with hypertrophy versus advanced heart failure. Circulation, 103**:** 670-677.

Hart CY, Meyer DM, Tazelaar HD, Grande JP, Burnett JC, Jr., Housmans PR, Redfield MM. (2001) Load versus humoral activation in the genesis of early hypertensive heart disease. Circulation, 104**:** 215-220.

Hawkins NM, Wang D, McMurray JJ, Pfeffer MA, Swedberg K, Granger CB, Yusuf S, Pocock SJ, Ostergren J, Michelson EL, Dunn FG, CHARM Investigators Committees. (2007) Prevalence and prognostic implications of electrocardiographic left ventricular hypertrophy in heart failure: evidence from the CHARM programme. Heart, 93**:** 59-64.

Heineke J, Molkentin JD. (2006) Regulation of cardiac hypertrophy by intracellular signalling pathways. Nat Rev Mol Cell Biol, 7**:** 589-600.

Heinzel FR, Hohendanner F, Jin G, Sedej S, Edelmann F. (2015) Myocardial hypertrophy and its role in heart failure with preserved ejection fraction. J Appl Physiol (1985), 119**:** 1233-1242.

Hilfiker-Kleiner D, Hilfiker A, Kaminski K, Schaefer A, Park JK, Michel K, Quint A, Yaniv M, Weitzman JB, Drexler H. (2005) Lack of JunD promotes pressure overload-induced apoptosis, hypertrophic growth, and angiogenesis in the heart. Circulation, 112**:** 1470-1477.

Hill JA, Karimi M, Kutschke W, Davisson RL, Zimmerman K, Wang Z, Kerber RE, Weiss RM. (2000) Cardiac hypertrophy is not a required compensatory response to short-term pressure overload. Circulation, 101**:** 2863-2869.

Hill JA, Rothermel B, Yoo KD, Cabuay B, Demetroulis E, Weiss RM, Kutschke W, Bassel-Duby R, Williams RS. (2002) Targeted inhibition of calcineurin in pressure-overload cardiac hypertrophy. Preservation of systolic function. J Biol Chem, 277**:** 10251-10255.

Hirschberg K, Tarcea V, Pali S, Barnucz E, Gwanmesia PN, Korkmaz S, Radovits T, Loganathan S, Merkely B, Karck M, Szabo G. (2013) Cinaciguat prevents neointima formation after arterial injury by decreasing vascular smooth muscle cell migration and proliferation. Int J Cardiol, 167**:** 470-477.

Hoch B, Meyer R, Hetzer R, Krause EG, Karczewski P. (1999) Identification and expression of delta-isoforms of the multifunctional Ca^{2+}/calmodulin-dependent protein kinase in failing and nonfailing human myocardium. Circ Res, 84**:** 713-721.

Hofmann F. (2018) A concise discussion of the regulatory role of cGMP kinase I in cardiac physiology and pathology. Basic Res Cardiol, 113**:** 31.

Hofmann F, Bernhard D, Lukowski R, Weinmeister P. (2009) cGMP regulated protein kinases (cGK). Handb Exp Pharmacol**:** 137-162.

Hood WP, Jr., Rackley CE, Rolett EL. (1968) Wall stress in the normal and hypertrophied human left ventricle. Am J Cardiol, 22**:** 550-558.

Huss JM, Imahashi K, Dufour CR, Weinheimer CJ, Courtois M, Kovacs A, Giguere V, Murphy E, Kelly DP. (2007) The nuclear receptor ERRalpha is required for the bioenergetic and functional adaptation to cardiac pressure overload. Cell Metab, 6**:** 25-37.

Iemitsu M, Miyauchi T, Maeda S, Sakai S, Kobayashi T, Fujii N, Miyazaki H, Matsuda M, Yamaguchi I. (2001) Physiological and pathological cardiac hypertrophy induce different molecular phenotypes in the rat. Am J Physiol Regul Integr Comp Physiol, 281**:** R2029-2036.

Ikeda H, Shiojima I, Ozasa Y, Yoshida M, Holzenberger M, Kahn CR, Walsh K, Igarashi T, Abel ED, Komuro I. (2009) Interaction of myocardial insulin receptor and IGF receptor signaling in exercise-induced cardiac hypertrophy. J Mol Cell Cardiol, 47**:** 664-675.

Ingelsson E, Sundstrom J, Arnlov J, Zethelius B, Lind L. (2005) Insulin resistance and risk of congestive heart failure. JAMA, 294**:** 334-341.

Irvine JC, Ganthavee V, Love JE, Alexander AE, Horowitz JD, Stasch JP, Kemp-Harper BK, Ritchie RH. (2012) The Soluble Guanylyl Cyclase Activator Bay 58-2667 Selectively Limits Cardiomyocyte Hypertrophy. PLoS ONE, 7**:** e44481.

Izumo S, Lompre AM, Matsuoka R, Koren G, Schwartz K, Nadal-Ginard B, Mahdavi V. (1987) Myosin heavy chain messenger RNA and protein isoform transitions during cardiac hypertrophy. Interaction between hemodynamic and thyroid hormone-induced signals. J Clin Invest, 79**:** 970-977.

Javadov S, Jang S, Agostini B. (2014) Crosstalk between mitogen-activated protein kinases and mitochondria in cardiac diseases: therapeutic perspectives. Pharmacol Ther, 144**:** 202-225.

Juric D, Wojciechowski P, Das DK, Netticadan T. (2007) Prevention of concentric hypertrophy and diastolic impairment in aortic-banded rats treated with resveratrol. Am J Physiol Heart Circ Physiol, 292**:** H2138-2143.

Kaiser RA, Bueno OF, Lips DJ, Doevendans PA, Jones F, Kimball TF, Molkentin JD. (2004) Targeted inhibition of p38 mitogen-activated protein kinase antagonizes cardiac injury and cell death following ischemia-reperfusion in vivo. J Biol Chem, 279**:** 15524-15530.

Kalk P, Godes M, Relle K, Rothkegel C, Hucke A, Stasch JP, Hocher B. (2006) NO-independent activation of soluble guanylate cyclase prevents disease progression in rats with 5/6 nephrectomy. Br J Pharmacol, 148**:** 853-859.

Kass DA, Beyar R, Lankford E, Heard M, Maughan WL, Sagawa K. (1989) Influence of contractile state on curvilinearity of in situ end-systolic pressure-volume relations. Circulation, 79**:** 167-178.

Kaye DM, Wiviott SD, Kelly RA. (1999) Activation of Nitric Oxide Synthase (NOS3) by Mechanical Activity Alters Contractile Activity in a Ca^{2+}-Independent Manner in Cardiac Myocytes: Role of Troponin I Phosphorylation. Biochem Biophys Res Commun, 256**:** 398-403.

Kehat I, Davis J, Tiburcy M, Accornero F, Saba-El-Leil MK, Maillet M, York AJ, Lorenz JN, Zimmermann WH, Meloche S, Molkentin JD. (2011) Extracellular signal-regulated kinases 1 and 2 regulate the balance between eccentric and concentric cardiac growth. Circ Res, 108**:** 176-183.

Kelly JP, Mentz RJ, Mebazaa A, Voors AA, Butler J, Roessig L, Fiuzat M, Zannad F, Pitt B, O'Connor CM, Lam CS. (2015) Patient selection in heart failure with preserved ejection fraction clinical trials. J Am Coll Cardiol, 65**:** 1668-1682.

Kemi OJ, Ceci M, Wisloff U, Grimaldi S, Gallo P, Smith GL, Condorelli G, Ellingsen O. (2008) Activation or inactivation of cardiac Akt/mTOR signaling diverges physiological from pathological hypertrophy. J Cell Physiol, 214**:** 316-321.

Kerckhoffs RC, Omens J, McCulloch AD. (2012) A single strain-based growth law predicts concentric and eccentric cardiac growth during pressure and volume overload. Mech Res Commun, 42**:** 40-50.

Kim YK, Kim SJ, Yatani A, Huang Y, Castelli G, Vatner DE, Liu J, Zhang Q, Diaz G, Zieba R, Thaisz J, Drusco A, Croce C, Sadoshima J, Condorelli G, Vatner SF. (2003) Mechanism of enhanced cardiac function in mice with hypertrophy induced by overexpressed Akt. J Biol Chem, 278**:** 47622-47628.

Kinugawa K, Jeong MY, Bristow MR, Long CS. (2005) Thyroid hormone induces cardiac myocyte hypertrophy in a thyroid hormone receptor alpha1-specific manner that requires TAK1 and p38 mitogen-activated protein kinase. Mol Endocrinol, 19**:** 1618-1628.

Kirchhefer U, Schmitz W, Scholz H, Neumann J. (1999) Activity of cAMP-dependent protein kinase and Ca^{2+}/calmodulin-dependent protein kinase in failing and nonfailing human hearts. Cardiovasc Res, 42**:** 254-261.

Kizer JR, Arnett DK, Bella JN, Paranicas M, Rao DC, Province MA, Oberman A, Kitzman DW, Hopkins PN, Liu JE, Devereux RB. (2004) Differences in left ventricular structure between black and white hypertensive adults: the Hypertension Genetic Epidemiology Network study. Hypertension, 43**:** 1182-1188.

Knoll R, Hoshijima M, Hoffman HM, Person V, Lorenzen-Schmidt I, Bang ML, Hayashi T, Shiga N, Yasukawa H, Schaper W, McKenna W, Yokoyama M, Schork NJ, Omens JH, McCulloch AD, Kimura A, Gregorio CC, Poller W, Schaper J, Schultheiss HP, Chien KR. (2002) The cardiac mechanical stretch sensor machinery involves a Z

disc complex that is defective in a subset of human dilated cardiomyopathy. Cell, 111**:** 943-955.

Koitabashi N, Aiba T, Hesketh GG, Rowell J, Zhang ML, Takimoto E, Tomaselli GF, Kass DA. (2010) Cyclic GMP/PKG-dependent inhibition of TRPC6 channel activity and expression negatively regulates cardiomyocyte NFAT activation Novel mechanism of cardiac stress modulation by PDE5 inhibition. J Mol Cell Cardiol, 48**:** 713-724.

Koivisto E, Kaikkonen L, Tokola H, Pikkarainen S, Aro J, Pennanen H, Karvonen T, Rysa J, Kerkela R, Ruskoaho H. (2011) Distinct regulation of B-type natriuretic peptide transcription by p38 MAPK isoforms. Mol Cell Endocrinol, 338**:** 18-27.

Kompa AR, Wang BH, Phrommintikul A, Ho PY, Kelly DJ, Behm DJ, Douglas SA, Krum H. (2010) Chronic urotensin II receptor antagonist treatment does not alter hypertrophy or fibrosis in a rat model of pressure-overload hypertrophy. Peptides, 31**:** 1523-1530.

Koren MJ, Devereux RB, Casale PN, Savage DD, Laragh JH. (1991) Relation of left ventricular mass and geometry to morbidity and mortality in uncomplicated essential hypertension. Ann Intern Med, 114**:** 345-352.

Korkmaz S, Loganathan S, Mikles B, Radovits T, Barnucz E, Hirschberg K, Li S, Hegedus P, Pali S, Weymann A, Karck M, Szabo G. (2013) Nitric oxide- and heme-independent activation of soluble guanylate cyclase attenuates peroxynitrite-induced endothelial dysfunction in rat aorta. J Cardiovasc Pharmacol Ther, 18**:** 70-77.

Korkmaz S, Radovits T, Barnucz E, Hirschberg K, Neugebauer P, Loganathan S, Veres G, Pali S, Seidel B, Zollner S, Karck M, Szabo G. (2009) Pharmacological activation of soluble guanylate cyclase protects the heart against ischemic injury. Circulation, 120**:** 677-686.

Kostetskii I, Li J, Xiong Y, Zhou R, Ferrari VA, Patel VV, Molkentin JD, Radice GL. (2005) Induced deletion of the N-cadherin gene in the heart leads to dissolution of the intercalated disc structure. Circ Res, 96**:** 346-354.

Kovacs A, Apor A, Nagy A, Vago H, Toth A, Nagy AI, Kovats T, Sax B, Szeplaki G, Becker D, Merkely B. (2014) Left ventricular untwisting in athlete's heart: key role in early diastolic filling? Int J Sports Med, 35**:** 259-264.

Kovacs A, Olah A, Lux A, Matyas C, Nemeth BT, Kellermayer D, Ruppert M, Torok M, Szabo L, Meltzer A, Assabiny A, Birtalan E, Merkely B, Radovits T. (2015) Strain and strain rate by speckle-tracking echocardiography correlate with pressure-volume loop-derived contractility indices in a rat model of athlete's heart. Am J Physiol Heart Circ Physiol, 308**:** H743-748.

Krege JH, Hodgin JB, Hagaman JR, Smithies O. (1995) A noninvasive computerized tail-cuff system for measuring blood pressure in mice. Hypertension, 25**:** 1111-1115.

Krishnamurthy P, Subramanian V, Singh M, Singh K. (2007) Beta1 integrins modulate beta-adrenergic receptor-stimulated cardiac myocyte apoptosis and myocardial remodeling. Hypertension, 49**:** 865-872.

Kruger M, Kotter S, Grutzner A, Lang P, Andresen C, Redfield MM, Butt E, dos Remedios CG, Linke WA. (2009) Protein Kinase G Modulates Human Myocardial Passive Stiffness by Phosphorylation of the Titin Springs. Circ Res, 104**:** 87-U230.

Krumholz HM, Larson M, Levy D. (1993) Sex differences in cardiac adaptation to isolated systolic hypertension. Am J Cardiol, 72**:** 310-313.

Kuhn M. (2003) Structure, regulation, and function of mammalian membrane guanylyl cyclase receptors, with a focus on guanylyl cyclase-A. Circ Res, 93**:** 700-709.

Kuhn M. (2009) Function and dysfunction of mammalian membrane guanylyl cyclase receptors: lessons from genetic mouse models and implications for human diseases. Handb Exp Pharmacol**:** 47-69.

Kuwahara K, Wang YG, McAnally J, Richardson JA, Bassel-Duby R, Hill JA, Olson EN. (2006) TRPC6 fulfills a calcineurin signaling circuit during pathologic cardiac remodeling. J Clin Invest, 116**:** 3114-3126.

Lam CS, Grewal J, Borlaug BA, Ommen SR, Kane GC, McCully RB, Pellikka PA. (2010) Size, shape, and stamina: the impact of left ventricular geometry on exercise capacity. Hypertension, 55**:** 1143-1149.

Lancel S, Qin F, Lennon SL, Zhang J, Tong X, Mazzini MJ, Kang YJ, Siwik DA, Cohen RA, Colucci WS. (2010) Oxidative posttranslational modifications mediate decreased SERCA activity and myocyte dysfunction in Galphaq-overexpressing mice. Circ Res, 107**:** 228-232.

Lee DI, Vahebi S, Tocchetti CG, Barouch LA, Solaro RJ, Takimoto E, Kass DA. (2010) PDE5A suppression of acute beta-adrenergic activation requires modulation of myocyte beta-3 signaling coupled to PKG-mediated troponin I phosphorylation. Basic Res Cardiol, 105**:** 337-347.

Lee DI, Zhu G, Sasaki T, Cho GS, Hamdani N, Holewinski R, Jo SH, Danner T, Zhang M, Rainer PP, Bedja D, Kirk JA, Ranek MJ, Dostmann WR, Kwon C, Margulies KB, Van Eyk JE, Paulus WJ, Takimoto E, Kass DA. (2015) Phosphodiesterase 9A controls nitric-oxide-independent cGMP and hypertrophic heart disease. Nature, 519**:** 472-476.

Levy D, Garrison RJ, Savage DD, Kannel WB, Castelli WP. (1990) Prognostic implications of echocardiographically determined left ventricular mass in the Framingham Heart Study. N Engl J Med, 322**:** 1561-1566.

Li JM, Brooks G. (1997) Differential protein expression and subcellular distribution of TGFbeta1, beta2 and beta3 in cardiomyocytes during pressure overload-induced hypertrophy. J Mol Cell Cardiol, 29**:** 2213-2224.

Li Y, Wu J, He Q, Shou Z, Zhang P, Pen W, Zhu Y, Chen J. (2009) Angiotensin (1-7) prevent heart dysfunction and left ventricular remodeling caused by renal dysfunction in 5/6 nephrectomy mice. Hypertens Res, 32**:** 369-374.

Liang Q, Bueno OF, Wilkins BJ, Kuan CY, Xia Y, Molkentin JD. (2003) c-Jun N-terminal kinases (JNK) antagonize cardiac growth through cross-talk with calcineurin-NFAT signaling. EMBO J, 22**:** 5079-5089.

Liang Q, Molkentin JD. (2003) Redefining the roles of p38 and JNK signaling in cardiac hypertrophy: dichotomy between cultured myocytes and animal models. J Mol Cell Cardiol, 35**:** 1385-1394.

Liao P, Georgakopoulos D, Kovacs A, Zheng M, Lerner D, Pu H, Saffitz J, Chien K, Xiao RP, Kass DA, Wang Y. (2001) The in vivo role of p38 MAP kinases in cardiac remodeling and restrictive cardiomyopathy. Proc Natl Acad Sci U. S. A., 98**:** 12283-12288.

Lima B, Forrester MT, Hess DT, Stamler JS. (2010) S-Nitrosylation in Cardiovascular Signaling. Circ Res, 106**:** 633-646.

Ling HY, Zhang T, Pereira L, Means CK, Cheng HQ, Gu YS, Dalton ND, Peterson KL, Chen J, Bers D, Brown JH. (2009) Requirement for Ca^{2+}/calmodulin-dependent kinase II in the transition from pressure overload-induced cardiac hypertrophy to heart failure in mice. J Clin Invest, 119**:** 1230-1240.

Litwin SE, Katz SE, Weinberg EO, Lorell BH, Aurigemma GP, Douglas PS. (1995) Serial Echocardiographic-Doppler Assessment of Left Ventricular Geometry and Function in Rats With Pressure-Overload Hypertrophy: Chronic Angiotensin-

Converting Enzyme Inhibition Attenuates the Transition to Heart Failure. Circulation, 91**:** 2642-2654.

Liu JP, Baker J, Perkins AS, Robertson EJ, Efstratiadis A. (1993) Mice carrying null mutations of the genes encoding insulin-like growth factor I (Igf-1) and type 1 IGF receptor (Igf1r). Cell, 75**:** 59-72.

Liu YH, Wang D, Rhaleb NE, Yang XP, Xu J, Sankey SS, Rudolph AE, Carretero OA. (2005) Inhibition of p38 mitogen-activated protein kinase protects the heart against cardiac remodeling in mice with heart failure resulting from myocardial infarction. J Card Fail, 11**:** 74-81.

Loganathan S, Korkmaz-Icoz S, Radovits T, Li S, Mikles B, Barnucz E, Hirschberg K, Karck M, Szabo G. (2015) Effects of soluble guanylate cyclase activation on heart transplantation in a rat model. J Heart Lung Transplant, 34**:** 1346-1353.

Lorell BH, Apstein CS, Weinberg EO, Cunningham MJ. (1990) Diastolic function in left ventricular hypertrophy: clinical and experimental relationships. Eur Heart J, 11 Suppl G**:** 54-64.

Lorell BH, Carabello BA. (2000) Left ventricular hypertrophy: pathogenesis, detection, and prognosis. Circulation 102**:** 470-479.

Lyon RC, Zanella F, Omens JH, Sheikh F. (2015) Mechanotransduction in cardiac hypertrophy and failure. Circ Res, 116**:** 1462-1476.

Maillet M, van Berlo JH, Molkentin JD. (2013) Molecular basis of physiological heart growth: fundamental concepts and new players. Nat Rev Mol Cell Biol, 14**:** 38-48.

Manso AM, Li R, Monkley SJ, Cruz NM, Ong S, Lao DH, Koshman YE, Gu Y, Peterson KL, Chen J, Abel ED, Samarel AM, Critchley DR, Ross RS. (2013) Talin1 has

unique expression versus talin 2 in the heart and modifies the hypertrophic response to pressure overload. J Biol Chem, 288**:** 4252-4264.

Markus MR, Stritzke J, Wellmann J, Duderstadt S, Siewert U, Lieb W, Luchner A, Doring A, Keil U, Schunkert H, Hense HW. (2011) Implications of prevalent and incident diabetes mellitus on left ventricular geometry and function in the ageing heart: the MONICA/KORA Augsburg cohort study. Nutr Metab Cardiovasc Dis, 21**:** 189-196.

Maron BJ. (1986) Structural features of the athlete heart as defined by echocardiography. J Am Coll Cardiol, 7**:** 190-203.

Matsui T, Li L, Wu JC, Cook SA, Nagoshi T, Picard MH, Liao R, Rosenzweig A. (2002) Phenotypic spectrum caused by transgenic overexpression of activated Akt in the heart. J Biol Chem, 277**:** 22896-22901.

Matyas C, Nemeth BT, Olah A, Hidi L, Birtalan E, Kellermayer D, Ruppert M, Korkmaz-Icoz S, Kokeny G, Horvath EM, Szabo G, Merkely B, Radovits T. (2015) The soluble guanylate cyclase activator cinaciguat prevents cardiac dysfunction in a rat model of type-1 diabetes mellitus. Cardiovasc Diabetol, 14**:** 145.

Maytin M, Siwik DA, Ito M, Xiao L, Sawyer DB, Liao R, Colucci WS. (2004) Pressure overload-induced myocardial hypertrophy in mice does not require gp91phox. Circulation, 109**:** 1168-1171.

McMullen JR, Jennings GL. (2007) Differences between pathological and physiological cardiac hypertrophy: novel therapeutic strategies to treat heart failure. Clin Exp Pharmacol Physiol, 34**:** 255-262.

McMullen JR, Shioi T, Zhang L, Tarnavski O, Sherwood MC, Kang PM, Izumo S. (2003) Phosphoinositide 3-kinase(p110alpha) plays a critical role for the induction of physiological, but not pathological, cardiac hypertrophy. Proc Natl Acad Sci U. S. A., 100**:** 12355-12360.

Megson IL, Miller MR. (2009) NO and sGC-stimulating NO donors. Handb Exp Pharmacol**:** 247-276.

Melenovsky V, Borlaug BA, Rosen B, Hay I, Ferruci L, Morell CH, Lakatta EG, Najjar SS, Kass DA. (2007) Cardiovascular features of heart failure with preserved ejection fraction versus nonfailing hypertensive left ventricular hypertrophy in the urban Baltimore community: the role of atrial remodeling/dysfunction. J Am Coll Cardiol, 49**:** 198-207.

Messerli FH, Rimoldi SF, Bangalore S. (2017) The Transition From Hypertension to Heart Failure: Contemporary Update. JACC Heart Fail, 5**:** 543-551.

Meyer M, McEntee RK, Nyotowidjojo I, Chu G, LeWinter MM. (2015) Relationship of exercise capacity and left ventricular dimensions in patients with a normal ejection fraction. An exploratory study. PLoS One, 10**:** e0119432.

Miller MK, Bang ML, Witt CC, Labeit D, Trombitas C, Watanabe K, Granzier H, McElhinny AS, Gregorio CC, Labeit S. (2003) The muscle ankyrin repeat proteins: CARP, ankrd2/Arpp and DARP as a family of titin filament-based stress response molecules. J Mol Biol, 333**:** 951-964.

Mitchell JH, Haskell W, Snell P, Van Camp SP. (2005) Task Force 8: classification of sports. J Am Coll Cardiol, 45**:** 1364-1367.

Moens AL, Takimoto E, Tocchetti CG, Chakir K, Bedja D, Cormaci G, Ketner EA, Majmudar M, Gabrielson K, Halushka MK, Mitchell JB, Biswal S, Channon KM, Wolin MS, Alp NJ, Paolocci N, Champion HC, Kass DA. (2008) Reversal of cardiac hypertrophy and fibrosis from pressure overload by tetrahydrobiopterin: efficacy of recoupling nitric oxide synthase as a therapeutic strategy. Circulation, 117**:** 2626-2636.

Mohammed SF, Hussain S, Mirzoyev SA, Edwards WD, Maleszewski JJ, Redfield MM. (2015) Coronary microvascular rarefaction and myocardial fibrosis in heart failure with preserved ejection fraction. Circulation, 131**:** 550-559.

Molkentin JD, Lu JR, Antos CL, Markham B, Richardson J, Robbins J, Grant SR, Olson EN. (1998) A calcineurin-dependent transcriptional pathway for cardiac hypertrophy. Cell, 93**:** 215-228.

Munzel T, Daiber A, Mulsch A. (2005) Explaining the phenomenon of nitrate tolerance. Circ Res, 97**:** 618-628.

Muscholl MW, Schunkert H, Muders F, Elsner D, Kuch B, Hense HW, Riegger GA. (1998) Neurohormonal activity and left ventricular geometry in patients with essential arterial hypertension. Am Heart J, 135**:** 58-66.

Nagueh SF, Appleton CP, Gillebert TC, Marino PN, Oh JK, Smiseth OA, Waggoner AD, Flachskampf FA, Pellikka PA, Evangelista A. (2009) Recommendations for the evaluation of left ventricular diastolic function by echocardiography. J Am Soc Echocardiogr, 22**:** 107-133.

Nakahara T, Takata Y, Hirayama Y, Asano K, Adachi H, Shiokawa G, Sumi T, Ogawa T, Yamashina A. (2007) Left ventricular hypertrophy and geometry in untreated essential hypertension is associated with blood levels of aldosterone and procollagen type III amino-terminal peptide. Circ J, 71**:** 716-721.

Nakamura T, Ranek MJ, Lee DI, Shalkey Hahn V, Kim C, Eaton P, Kass DA. (2015) Prevention of PKG1alpha oxidation augments cardioprotection in the stressed heart. J Clin Invest, 125**:** 2468-2472.

Neri Serneri GG, Boddi M, Modesti PA, Cecioni I, Coppo M, Padeletti L, Michelucci A, Colella A, Galanti G. (2001) Increased cardiac sympathetic activity and insulin-like

growth factor-I formation are associated with physiological hypertrophy in athletes. Circ Res, 89**:** 977-982.

Nishida K, Yamaguchi O, Hirotani S, Hikoso S, Higuchi Y, Watanabe T, Takeda T, Osuka S, Morita T, Kondoh G, Uno Y, Kashiwase K, Taniike M, Nakai A, Matsumura Y, Miyazaki J, Sudo T, Hongo K, Kusakari Y, Kurihara S, Chien KR, Takeda J, Hori M, Otsu K. (2004) p38alpha mitogen-activated protein kinase plays a critical role in cardiomyocyte survival but not in cardiac hypertrophic growth in response to pressure overload. Mol Cell Biol, 24**:** 10611-10620.

Nitenberg A, Loiseau A, Antony I. (2001) Left ventricular mechanical efficiency in hypertensive patients with and without increased myocardial mass and with normal pump function. Am J Hypertens, 14**:** 1231-1238.

Ohara T, Niebel CL, Stewart KC, Charonko JJ, Pu M, Vlachos PP, Little WC. (2012) Loss of adrenergic augmentation of diastolic intra-LV pressure difference in patients with diastolic dysfunction: evaluation by color M-mode echocardiography. JACC Cardiovasc Imaging, 5**:** 861-870.

Okamoto K, Aoki K. (1963) Development of a strain of spontaneously hypertensive rats. Jpn Circ J, 27**:** 282-293.

Oláh A, Németh BT, Mátyás C, Horváth EM, Hidi L, Birtalan E, Kellermayer D, Ruppert M, Merkely G, Szabó G, Merkely B, Radovits T. (2015) Cardiac effects of acute exhaustive exercise in a rat model. Int J Cardiol, 182**:** 258-266.

Olsen MH, Wachtell K, Hermann KL, Frandsen E, Dige-Petersen H, Rokkedal J, Devereux RB, Ibsen H. (2002) Is cardiovascular remodeling in patients with essential hypertension related to more than high blood pressure? A LIFE substudy. Losartan Intervention For Endpoint-Reduction in Hypertension. Am Heart J, 144**:** 530-537.

Opdahl A, Remme EW, Helle-Valle T, Lyseggen E, Vartdal T, Pettersen E, Edvardsen T, Smiseth OA. (2009) Determinants of left ventricular early-diastolic lengthening velocity: independent contributions from left ventricular relaxation, restoring forces, and lengthening load. Circulation, 119**:** 2578-2586.

Pacher P, Beckman JS, Liaudet L. (2007) Nitric oxide and peroxynitrite in health and disease. Physiol Rev, 87**:** 315-424.

Pacher P, Nagayama T, Mukhopadhyay P, Batkai S, Kass DA. (2008) Measurement of cardiac function using pressure-volume conductance catheter technique in mice and rats. Nat Protoc, 3**:** 1422-1434.

Packer M, Coats AJ, Fowler MB, Katus HA, Krum H, Mohacsi P, Rouleau JL, Tendera M, Castaigne A, Roecker EB, Schultz MK, DeMets DL, Carvedilol Prospective Randomized Cumulative Survival Study G. (2001) Effect of carvedilol on survival in severe chronic heart failure. N Engl J Med, 344**:** 1651-1658.

Pallafacchina G, Calabria E, Serrano AL, Kalhovde JM, Schiaffino S. (2002) A protein kinase B-dependent and rapamycin-sensitive pathway controls skeletal muscle growth but not fiber type specification. Proc Natl Acad Sci U. S. A., 99**:** 9213-9218.

Palmieri V, Bella JN, Arnett DK, Liu JE, Oberman A, Schuck MY, Kitzman DW, Hopkins PN, Morgan D, Rao DC, Devereux RB. (2001) Effect of type 2 diabetes mellitus on left ventricular geometry and systolic function in hypertensive subjects: Hypertension Genetic Epidemiology Network (HyperGEN) study. Circulation, 103**:** 102-107.

Pantos C, Mourouzis I, Cokkinos DV. (2011) New insights into the role of thyroid hormone in cardiac remodeling: time to reconsider? Heart Fail Rev, 16**:** 79-96.

Pantos C, Xinaris C, Mourouzis I, Malliopoulou V, Kardami E, Cokkinos DV. (2007) Thyroid hormone changes cardiomyocyte shape and geometry via ERK signaling

pathway: potential therapeutic implications in reversing cardiac remodeling? Mol Cell Biochem, 297**:** 65-72.

Passier R, Zeng H, Frey N, Naya FJ, Nicol RL, McKinsey TA, Overbeek P, Richardson JA, Grant SR, Olson EN. (2000) CaM kinase signaling induces cardiac hypertrophy and activates the MEF2 transcription factor in vivo. J Clin Invest, 105**:** 1395-1406.

Patel JB, Valencik ML, Pritchett AM, Burnett JC, Jr., McDonald JA, Redfield MM. (2005) Cardiac-specific attenuation of natriuretic peptide A receptor activity accentuates adverse cardiac remodeling and mortality in response to pressure overload. Am J Physiol Heart Circ Physiol, 289**:** H777-784.

Paulus WJ, Tschope C. (2013) A novel paradigm for heart failure with preserved ejection fraction: comorbidities drive myocardial dysfunction and remodeling through coronary microvascular endothelial inflammation. J Am Coll Cardiol, 62**:** 263-271.

Pavlik G, Major Z, Csajagi E, Jeserich M, Kneffel Z. (2013) The athlete's heart. Part II: influencing factors on the athlete's heart: types of sports and age (review). Acta Physiol Hung, 100**:** 1-27.

Pelliccia A, Maron BJ, Spataro A, Proschan MA, Spirito P. (1991) The upper limit of physiologic cardiac hypertrophy in highly trained elite athletes. N Engl J Med, 324**:** 295-301.

Petrich BG, Gong X, Lerner DL, Wang X, Brown JH, Saffitz JE, Wang Y. (2002) c-Jun N-terminal kinase activation mediates downregulation of connexin43 in cardiomyocytes. Circ Res, 91**:** 640-647.

Pfeffer JM, Pfeffer MA, Mirsky I, Braunwald E. (1982) Regression of left ventricular hypertrophy and prevention of left ventricular dysfunction by captopril in the spontaneously hypertensive rat. Proc Natl Acad Sci U. S. A., 79**:** 3310-3314.

Pimentel DR, Amin JK, Xiao L, Miller T, Viereck J, Oliver-Krasinski J, Baliga R, Wang J, Siwik DA, Singh K, Pagano P, Colucci WS, Sawyer DB. (2001) Reactive oxygen species mediate amplitude-dependent hypertrophic and apoptotic responses to mechanical stretch in cardiac myocytes. Circ Res, 89**:** 453-460.

Pluim BM, Zwinderman AH, van der Laarse A, van der Wall EE. (2000) The athlete's heart. A meta-analysis of cardiac structure and function. Circulation, 101**:** 336-344.

Poehlman ET, Rosen CJ, Copeland KC. (1994) The influence of endurance training on insulin-like growth factor-1 in older individuals. Metabolism, 43**:** 1401-1405.

Poole-Wilson PA, Swedberg K, Cleland JG, Di Lenarda A, Hanrath P, Komajda M, Lubsen J, Lutiger B, Metra M, Remme WJ, Torp-Pedersen C, Scherhag A, Skene A, Carvedilol Or Metoprolol European Trial Investigators. (2003) Comparison of carvedilol and metoprolol on clinical outcomes in patients with chronic heart failure in the Carvedilol Or Metoprolol European Trial (COMET): randomised controlled trial. Lancet, 362**:** 7-13.

Powell-Braxton L, Hollingshead P, Warburton C, Dowd M, Pitts-Meek S, Dalton D, Gillett N, Stewart TA. (1993) IGF-I is required for normal embryonic growth in mice. Genes Dev, 7**:** 2609-2617.

Prior DL, La Gerche A. (2012) The athlete’s heart. Heart, 98**:** 947-955.

Purcell NH, Wilkins BJ, York A, Saba-El-Leil MK, Meloche S, Robbins J, Molkentin JD. (2007) Genetic inhibition of cardiac ERK1/2 promotes stress-induced apoptosis and heart failure but has no effect on hypertrophy in vivo. Proc Natl Acad Sci U. S. A., 104**:** 14074-14079.

Radovits T, Korkmaz S, Miesel-Groschel C, Seidel B, Stasch JP, Merkely B, Karck M, Szabo G. (2011) Pre-conditioning with the soluble guanylate cyclase activator

Cinaciguat reduces ischaemia-reperfusion injury after cardiopulmonary bypass. Eur J Cardiothorac Surg, 39**:** 248-255.

Radovits T, Olah A, Lux A, Nemeth BT, Hidi L, Birtalan E, Kellermayer D, Matyas C, Szabo G, Merkely B. (2013) Rat model of exercise-induced cardiac hypertrophy: hemodynamic characterization using left ventricular pressure-volume analysis. Am J Physiol Heart Circ Physiol, 305**:** H124-134.

Raff GL, Glantz SA. (1981) Volume loading slows left ventricular isovolumic relaxation rate. Evidence of load-dependent relaxation in the intact dog heart. Circ Res, 48**:** 813-824.

Rainer PP, Kass DA. (2016) Old dog, new tricks: novel cardiac targets and stress regulation by protein kinase G. Cardiovasc Res, 111**:** 154-162.

Rakowski H, Appleton C, Chan KL, Dumesnil JG, Honos G, Jue J, Koilpillai C, Lepage S, Martin RP, Mercier LA, O'Kelly B, Prieur T, Sanfilippo A, Sasson Z, Alvarez N, Pruitt R, Thompson C, Tomlinson C. (1996) Canadian consensus recommendations for the measurement and reporting of diastolic dysfunction by echocardiography: from the Investigators of Consensus on Diastolic Dysfunction by Echocardiography. J Am Soc Echocardiogr, 9**:** 736-760.

Ranek MJ, Terpstra EJ, Li J, Kass DA, Wang X. (2013) Protein kinase g positively regulates proteasome-mediated degradation of misfolded proteins. Circulation, 128**:** 365-376.

Rapp JP, Dene H. (1985) Development and characteristics of inbred strains of Dahl salt-sensitive and salt-resistant rats. Hypertension, 7**:** 340-349.

Ren J, Zhang S, Kovacs A, Wang Y, Muslin AJ. (2005) Role of p38alpha MAPK in cardiac apoptosis and remodeling after myocardial infarction. J Mol Cell Cardiol, 38**:** 617-623.

Richand V, Lafitte S, Reant P, Serri K, Lafitte M, Brette S, Kerouani A, Chalabi H, Dos Santos P, Douard H, Roudaut R. (2007) An ultrasound speckle tracking (two-dimensional strain) analysis of myocardial deformation in professional soccer players compared with healthy subjects and hypertrophic cardiomyopathy. Am J Cardiol, 100**:** 128-132.

Rimbaud S, Garnier A, Ventura-Clapier R. (2009) Mitochondrial biogenesis in cardiac pathophysiology. Pharmacol Rep, 61**:** 131-138.

Ross J, Jr. (1997) On variations in the cardiac hypertrophic response to pressure overload. Circulation, 95**:** 1349-1351.

Sack MN, Fyhrquist FY, Saijonmaa OJ, Fuster V, Kovacic JC. (2017) Basic Biology of Oxidative Stress and the Cardiovascular System: Part 1 of a 3-Part Series. J Am Coll Cardiol, 70**:** 196-211.

Saltiel AR, Kahn CR. (2001) Insulin signalling and the regulation of glucose and lipid metabolism. Nature, 414**:** 799-806.

Samuelsson AM, Bollano E, Mobini R, Larsson BM, Omerovic E, Fu M, Waagstein F, Holmang A. (2006) Hyperinsulinemia: effect on cardiac mass/function, angiotensin II receptor expression, and insulin signaling pathways. Am J Physiol Heart Circ Physiol, 291**:** H787-796.

Sandler H, Dodge HT. (1963) Left Ventricular Tension and Stress in Man. Circ Res, 13**:** 91-104.

Sano M, Minamino T, Toko H, Miyauchi H, Orimo M, Qin Y, Akazawa H, Tateno K, Kayama Y, Harada M, Shimizu I, Asahara T, Hamada H, Tomita S, Molkentin JD, Zou Y, Komuro I. (2007) p53-induced inhibition of Hif-1 causes cardiac dysfunction during pressure overload. Nature, 446**:** 444-448.

Sartoretto JL, Jin BY, Bauer M, Gertler FB, Liao R, Michel T. (2009) Regulation of VASP phosphorylation in cardiac myocytes: differential regulation by cyclic nucleotides and modulation of protein expression in diabetic and hypertrophic heart. Am J Physiol Heart Circ Physiol, 297**:** H1697-1710.

Sawabe T, Chiba T, Kobayashi A, Nagasaka K, Aihara K, Takaya A. (2019) A novel soluble guanylate cyclase activator with reduced risk of hypotension by short-acting vasodilation. Pharmacol Res Perspect, 7**:** e00463.

Schaeffer PJ, Desantiago J, Yang J, Flagg TP, Kovacs A, Weinheimer CJ, Courtois M, Leone TC, Nichols CG, Bers DM, Kelly DP. (2009) Impaired contractile function and calcium handling in hearts of cardiac-specific calcineurin b1-deficient mice. Am J Physiol Heart Circ Physiol, 297**:** H1263-1273.

Scharf M, Brem MH, Wilhelm M, Schoepf UJ, Uder M, Lell MM. (2010a) Atrial and ventricular functional and structural adaptations of the heart in elite triathletes assessed with cardiac MR imaging. Radiology, 257**:** 71-79.

Scharf M, Brem MH, Wilhelm M, Schoepf UJ, Uder M, Lell MM. (2010b) Cardiac magnetic resonance assessment of left and right ventricular morphologic and functional adaptations in professional soccer players. Am Heart J, 159**:** 911-918.

Scharhag J, Schneider G, Urhausen A, Rochette V, Kramann B, Kindermann W. (2002) Athlete's heart: right and left ventricular mass and function in male endurance athletes and untrained individuals determined by magnetic resonance imaging. J Am Coll Cardiol, 40**:** 1856-1863.

Schmidt-Trucksass A, Schmid A, Haussler C, Huber G, Huonker M, Keul J. (2001) Left ventricular wall motion during diastolic filling in endurance-trained athletes. Med Sci Sports Exerc, 33**:** 189-195.

Schmidt HH, Schmidt PM, Stasch JP. (2009) NO- and haem-independent soluble guanylate cyclase activators. Handb Exp Pharmacol**:** 309-339.

Schnell F, Donal E, Bernard-Brunet A, Reynaud A, Wilson MG, Thebault C, Ridard C, Mabo P, Carre F. (2013) Strain analysis during exercise in patients with left ventricular hypertrophy: impact of etiology. J Am Soc Echocardiogr, 26**:** 1163-1169.

Schunkert H, Dzau VJ, Tang SS, Hirsch AT, Apstein CS, Lorell BH. (1990) Increased rat cardiac angiotensin converting enzyme activity and mRNA expression in pressure overload left ventricular hypertrophy. Effects on coronary resistance, contractility, and relaxation. J Clin Invest, 86**:** 1913-1920.

Sehgal S, Drazner MH. (2007) Left ventricular geometry: does shape matter? Am Heart J, 153**:** 153-155.

Selby DE, Palmer BM, LeWinter MM, Meyer M. (2011) Tachycardia-induced diastolic dysfunction and resting tone in myocardium from patients with a normal ejection fraction. J Am Coll Cardiol, 58**:** 147-154.

Seliger SL, de Lemos J, Neeland IJ, Christenson R, Gottdiener J, Drazner MH, Berry J, Sorkin J, deFilippi C. (2015) Older Adults, "Malignant" Left Ventricular Hypertrophy, and Associated Cardiac-Specific Biomarker Phenotypes to Identify the Differential Risk of New-Onset Reduced Versus Preserved Ejection Fraction Heart Failure: CHS (Cardiovascular Health Study). JACC Heart Fail, 3**:** 445-455.

Sena S, Hu P, Zhang D, Wang X, Wayment B, Olsen C, Avelar E, Abel ED, Litwin SE. (2009) Impaired insulin signaling accelerates cardiac mitochondrial dysfunction after myocardial infarction. J Mol Cell Cardiol, 46**:** 910-918.

Seo K, Rainer PP, Lee DI, Hao S, Bedja D, Birnbaumer L, Cingolani OH, Kass DA. (2014) Hyperactive adverse mechanical stress responses in dystrophic heart are coupled

to transient receptor potential canonical 6 and blocked by cGMP-protein kinase G modulation. Circ Res, 114**:** 823-832.

Seymour AM, Giles L, Ball V, Miller JJ, Clarke K, Carr CA, Tyler DJ. (2015) In vivo assessment of cardiac metabolism and function in the abdominal aortic banding model of compensated cardiac hypertrophy. Cardiovasc Res, 106**:** 249-260.

Shah AM, Claggett B, Sweitzer NK, Shah SJ, Anand IS, O'Meara E, Desai AS, Heitner JF, Li G, Fang J, Rouleau J, Zile MR, Markov V, Ryabov V, Reis G, Assmann SF, McKinlay SM, Pitt B, Pfeffer MA, Solomon SD. (2014) Cardiac structure and function and prognosis in heart failure with preserved ejection fraction: findings from the echocardiographic study of the Treatment of Preserved Cardiac Function Heart Failure with an Aldosterone Antagonist (TOPCAT) Trial. Circ Heart Fail, 7**:** 740-751.

Shah AM, Solomon SD. (2012) Myocardial deformation imaging: current status and future directions. Circulation, 125**:** e244-248.

Sharma S, Maron BJ, Whyte G, Firoozi S, Elliott PM, McKenna WJ. (2002) Physiologic limits of left ventricular hypertrophy in elite junior athletes: relevance to differential diagnosis of athlete's heart and hypertrophic cardiomyopathy. J Am Coll Cardiol, 40**:** 1431-1436.

Sharp WW, Simpson DG, Borg TK, Samarel AM, Terracio L. (1997) Mechanical forces regulate focal adhesion and costamere assembly in cardiac myocytes. Am J Physiol, 273**:** H546-556.

Shibata S, Hastings JL, Prasad A, Fu Q, Bhella PS, Pacini E, Krainski F, Palmer MD, Zhang R, Levine BD. (2011) Congestive heart failure with preserved ejection fraction is associated with severely impaired dynamic Starling mechanism. J Appl Physiol (1985), 110**:** 964-971.

Shimizu I, Minamino T. (2016) Physiological and pathological cardiac hypertrophy. J Mol Cell Cardiol, 97**:** 245-262.

Shimizu I, Minamino T, Toko H, Okada S, Ikeda H, Yasuda N, Tateno K, Moriya J, Yokoyama M, Nojima A, Koh GY, Akazawa H, Shiojima I, Kahn CR, Abel ED, Komuro I. (2010) Excessive cardiac insulin signaling exacerbates systolic dysfunction induced by pressure overload in rodents. J Clin Invest, 120**:** 1506-1514.

Shimizu I, Yoshida Y, Katsuno T, Tateno K, Okada S, Moriya J, Yokoyama M, Nojima A, Ito T, Zechner R, Komuro I, Kobayashi Y, Minamino T. (2012) p53-induced adipose tissue inflammation is critically involved in the development of insulin resistance in heart failure. Cell Metab, 15**:** 51-64.

Shioi T, Kang PM, Douglas PS, Hampe J, Yballe CM, Lawitts J, Cantley LC, Izumo S. (2000) The conserved phosphoinositide 3-kinase pathway determines heart size in mice. EMBO J, 19**:** 2537-2548.

Shioi T, McMullen JR, Kang PM, Douglas PS, Obata T, Franke TF, Cantley LC, Izumo S. (2002) Akt/protein kinase B promotes organ growth in transgenic mice. Mol Cell Biol, 22**:** 2799-2809.

Shioi T, McMullen JR, Tarnavski O, Converso K, Sherwood MC, Manning WJ, Izumo S. (2003) Rapamycin attenuates load-induced cardiac hypertrophy in mice. Circulation, 107**:** 1664-1670.

Silver MA, Pick R, Brilla CG, Jalil JE, Janicki JS, Weber KT. (1990) Reactive and reparative fibrillar collagen remodelling in the hypertrophied rat left ventricle: two experimental models of myocardial fibrosis. Cardiovasc Res, 24**:** 741-747.

Simpson DG, Majeski M, Borg TK, Terracio L. (1999) Regulation of cardiac myocyte protein turnover and myofibrillar structure in vitro by specific directions of stretch. Circ Res, 85**:** e59-69.

Simsek Z, Hakan Tas M, Degirmenci H, Gokhan Yazici A, Ipek E, Duman H, Gundogdu F, Karakelleoglu S, Senocak H. (2013) Speckle tracking echocardiographic analysis of left ventricular systolic and diastolic functions of young elite athletes with eccentric and concentric type of cardiac remodeling. Echocardiography, 30**:** 1202-1208.

Spinale FG. (2007) Myocardial matrix remodeling and the matrix metalloproteinases: influence on cardiac form and function. Physiol Rev, 87**:** 1285-1342.

Spirito P, Pelliccia A, Proschan MA, Granata M, Spataro A, Bellone P, Caselli G, Biffi A, Vecchio C, Maron BJ. (1994) Morphology of the "athlete's heart" assessed by echocardiography in 947 elite athletes representing 27 sports. Am J Cardiol, 74**:** 802-806.

Stasch JP, Schlossmann J, Hocher B. (2015) Renal effects of soluble guanylate cyclase stimulators and activators: A review of the preclinical evidence. Curr Opin Pharmacol, 21**:** 95-104.

Stasch JP, Hobbs AJ. (2009) NO-independent, haem-dependent soluble guanylate cyclase stimulators. Handb Exp Pharmacol**:** 277-308.

Stasch JP, Pacher P, Evgenov OV. (2011) Soluble guanylate cyclase as an emerging therapeutic target in cardiopulmonary disease. Circulation, 123**:** 2263-2273.

Stasch JP, Schmidt P, Alonso-Alija C, Apeler H, Dembowsky K, Haerter M, Heil M, Minuth T, Perzborn E, Pleiss U, Schramm M, Schroeder W, Schroder H, Stahl E, Steinke W, Wunder F. (2002) NO- and haem-independent activation of soluble guanylyl cyclase: molecular basis and cardiovascular implications of a new pharmacological principle. Br J Pharmacol, 136**:** 773-783.

Steinberg BA, Zhao X, Heidenreich PA, Peterson ED, Bhatt DL, Cannon CP, Hernandez AF, Fonarow GC. (2012) Trends in patients hospitalized with heart failure

and preserved left ventricular ejection fraction: prevalence, therapies, and outcomes. Circulation, 126**:** 65-75.

Stubbe P, Gatz J, Heidemann P, Muhlen A, Hesch R. (1978) Thyroxine-binding globulin, triiodothyronine, thyroxine and thyrotropin in newborn infants and children. Horm Metab Res, 10**:** 58-61.

Suga H, Hayashi T, Shirahata M. (1981) Ventricular systolic pressure-volume area as predictor of cardiac oxygen consumption. Am J Physiol, 240**:** H39-44.

Sunagawa K, Maughan WL, Burkhoff D, Sagawa K. (1983) Left ventricular interaction with arterial load studied in isolated canine ventricle. Am J Physiol, 245**:** H773-780.

Swynghedauw B. (2006) Phenotypic plasticity of adult myocardium: molecular mechanisms. J Exp Biol, 209**:** 2320-2327.

Tagawa H, Koide M, Sato H, Zile MR, Carabello BA, Cooper G 4th. (1998) Cytoskeletal role in the transition from compensated to decompensated hypertrophy during adult canine left ventricular pressure overloading. Circ Res, 82**:** 751-761.

Takeda N, Manabe I, Uchino Y, Eguchi K, Matsumoto S, Nishimura S, Shindo T, Sano M, Otsu K, Snider P, Conway SJ, Nagai R. (2010) Cardiac fibroblasts are essential for the adaptive response of the murine heart to pressure overload. J Clin Invest, 120**:** 254-265.

Takimoto E, Champion HC, Li MX, Belardi D, Ren SX, Rodriguez ER, Bedja D, Gabrielson KL, Wang YB, Kass DA. (2005a) Chronic inhibition of cyclic GMP phosphodiesterase 5A prevents and reverses cardiac hypertrophy. Nat Med, 11**:** 214-222.

Takimoto E, Champion HC, Li MX, Ren SX, Rodriguez ER, Tavazzi B, Lazzarino G, Paolocci N, Gabrielson KL, Wang YB, Kass DA. (2005b) Oxidant stress from nitric

oxide synthase-3 uncoupling stimulates cardiac pathologic remodeling from chronic pressure load. J Clin Invest, 115**:** 1221-1231.

Takimoto E, Koitabashi N, Hsu S, Ketner EA, Zhang M, Nagayarna T, Bedja D, Gabrielson KL, Blanton R, Siderovski DP, Mendelsohn ME, Kass DA. (2009) Regulator of G protein signaling 2 mediates cardiac compensation to pressure overload and antihypertrophic effects of PDE5 inhibition in mice. J Clin Invest, 119**:** 408-420.

Tamura N, Ogawa Y, Chusho H, Nakamura K, Nakao K, Suda M, Kasahara M, Hashimoto R, Katsuura G, Mukoyama M, Itoh H, Saito Y, Tanaka I, Otani H, Katsuki M. (2000) Cardiac fibrosis in mice lacking brain natriuretic peptide. Proc Natl Acad Sci U. S. A., 97**:** 4239-4244.

Tan YT, Wenzelburger F, Lee E, Heatlie G, Leyva F, Patel K, Frenneaux M, Sanderson JE. (2009) The pathophysiology of heart failure with normal ejection fraction: exercise echocardiography reveals complex abnormalities of both systolic and diastolic ventricular function involving torsion, untwist, and longitudinal motion. J Am Coll Cardiol, 54**:** 36-46.

Tatar M, Bartke A, Antebi A. (2003) The endocrine regulation of aging by insulin-like signals. Science, 299**:** 1346-1351.

Terentyev D, Gyorke I, Belevych AE, Terentyeva R, Sridhar A, Nishijima Y, de Blanco EC, Khanna S, Sen CK, Cardounel AJ, Carnes CA, Gyorke S. (2008) Redox modification of ryanodine receptors contributes to sarcoplasmic reticulum Ca^{2+} leak in chronic heart failure. Circ Res, 103**:** 1466-1472.

Thiedemann KU, Holubarsch C, Medugorac I, Jacob R. (1983) Connective tissue content and myocardial stiffness in pressure overload hypertrophy. A combined study of morphologic, morphometric, biochemical, and mechanical parameters. Basic Res Cardiol, 78**:** 140-155.

Toischer K, Rokita AG, Unsold B, Zhu W, Kararigas G, Sossalla S, Reuter SP, Becker A, Teucher N, Seidler T, Grebe C, Preuss L, Gupta SN, Schmidt K, Lehnart SE, Kruger M, Linke WA, Backs J, Regitz-Zagrosek V, Schafer K, Field LJ, Maier LS, Hasenfuss G. (2010) Differential cardiac remodeling in preload versus afterload. Circulation, 122**:** 993-1003.

Touyz RM, Mercure C, He Y, Javeshghani D, Yao G, Callera GE, Yogi A, Lochard N, Reudelhuber TL. (2005) Angiotensin II-dependent chronic hypertension and cardiac hypertrophy are unaffected by gp91phox-containing NADPH oxidase. Hypertension, 45**:** 530-537.

Troncoso R, Ibarra C, Vicencio JM, Jaimovich E, Lavandero S. (2014) New insights into IGF-1 signaling in the heart. Trends Endocrinol Metab, 25**:** 128-137.

Tsai EJ, Kass DA. (2009) Cyclic GMP signaling in cardiovascular pathophysiology and therapeutics. Pharmacol Ther, 122**:** 216-238.

Tsai EJ, Liu Y, Koitabashi N, Bedja D, Danner T, Jasmin J-F, Lisanti MP, Friebe A, Takimoto E, Kass DA. (2012) Pressure-overload-induced subcellular relocalization/oxidation of soluble guanylyl cyclase in the heart modulates enzyme stimulation. Circ Res, 110**:** 295-303.

Tsuji T, del Monte F, Yoshikawa Y, Abe T, Shimizu J, Nakajima-Takenaka C, Taniguchi S, Hajjar RJ, Takaki M. (2009) Rescue of Ca^{2+} overload-induced left ventriclur dysfunction by targeted ablation of phospholamban. Am J Physiol Heart Circ Physiol, 296**:** H310-H317.

Ungvari Z, Csiszar A. (2012) The emerging role of IGF-1 deficiency in cardiovascular aging: recent advances. J Gerontol A Biol Sci Med Sci, 67**:** 599-610.

Utomi V, Oxborough D, Whyte GP, Somauroo J, Sharma S, Shave R, Atkinson G, George K. (2013) Systematic review and meta-analysis of training mode, imaging

modality and body size influences on the morphology and function of the male athlete's heart. Heart, 99**:** 1727-1733.

Valko M, Leibfritz D, Moncol J, Cronin MT, Mazur M, Telser J. (2007) Free radicals and antioxidants in normal physiological functions and human disease. Int J Biochem Cell Biol, 39**:** 44-84.

van de Weijer T, van Ewijk PA, Zandbergen HR, Slenter JM, Kessels AG, Wildberger JE, Hesselink MKC, Schrauwen P, Schrauwen-Hinderling VB, Kooi ME. (2012) Geometrical models for cardiac MRI in rodents: comparison of quantification of left ventricular volumes and function by various geometrical models with a full-volume MRI data set in rodents. Am J Physiol Heart Circ Physiol, 302**:** H709-H715.

van Rooij E, Sutherland LB, Qi X, Richardson JA, Hill J, Olson EN. (2007) Control of stress-dependent cardiac growth and gene expression by a microRNA. Science, 316**:** 575-579

Velagaleti RS, Gona P, Levy D, Aragam J, Larson MG, Tofler GH, Lieb W, Wang TJ, Benjamin EJ, Vasan RS. (2008) Relations of biomarkers representing distinct biological pathways to left ventricular geometry. Circulation, 118**:** 2252-2258.

Villari B, Vassalli G, Monrad ES, Chiariello M, Turina M, Hess OM. (1995) Normalization of diastolic dysfunction in aortic stenosis late after valve replacement. Circulation, 91**:** 2353-2358.

Vinciguerra M, Santini MP, Claycomb WC, Ladurner AG, Rosenthal N. (2009) Local IGF-1 isoform protects cardiomyocytes from hypertrophic and oxidative stresses via SirT1 activity. Aging (Albany, NY), 2**:** 43-62.

Vinciguerra M, Santini MP, Martinez C, Pazienza V, Claycomb WC, Giuliani A, Rosenthal N. (2012) mIGF-1/JNK1/SirT1 signaling confers protection against oxidative stress in the heart. Aging Cell, 11**:** 139-149.

Wagner S, Ruff HM, Weber SL, Bellmann S, Sowa T, Schulte T, Anderson ME, Grandi E, Bers DM, Backs J, Belardinelli L, Maier LS. (2011) Reactive oxygen species-activated Ca/calmodulin kinase IIdelta is required for late I(Na) augmentation leading to cellular Na and Ca overload. Circ Res, 108**:** 555-565.

Wang J, Khoury DS, Yue Y, Torre-Amione G, Nagueh SF. (2008) Preserved left ventricular twist and circumferential deformation, but depressed longitudinal and radial deformation in patients with diastolic heart failure. Eur Heart J, 29**:** 1283-1289.

Wang Y, Su B, Sah VP, Brown JH, Han J, Chien KR. (1998) Cardiac hypertrophy induced by mitogen-activated protein kinase kinase 7, a specific activator for c-Jun NH2-terminal kinase in ventricular muscle cells. J Biol Chem, 273**:** 5423-5426.

Wang Y, Wisloff U, Kemi OJ. (2010) Animal models in the study of exercise-induced cardiac hypertrophy. Physiol Res, 59**:** 633-644.

Weeks KL, McMullen JR. (2011) The athlete's heart vs. the failing heart: can signaling explain the two distinct outcomes? Physiology (Bethesda), 26**:** 97-105.

Weiner RB, Baggish AL. (2012) Exercise-induced cardiac remodeling. Prog Cardiovasc Dis, 54**:** 380-386.

Weiss MB, Ellis K, Sciacca RR, Johnson LL, Schmidt DH, Cannon PJ. (1976) Myocardial blood flow in congestive and hypertrophic cardiomyopathy: relationship to peak wall stress and mean velocity of circumferential fiber shortening. Circulation, 54**:** 484-494.

Wilhelm M, Roten L, Tanner H, Schmid JP, Wilhelm I, Saner H. (2012) Long-term cardiac remodeling and arrhythmias in nonelite marathon runners. Am J Cardiol, 110**:** 129-135.

Wilkins BJ, Dai YS, Bueno OF, Parsons SA, Xu J, Plank DM, Jones F, Kimball TR, Molkentin JD. (2004) Calcineurin/NFAT coupling participates in pathological, but not physiological, cardiac hypertrophy. Circ Res, 94**:** 110-118.

Witteles RM, Tang WH, Jamali AH, Chu JW, Reaven GM, Fowler MB. (2004) Insulin resistance in idiopathic dilated cardiomyopathy: a possible etiologic link. J Am Coll Cardiol, 44**:** 78-81.

Wu X, Eder P, Chang B, Molkentin JD. (2010) TRPC channels are necessary mediators of pathologic cardiac hypertrophy. Proc Natl Acad Sci U. S. A., 107**:** 7000-7005.

Yamaguchi O, Higuchi Y, Hirotani S, Kashiwase K, Nakayama H, Hikoso S, Takeda T, Watanabe T, Asahi M, Taniike M, Matsumura Y, Tsujimoto I, Hongo K, Kusakari Y, Kurihara S, Nishida K, Ichijo H, Hori M, Otsu K. (2003) Targeted deletion of apoptosis signal-regulating kinase 1 attenuates left ventricular remodeling. Proc Natl Acad Sci U. S. A., 100**:** 15883-15888.

Yamaguchi O, Watanabe T, Nishida K, Kashiwase K, Higuchi Y, Takeda T, Hikoso S, Hirotani S, Asahi M, Taniike M, Nakai A, Tsujimoto I, Matsumura Y, Miyazaki J, Chien KR, Matsuzawa A, Sadamitsu C, Ichijo H, Baccarini M, Hori M, Otsu K. (2004) Cardiac-specific disruption of the c-raf-1 gene induces cardiac dysfunction and apoptosis. J Clin Invest, 114**:** 937-943.

Yamashita K, Kajstura J, Discher DJ, Wasserlauf BJ, Bishopric NH, Anversa P, Webster KA. (2001) Reperfusion-activated Akt kinase prevents apoptosis in transgenic mouse hearts overexpressing insulin-like growth factor-1. Circ Res, 88**:** 609-614.

Yasoda A, Komatsu Y, Chusho H, Miyazawa T, Ozasa A, Miura M, Kurihara T, Rogi T, Tanaka S, Suda M, Tamura N, Ogawa Y, Nakao K. (2004) Overexpression of CNP in chondrocytes rescues achondroplasia through a MAPK-dependent pathway. Nat Med, 10**:** 80-86.

Yin FC, Spurgeon HA, Rakusan K, Weisfeldt ML, Lakatta EG. (1982) Use of tibial length to quantify cardiac hypertrophy: application in the aging rat. Am J Physiol, 243**:** H941-947.

Yin H, Zhang J, Lin H, Wang R, Qiao Y, Wang B, Liu F. (2008) p38 mitogen-activated protein kinase inhibition decreases TNFalpha secretion and protects against left ventricular remodeling in rats with myocardial ischemia. Inflammation, 31**:** 65-73.

Zabalgoitia M, Berning J, Koren MJ, Stoylen A, Nieminen MS, Dahlof B, Devereux RB, Investigators LS. (2001) Impact of coronary artery disease on left ventricular systolic function and geometry in hypertensive patients with left ventricular hypertrophy (the LIFE study). Am J Cardiol, 88**:** 646-650.

Zarain-Herzberg A, Fragoso-Medina J, Estrada-Aviles R. (2011) Calcium-regulated transcriptional pathways in the normal and pathologic heart. IUBMB Life, 63**:** 847-855.

Zhang S, Weinheimer C, Courtois M, Kovacs A, Zhang CE, Cheng AM, Wang Y, Muslin AJ. (2003) The role of the Grb2-p38 MAPK signaling pathway in cardiac hypertrophy and fibrosis. J Clin Invest, 111**:** 833-841.

Zhang X, Javan H, Li L, Szucsik A, Zhang R, Deng Y, Selzman CH. (2013) A modified murine model for the study of reverse cardiac remodelling. Exp Clin Cardiol, 18**:** e115-117.

Zhao W, Choi JH, Hong GR, Vannan MA. (2008) Left ventricular relaxation. Heart Fail Clin, 4**:** 37-46.

Zheng M, Dilly K, Dos Santos Cruz J, Li M, Gu Y, Ursitti JA, Chen J, Ross J, Jr., Chien KR, Lederer JW, Wang Y. (2004) Sarcoplasmic reticulum calcium defect in Ras-induced hypertrophic cardiomyopathy heart. Am J Physiol Heart Circ Physiol, 286**:** H424-433.

Zhu W, Zou Y, Shiojima I, Kudoh S, Aikawa R, Hayashi D, Mizukami M, Toko H, Shibasaki F, Yazaki Y, Nagai R, Komuro I. (2000) Ca^{2+}/calmodulin-dependent kinase II and calcineurin play critical roles in endothelin-1-induced cardiomyocyte hypertrophy. J Biol Chem, 275**:** 15239-15245.

Zile MR, Brutsaert DL. (2002a) New concepts in diastolic dysfunction and diastolic heart failure: Part I: diagnosis, prognosis, and measurements of diastolic function. Circulation, 105**:** 1387-1393.

Zile MR, Brutsaert DL. (2002b) New concepts in diastolic dysfunction and diastolic heart failure: Part II: causal mechanisms and treatment. Circulation, 105**:** 1503-1508.

Zima AV, Blatter LA. (2006) Redox regulation of cardiac calcium channels and transporters. Cardiovasc Res, 71**:** 310-321.

11. List of publications

11.1. Publications related to the dissertation

Németh BT, Mátyás C, Oláh A, Lux Á, Hidi L, Ruppert M, Kellermayer D, Kökény G, Szabó G, Merkely B, Radovits T. (2016) Cinaciguat prevents the development of pathologic hypertrophy in a rat model of left ventricular pressure overload. Sci Rep, 6**:** 37166.
IF_{2016}: 4.259

Oláh A, **Németh BT**, Mátyás C, Hidi L, Lux Á, Ruppert M, Kellermayer D, Sayour AA, Szabó L, Török M, Meltzer A, Gellér L, Merkely B, Radovits T. (2016) Physiological and pathological left ventricular hypertrophy of comparable degree is associated with characteristic differences of in vivo hemodynamics. Am J Physiol Heart Circ Physiol, 310**:** H587-97.
IF_{2016}: 3.348

Oláh A, Sayour AA, **Németh BT**, Mátyás Cs, Hidi L, Lux Á, Ruppert M, Kellermayer D, Szabó L, Török M, Meltzer A, Gellér L, Merkely B, Radovits T. (2018) A hasonló fokú fiziológiás és patológiás balkamra-hipertrófia különböző in vivo hemodinamikai következményekhez vezet. Cardiol Hung, 48**:** 20-30.

Németh BT, Mátyás Cs, Oláh A, Lux Á, Hidi L, Ruppert M, Kellermayer D, Kökény G, Szabó G, Merkely B, Radovits T. (2017) A cinaciguat megelőzi a patológiás szívizom-hipertrófia kialakulását bal kamrai nyomás-túlterhelés patkánymodelljén. Cardiol Hung, 47**:** 183-194.

11.2. Publications not related to the dissertation

Ruppert M, Korkmaz-Icöz S, Li S, Brlecic P, **Németh BT**, Oláh A, Horváth EM, Veres G, Pleger S, Grabe N, Merkely B, Karck M, Radovits T, Szabó G. (2019) Comparison of the Reverse-Remodeling Effect of Pharmacological Soluble Guanylate Cyclase

Activation With Pressure Unloading in Pathological Myocardial Left Ventricular Hypertrophy. Front Physiol, 9**:** 1869.
IF_{2017}: 3.394

Varga ZV, Erdelyi K, Paloczi J, Cinar R, Zsengeller ZK, Jourdan T, Matyas C, **Nemeth BT**, Guillot A, Xiang X, Mehal A, Hasko G, Stillman IE, Rosen S, Gao B, Kunos G, Pacher P. (2018) Disruption of renal arginine metabolism promotes kidney injury in hepatorenal syndrome. Hepatology, 68**:** 1519-1533.
IF_{2017}: 14.079

Mátyás C, Kovács A, **Németh BT**, Oláh A, Braun S, Tokodi M, Barta BA, Benke K, Ruppert M, Lakatos BK, Merkely B, Radovits T. (2018) Comparison of speckle-tracking echocardiography with invasive hemodynamics for the detection of characteristic cardiac dysfunction in type-1 and type-2 diabetes mellitus. Cardiovasc Diabetol, 17**:** 13.
IF_{2017}: 5.235

Ouyang X, Han SN, Zhang JY, **Nemeth BT**, Pacher P, Feng D, Bataller R, Cabezas J, Stärkel P, Caballeria J, LePine Pongratz R, Cai SY, Schnabl B, Hoque R, Chen Y, Yang W, Martinez IG, Wang FS, Gao B, Torok NJ, Kibbey RG, Mehal WZ. (2018) Digoxin Suppresses Pyruvate Kinase M2 Promoted HIF-1α Transactivation in Steatohepatitis. Cell Metab, 27**:** 339-350.
IF_{2017}: 20.565

Varga ZV, Matyas C, Erdelyi K, Cinar R, Nieri D, Chicca A, **Nemeth BT**, Paloczi J, Lajtos T, Corey L, Hasko G, Gao B, Kunos G, Gertsch J, Pacher P. (2018) Beta-caryophyllene protects against alcoholic steatohepatitis by attenuating inflammation and metabolic dysregulation in mice. Br J Pharmacol, 175**:** 320-334.
IF_{2017}: 6.810

Benke K, Matyas C, Sayour AA, Oláh A, **Németh BT**, Ruppert M, Szabo G, Kökény G, Horváth EM, Hartyánszky I, Szabolcs Z, Merkely B, Radovits T. (2017) Pharmacological preconditioning with gemfibrozil preserves cardiac function after heart transplantation. Sci Rep, 7**:** 14232.
IF_{2017}: 4.122

Nemeth BT, Varga ZV, Wu WJ, Pacher P. (2017) Trastuzumab cardiotoxicity: from clinical trials to experimental studies. Br J Pharmacol, 174**:** 3727-3748.
IF_{2017}: 6.810

Mátyás C, **Németh BT**, Oláh A, Török M, Ruppert M, Kellermayer D, Barta BA, Szabó G, Kökény G, Horváth EM, Bódi B, Papp Z, Merkely B, Radovits T. (2017) Prevention of the development of heart failure with preserved ejection fraction by the phosphodiesterase-5A inhibitor vardenafil in rats with type 2 diabetes. Eur J Heart Fail, 19**:** 326-336.
IF_{2017}: 10.683

Mukhopadhyay P, Horváth B, Rajesh M, Varga ZV, Gariani K, Ryu D, Cao Z, Holovac E, Park O, Zhou Z, Xu MJ, Wang W, Godlewski G, Paloczi J, **Nemeth BT**, Persidsky Y, Liaudet L, Haskó G, Bai P, Hamid Boulares A, Auwerx J, Gao B, Pacher P. (2017) PARP inhibition protects against alcoholic and nonalcoholic steatohepatitis. J Hepatol, 66**:** 589-600.
IF_{2017}: 14.911

Benke K, Sayour AA, Mátyás C, Ágg B, **Németh BT**, Oláh A, Ruppert M, Hartyánszky I, Szabolcs Z, Radovits T, Merkely B, Szabó G. (2017) Heterotopic Abdominal Rat Heart Transplantation as a Model to Investigate Volume Dependency of Myocardial Remodeling. Transplantation, 101**:** 498-505.
IF_{2017}: 3.960

Oláh A, Kellermayer D, Mátyás C, **Németh BT**, Lux Á, Szabó L, Török M, Ruppert M, Meltzer A, Sayour AA, Benke K, Hartyánszky I, Merkely B, Radovits T. (2017) Complete Reversion of Cardiac Functional Adaptation Induced by Exercise Training. Med Sci Sports Exerc, 49**:** 420-429.
IF_{2017}: 4.291

Ruppert M, Korkmaz-Icöz S, Li S, **Németh BT**, Hegedűs P, Brlecic P, Mátyás C, Zorn M, Merkely B, Karck M, Radovits T, Szabó G. (2016) Myocardial reverse remodeling after pressure unloading is associated with maintained cardiac mechanoenergetics in a rat model of left ventricular hypertrophy. Am J Physiol Heart Circ Physiol, 311**:** H592-603.
IF_{2016}: 3.348

Matyas C, Varga ZV, Mukhopadhyay P, Paloczi J, Lajtos T, Erdelyi K, **Nemeth BT**, Nan M, Hasko G, Gao B, Pacher P. (2016) Chronic plus binge ethanol feeding induces myocardial oxidative stress, mitochondrial and cardiovascular dysfunction, and steatosis. Am J Physiol Heart Circ Physiol, 310**:** H1658-1670.
IF_{2016}: 3.348

Mátyás Cs, **Németh BT**, Oláh A, Hidi L, Birtalan E, Kellermayer D, Ruppert M, Korkmaz S, Kökény G, Horváth EM, Szabó G, Merkely B, Radovits T. (2015) The soluble guanylate cyclase activator cinaciguat prevents cardiac dysfunction in a rat model of type-1 diabetes mellitus. Cardiovasc Diabetol, 14**:** 145.
IF_{2015}: 4.534

Kovács A, Oláh A, Lux Á, Mátyás Cs, **Németh BT**, Kellermayer D, Ruppert M, Török M, Szabó L, Assabiny A, Birtalan E, Merkely B, Radovits T. (2015) Strain and strain rate by speckle tracking echocardiography correlate with pressure-volume loop derived contractility indices in a rat model of athlete's heart. Am J Physiol Heart Circ Physiol, 308**:** H743-748.
IF_{2015}: 3.324

Oláh A, **Németh BT**, Mátyás Cs, Horváth EM, Hidi L, Birtalan E, Kellermayer D, Ruppert M, Merkely G, Szabó G, Merkely B, Radovits T. (2015) Cardiac effects of acute exhaustive exercise in a rat model. Int J Cardiol, 182**:** 258-266.
IF_{2015}: 4.638

Radovits T, Korkmaz S, Mátyás Cs, Oláh A, **Németh BT**, Páli Sz, Hirschberg K, Zubarevich A, Gwanmesia PN, Li S, Loganathan S, Barnucz E, Merkely B, Szabó G. (2014) An altered pattern of myocardial histopathological and molecular changes underlies the different characteristics of type-1 and type-2 diabetic cardiac dysfunction. J Diabetes Res, 2015**:** 728741.
IF_{2015}: 2.431

Weymann A, Radovits T, Schmack B, Korkmaz S, Li S, Chaimow N, Pätzold I, Becher PM, Hartyánszky I, Soós P, Merkely G, **Németh BT**, Istók R, Veres G, Merkely B, Terytze K, Karck M, Szabó G. (2014) Total aortic arch replacement: Superior ventriculo-arterial coupling with decellularized allografts compared with conventional prostheses. PLoS One, 9**:** e103588.
IF_{2014}: 3.234

Radovits T, Oláh A, Lux A, **Németh BT**, Hidi L, Birtalan E, Kellermayer D, Mátyás C, Szabó G, Merkely B. (2013) Rat model of exercise-induced cardiac hypertrophy - hemodynamic characterization using left ventricular pressure-volume analysis. Am J Physiol Heart Circ Physiol, 305**:** H124-134.
IF_{2013}: 4.012

Ruppert M, Barta B, Korkmaz-Icöz S, Li S, Oláh A, Mátyás Cs, **Németh BT**, Benke K, Sayour AA, Karck M, Merkely B, Radovits T, Szabó G. (2018) A hipertrófiás myocardium reverz elektromos remodellációjának vizsgálata patkánymodellben. Cardiol Hung, 48**:** 118-128.

Mátyás Cs, Sayour A, Korkmaz-Icöz S, Oláh A, **Németh BT**, Páli Sz, Hirschberg K, Zubarevich A, Gwanmesia PN, Li S, Loganathan S, Barnucz E, Merkely B, Szabó G, Radovits T. (2017) Az 1-es és 2-es típusú diabéteszes kardiális diszfunkció hátterében álló eltérő miokardiális szövettani és molekuláris jellegzetességek. Cardiol Hung, 47**:** 102-111.

Mátyás Cs, Barta B, **Németh BT**, Oláh A, Hidi L, Birtalan E, Kellermayer D, Ruppert M, Korkmaz-Icöz S, Kökény G, Horváth EM, Szabó G, Merkely B, Radovits T. (2017) A szolubilis guanilát-cikláz aktivátor cinaciguat megelőzi a kardiális diszfunkció kialakulását 1-es típusú cukorbetegség patkánymodelljében. Cardiol Hung, 47**:** 34-45.

Benke K, Sayour AA, Ágg B, Radovits T, Szilveszter B, Odler B, **Németh BT**, Pólos M, Oláh A, Mátyás Cs, Ruppert M, Hartyánszky I, Maurovich-Horvat P, Merkely B, Szabolcs Z. (2016) Génpolimorfizmusok, mint rizikófaktorok a Marfan-szindróma kardiovaszkuláris manifesztációinak előrejelzésében. Cardiol Hung, 46**:** 76-81.

Oláh A, **Németh BT**, Mátyás Cs, Horváth EM, Hidi L, Birtalan E, Kellermayer D, Ruppert M, Gellér L, Szabó G, Merkely B, Radovits T. (2016) Az egyszeri, kimerítő fizikai terhelés kardiális hatásainak vizsgálata patkánymodellen. Cardiol Hung, 46**:** 1-9.

Oláh A, Lux Á, **Németh BT**, Hidi L, Birtalan E, Kellermayer D, Mátyás C, Ruppert M, Merkely G, Szabó G, Merkely B, Radovits T. (2013) A sportszív részletes hemodinamikai jellemzése bal kamrai nyomás-térfogat analízis segítségével. Cardiol Hung, 43**:** 224-232.

Németh BT, Hidi L, Tóth R, Radovits T, Szabó G, Merkely B, Horkay F, Veres G. (2013) A szívizomvédelem lehetőségei a szívsebészeti gyakorlatban. Cardiol Hung, 43**:** 63-69.

12. Acknowledgements

First and foremost, I would like to express my deepest gratitude to my tutor, Dr. Tamás Radovits for his indefatigable support over our work together nearing almost a decade at the time of conception of this dissertation. I am positive I would never have reached this far without his patient guidance and expertise throughout these past years.

Sincere thanks to Prof. Dr. Béla Merkely for his supervision and encouragement during my work as a PhD student, as well as for the immense support in providing the resources and framework that allowed for conduction of the research discussed herein. I would also like to thank Dr. Violetta Kékesi, Dr. Gábor Kökény and Dr. Judit Skopál for their help and expert scientific advice on all and any of the questions I turned to them with.

Special thanks goes to Prof. Dr. Pál Pacher, whose brilliant ideas, originality and boundless insight were truly inspiring for me as a visiting fellow in his laboratory, leaving a permanent mark on my mentality not just as a scientist, but as a person as well.

This work would not have been possible without the expert assistance of Henriett Biró, Gábor Fritz, Dóra Juhász, Krisztina Fazekas, Tímea Fischinger and Edina Urbán. I am also deeply grateful to my fellow PhD students as well as members of the Students' Scientific Association in our lab, who were always there to give a hand, whether it be work or leisure. The author is grateful to Servier Medical Art for providing elements under CC BY 3.0 licensing to be freely used for the figures' artwork in this dissertation.

Last, but not least, my warmest and most sincere gratitude goes without doubt to my family and closest friends. You have been there for me since my very first steps, and there is no way of expressing the safety it gives to know you will always be there, no matter where the road bends.